Functionalization of Nanoparticles with Tyrosine Hydroxylase

Biotechnological and Therapeutic Implications

Maria Teresa Bezem

Thesis for the degree of Philosophiae Doctor (PhD)
University of Bergen, Norway
2022

UNIVERSITY OF BERGEN

Functionalization of Nanoparticles with Tyrosine Hydroxylase

Biotechnological and Therapeutic Implications

Maria Teresa Bezem

Thesis for the degree of Philosophiae Doctor (PhD)
at the University of Bergen

Date of defense: 30.09.2022

Year: 2022

Title: Functionalization of Nanoparticles with Tyrosine Hydroxylase

Name: Maria Teresa Bezem

Print: Skipnes Kommunikasjon / University of Bergen

Scientific environment

Most of the work presented in this thesis was carried out in the Biorecognition research group at the Department of Biomedicine, Faculty of Medicine, University of Bergen during the period 2012-2021. The main supervisor of the doctoral education was Aurora Martinez, and Knut Teigen was co-supervisor. The synthesis and initial characterization of porous silicon nanoparticles was conducted during a 6-month research stay in 2014 in the lab of Michael J. Sailor in the Department of Chemistry and Biochemistry, at the University of California San Diego.

The project was financially supported by the Faculty of Medicine, University of Bergen. Additional grants and training have been provided by the Meltzer Research Fund, the National Graduate School in Structural Biology (BioStruct), the National Graduate School in Biocatalysis (BioCat), Norwegian PhD School of Pharmacy and the Norwegian Biochemical Society (NBS).

Acknowledgements

Who would have thought that it would take me a decade to complete this PhD? Not I, but life happens… I now have two wonderful children: Sølve Elias and Eira, and I learned to walk again, which was not a matter of course all along.

Aurora, I am enormously grateful that you never gave up on me! Your support and wisdom have guided me through this journey. You have provided a wonderful research environment and plenty of opportunities. I will always remember your passion for the hydroxylases and their interactions. I'm glad you shared it with me. I am very thankful for the co-supervision and feedback on my thesis that I received from Knut, Rune and Lars H.

A big thanks goes to all the current and former members of the Biorecognition group, especially to Ann Kari, Dayne, Helene, Heli, Jarl, Juha, Karina, Lars S., Marte, Svein and Trond-André for creating a nice atmosphere both scientifically and socially. Thanks to Anne and Kunwar for being such great office mates. Fredrik, it has been a pleasure to work with you, I wish we could work more on nanoparticles together!

Mike, thanks for letting me stay in your lab. I felt well-integrated right from the start and could collaborate with many, which was fun. Thanks to Joanna, Tushar, BJ, Rhiannon and Nicole for great guidance and exciting experiments in the Sailor lab and all the nice conversations that came along.

At last, but not at least, I would like to thank my friends and family. Gunnar, Christine, Geir Olav, Alex, Trine, Tina, Anette, Ulle og Max, jeg er glad for at dere tar både meg og barna med på turer, seiling, kiting og andre aktiviteter. Annbjørg, Sindre, Øystein og Frie, takk for alle de fine klatreøktene og skiturene – det er god avveksling. Kjære Tore, tusen takk for alle de fine dagene sammen. Marc en Lidy, ik had dit niet kunnen voltooien zonder jullie steun. Heel erg bedankt voor alle hulp!

The figures 1 to 5 were made in BioRender and figure 7 in Illustrator (Adobe).

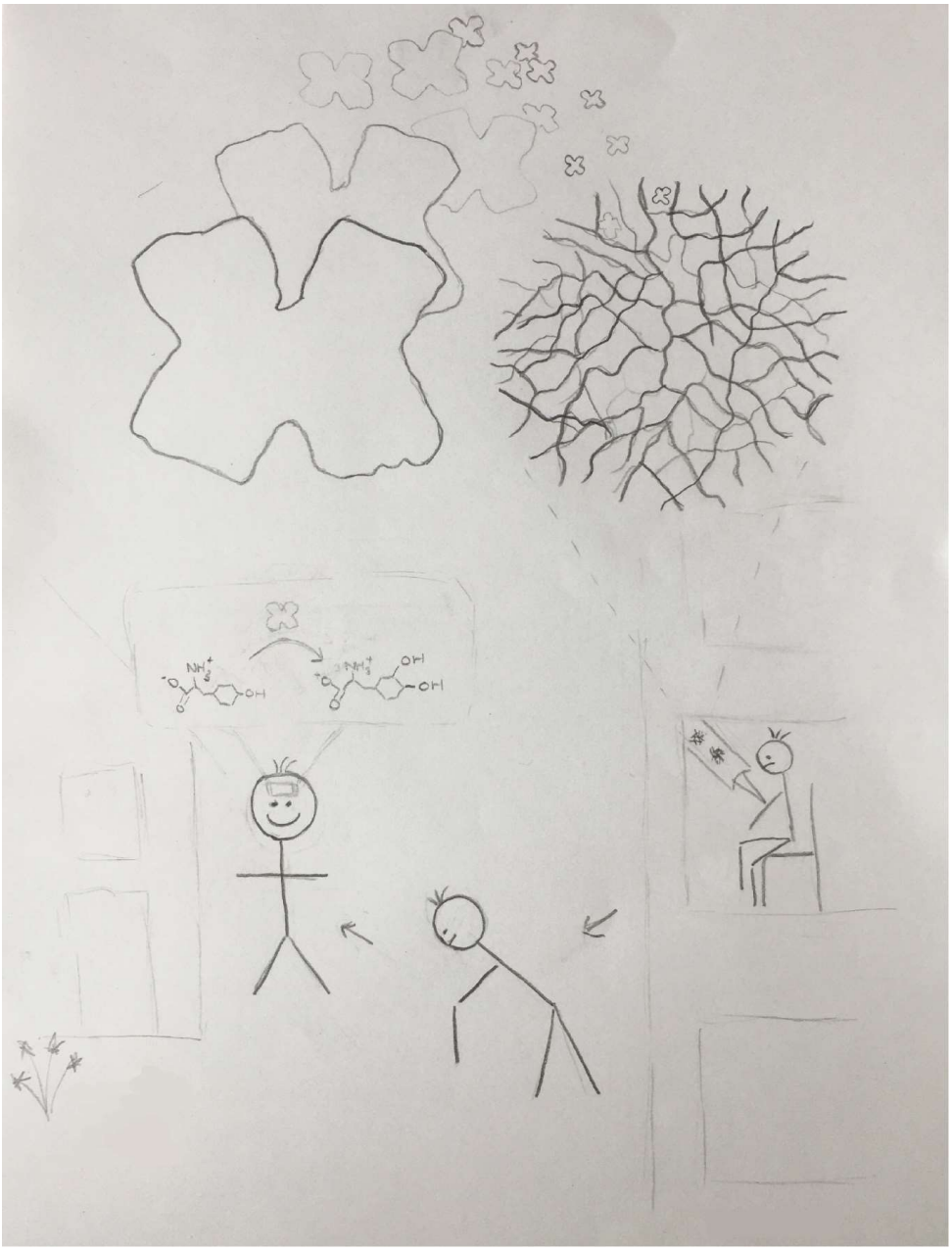

Sketch of the envisioned enzyme replacement therapy for Parkinson's patients.

Abstract

Tyrosine hydroxylase (TH) is important for neuronal function as it is the rate-limiting enzyme in the synthesis of dopamine, noradrenaline, and adrenaline. In Parkinson's disease, the levels of TH and dopamine decrease, due to progressive loss of the dopaminergic neurons in a part of the midbrain called substantia nigra. Treatment is typically with the dopamine precursor, levodopa, but its pharmacological effect wears off, and the patients develop serious side effects, so there is a need for better treatment options. One alternative could be to replace the lacking TH with an enzyme replacement therapy and thereby restore the dopamine levels. The main goal of this thesis has been to investigate how TH can be pharmacologically developed into a potential biological drug. We have therefore studied different nanoparticle (NP)-based formulations to stabilize and deliver TH and evaluated the therapeutic potential of TH-loaded NPs.

We started out by using fusion tags in the preparation of TH to obtain a stable enzyme of which we determined the full-length solution structure. Then we selected porous silicon and maltodextrin NPs as potential carriers of TH. Initial characterization revealed that the photoluminescent properties of porous silicon can be tuned to correlate with the release of a model protein, which can be useful in tracking of drug delivery. Furthermore, we found that TH loading in porous silicon NPs occurred through electrostatic interactions, but that it also induced TH aggregation. On the other hand, maltodextrin NPs absorbed large amounts of TH while preventing or delaying its aggregation. We observed functional delivery of TH by these NPs to neuronal cells and tissue, which significantly increased the intracellular TH activity.

All in all, this thesis has given insights into the structural mechanisms and functional prerequisites necessary for successful formulations of TH with NPs, which shows the therapeutic potential of enzyme replacement therapy with TH-loaded NPs.

Sammendrag

Tyrosine hydroxylase (TH) er et viktig enzym for nervesystemet, fordi det katalyserer det første steget i syntesen av dopamin, noradrenalin og adrenalin. Nivået på TH og dopamin synker hos Parkinsons pasienter pga. den gradvise celledøden i den hjernedelen som heter substantia nigra. Vanlig behandling går ut på å ta levodopa som er forløperen til dopamin, men effekten avtar etter hvert, og pasientene får alvorlige bivirkninger ved høye doser. Det trengs altså et bedre behandlingstilbud. En mulighet kan være å tilføre mer TH vha. en enzymerstatningsterapi som også vil gjenopprette dopaminnivået. Hovedformålet med denne avhandlingen er å finne ut hvordan TH kan bli brukt som biologisk medisin. Vi har derfor utviklet forskjellige nanopartikkel-baserte formuleringer som kan stabilisere og levere TH, og evaluert det terapeutiske potensiale til TH-lastede nanopartikler.

Vi begynte med å produsere TH sammen med forskjellige fusjonspartnere og fikk et stabilt enzym som vi målte strukturen av. Så valgte vi porøst silisium og maltodekstrin nanopartikler som mulige bærere av TH. De første forsøkene med porøst silisium viste at det er en sammenheng mellom fotoluminescensen og frigjøringen av et modellprotein som kan være nyttig i sporing av legemiddelleveringen i kroppen. Videre fant vi at TH kunne bindes i nanopartikler av porøst silisium, men at dette førte til aggregering av TH. Maltodekstrin-nanopartikler kunne derimot absorbere store mengder TH samtidig som de forhindret eller forsinket TH aggregeringen. Vi observerte at disse nanopartiklene kunne levere TH til nerveceller og hjernevev og dermed økte den intracellulære TH aktiviteten.

Alt i alt har denne avhandlingen gitt et godt innblikk i de strukturelle mekanismene og de funksjonelle forutsetningene som trengs for å kunne lage vellykkede nanopartikkel-baserte formuleringer av TH. TH-lastede nanopartikler har muligheten til å bli videreutviklet til enzymerstatningsterapi for sykdommer hvor det er for lite aktivt TH, som f.eks. ved Parkinsons sykdom.

Contents

Abbreviations

AAAH	Aromatic amino acid hydroxylase
ACT	a structural motif named after aspartate kinase, chorismate mutase, and tyrA
BBB	blood-brain barrier
BH4	tetrahydrobiopterin
BSA	bovine serum albumin
CNS	central nervous system
Cryo-EM	cryogenic electron microscopy
DBS	deep brain stimulation
DDC	DOPA decarboxylase
DRD	DOPA-responsive dystonia
ERT	enzyme replacement therapy
FDA	food and drug administration
GTP	guanosine triphosphate
L-DOPA	L-3,4-dihydroxyphenylalanine
L-Phe	L-phenylalanine
LSD	lysosomal storage disorder
L-Tyr	L-tyrosine
MBP	maltose binding protein
MDNP	maltodextrin nanoparticle
NMR	nuclear magnetic resonance
NP	nanoparticle
PD	Parkinson's disease
PEG	polyethylene glycol
PKU	phenylketonuria
PLGA	poly(lactic-co-glycolic acid)
pSiNP	porous silicon nanoparticle
SAXS	small angle x-ray scattering
TEV	tobacco etch virus
TH	tyrosine hydroxylase
THD	tyrosine hydroxylase deficiency
ZZ	a synthetic structural protein motif

List of Publications

I. Bezem, M. T., Baumann, A., Skjærven, L., Meyer, R., Kursula, P., Martinez, A., & Flydal, M. I. (2016). **Stable Preparations of Tyrosine Hydroxylase Provide the Solution Structure of the Full-Length Enzyme**. *Scientific Reports*, **6**(1), 1-14.

II. Wang, J., Kumeria, T., Bezem, M. T., Wang, J., & Sailor, M. J. (2018). **Self-Reporting Photoluminescent Porous Silicon Microparticles for Drug Delivery**. *ACS Applied Materials & Interfaces*, **10**(4), 3200-3209.

III. Bezem, M. T., Johannessen, F. G., Kråkenes, T.-A., Sailor, M. J., & Martinez, A. (2021) **Relevance of Electrostatics for the Interaction of Tyrosine Hydroxylase with Porous Silicon Nanoparticles**. *Molecular Pharmaceutics*, **18**(3), 976-985.

IV. Bezem, M. T., Johannessen, F. G., Jung-KC, K., Gundersen, E. T., Jorge-Finnigan, A., Ying, M., Betbeder, D., Herfindal, L. & Martinez, A. (2018). **Stabilization of Human Tyrosine Hydroxylase in Maltodextrin Nanoparticles for Delivery to Neuronal Cells and Tissue**. *Bioconjugate Chemistry*, **29**(2), 493-502.

1. General introduction

Proteins are considered to be the machinery of the human body as they are the macromolecules with the most diverse and dynamic roles in living organisms. They carry out specific tasks such as catalysis (as enzymes), transport of molecules and nutrients (as transporters and channels) and can function as structural components, signaling molecules and so forth. Proteins are composed of long chains of amino acids, with a sequence that is encoded in our genes, which determine the necessary protein structure for a specific biological function. The genes also regulate where, when and which proteins are produced, establishing a detailed organization of protein components in a cell that is dynamic to external responses. This homeostasis, together with protein folding into structures of higher levels, is highly complex, and a fascinating part of what makes life – as we know it on earth – possible. Many proteins are vital for survival and well-being of the hosting organism, and the lack or malfunctioning of one protein can distort this state of equilibrium and cause disease.

One protein in which I am particularly interested in, is tyrosine hydroxylase (TH). TH is a protein with complex structure and an important physiological role as enzyme, it is implicated in several disorders and therefore a target for potential treatment options, as I will describe in the following chapters.

1.1 Tyrosine hydroxylase – a vital enzyme for neuronal function

In 1964, Nagatsu and coworkers discovered TH (EC: 1.14.16.2), the enzyme that catalyzes the conversion of L-tyrosine (L-Tyr) to L-3,4-dihydroxyphenylalanine (L-DOPA) [1]. This reaction requires ferrous iron (Fe^{2+}), molecular oxygen (O_2), and the cofactor tetrahydrobiopterin (BH_4) [2, 3]. It is the first and rate-limiting step in the biosynthesis of the catecholamines: dopamine, noradrenaline (also called norepinephrine) and adrenaline (epinephrine) (Fig. 1).

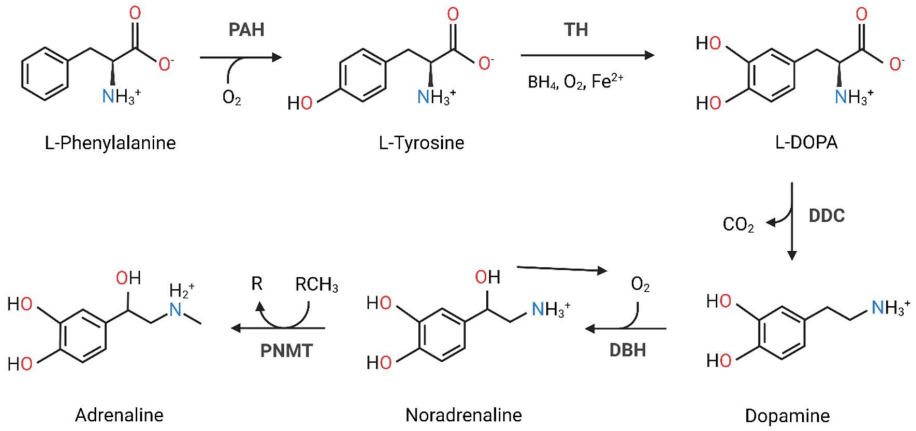

Figure 1: Biosynthesis of catecholamines and the enzymes catalyzing each step. The essential amino acid L-phenylalanine is hydroxylated by phenylalanine hydroxylase (PAH) into L-tyrosine, which can be further hydroxylated into L-3,4-dihydroxyphenylalanine (L-DOPA) by tyrosine hydroxylase (TH). L-DOPA is converted into dopamine through decarboxylation by dopa decarboxylase (DDC). Subsequent synthesis of noradrenaline is catalyzed by dopamine β-hydroxylase (DBH) and of adrenaline by phenylethanolamine N-methyltransferase (PNMT).

Catecholamines are neurotransmitters and hormones with essential roles in motor activity, cognition, digestion, and physiological responses to stress. Dopamine is a neurotransmitter, acting as a signaling molecule mainly in the central nervous system (CNS), controlling movement, behavior and metabolic functions [4]. Noradrenaline is primarily present in sympathetic nerve endings where it acts locally as a neurotransmitter on smooth muscle tissue involved in bowel movements, regulating vascular tone, and heart rate [5]. Adrenaline acts mainly as a hormone on peripheral organs after its release from the adrenal gland into the bloodstream, and is connected to the reactions such as increased glucose levels in blood and increased heart rate that are involved in the fight-or-fight response [6]. Impairment of catecholamine synthesis and/or function can have fatal consequences. A deletion of the *TH* gene leads to mid-gestational lethality, indicating that TH and catecholamines are also essential for fetal development and postnatal survival [7, 8].

1.1.1 Location and physiological function of TH

TH is expressed in both the CNS and peripheral nervous system. In the CNS, it is found in dopaminergic and noradrenergic neurons, including areas such as the

substantia nigra and ventral tegmental area, and to a minor extent in the hypothalamus and cortex [9]. TH staining of the brain revealed its location in dopaminergic and noradrenergic neurons and enabled recognition of the four major dopaminergic pathways connecting these brain areas [9]: the nigrostriatal pathway for control of motor function; the mesolimbic pathway constituting the reward system; the mesocortical pathway influencing cognitive control and emotional response; and the tuberoinfundibular pathway inhibiting the release of the peptide hormone prolactin from the pituitary gland. In the peripheral nervous system, TH is expressed in the superior cervical ganglia and in high amounts in chromaffin cells of the adrenal medulla [9]. TH is also found in intrinsic cardiac adrenergic cells during early fetal development [10], in minor amounts in dopaminergic cells of the retina [11] and enteric nerve endings in the gut [12]. The abundance of TH in dopaminergic neurons, both in cell bodies and axons, is so remarkable that the presence of TH is frequently used as an immunofluorescent marker for dopaminergic neurons, although it is also expressed in other cell types [13, 14].

TH is considered a soluble and intracellular protein mainly found in the cytoplasm [15], where L-Tyr is readily available for hydroxylation. There are, however, reports showing that TH is located in the nucleus [16], attached to the Golgi and synaptic vesicles [17] as well as in a particulate form in the nerve endings [18, 19]. Several studies have also demonstrated the binding of TH to natural and synthetic membranes, an interaction that appears to be modulated by the phosphorylation state [17, 20-22]. Nuclear location is thought to be related to proteasomal degradation [23], whereas at membranes TH interacts with other proteins, especially those involved in the synthesis and transport of catecholamines [24], 14-3-3 proteins [20], or vesicular monoamine transporter 2 (VMAT2) and α-synuclein [17, 25]. TH can also bind to membranes directly through the flexible N-terminal tail [21, 26], for instance, when located at the cytosolic side of synaptic vesicular membranes while bound to VMAT2 [25].

The hydroxylation reaction catalyzed by TH (Fig. 1) occurs in a stepwise manner initiated with the binding of molecular oxygen to the Fe^{II} atom in the catalytic site of

BH_4- and L-Tyr-bound TH, proceeding to consecutive radical reactions with formation of a Fe^{II}-O-O-BH_4 bridge structure and a subsequent Fe^{IV}=O hydroxylating intermediate. In the second step the L-Tyr substrate is hydroxylated followed by the protonation of the oxidized cofactor which is subsequently released as 4a-OH-BH_4, called pterin-4a-carbinolamine [27]. The substrate hydroxylation is coupled to the cofactor hydroxylation and under normal conditions no product is released before both oxidations have occurred [27]. The cofactor (now pterin-4a-carbinolamine) needs to be regenerated to its reduced form (BH_4) after each hydroxylation (Fig. 2). BH_4 is recycled through a regenerative pathway [28] and seems also to be the physiological reductant of the iron atom, although many other reductants work as well [29].

The TH reaction is sensitive to the oxidative environment of the cell, as it influences the oxidation state of the iron atom in the active site and the cofactor BH_4. TH-mediated catalysis requires iron in the ferrous (reduced) state, *i.e.*, Fe^{II} [2] and BH_4 is an essential cofactor for the TH reaction and can exist in different forms. TH-mediated catalysis requires BH_4 in the reduced form which it is synthesized through the *de novo* pathway or recycled in the regeneration or salvage pathways (Fig. 2) [28]. If tyrosine hydroxylation is uncoupled from the oxidation of BH_4, the TH reaction generates hydrogen peroxide (H_2O_2) leading to oxidative stress [30]. Catalase and superoxide dismutase (SOD) or mimetics, have a positive effect on TH activity by maintaining oxidative conditions low [31].

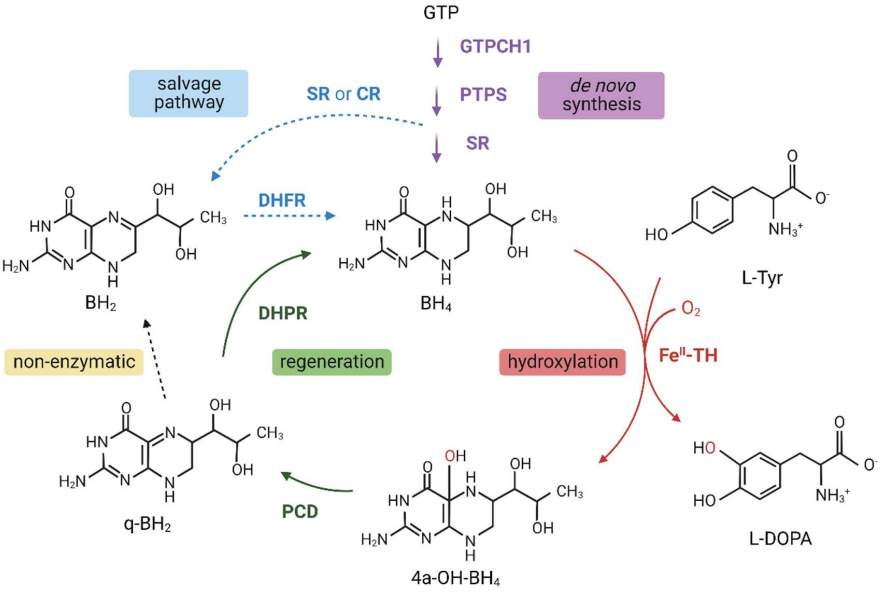

Figure 2: Metabolism of the cofactor BH_4. BH_4 is synthesized from guanosine triphosphate (GTP) through a *de novo* synthetic pathway involving several steps catalyzed by the enzymes GTP cyclohydroxylase I (GTPCH1), 6-pyruvoyltetrahydropterin synthase (PTPS) and sepiapterin reductase (SR). BH_4 is hydroxylated simultaneously with L-Tyr, mediated by binding to the atomic Fe^{II} in the active site of TH. Regeneration occurs through the quinoid dihydrobiopterin ($q\text{-}BH_2$) by pterin 4a-carbinolamine dehydratase (PCD) and dihydropteridine reductase (DHPR). Alternatively, $q\text{-}BH_2$ can be converted non-enzymatically to dihydrobiopterin (BH_2) and rescued through the salvage pathway by dihydrofolate reductase (DHFR). Illustration was based on [28, 32, 33].

Hydroxylation of L-Tyr into L-DOPA can also be catalyzed by tyrosinase, a copper-dependent enzyme. Actually, tyrosinase was considered to be the enzyme catalyzing the first step of the catecholamine synthesis before the discovery of TH [1] The reaction mechanism of tyrosinase is similar, but different from that of TH. Tyrosinase requires molecular oxygen and a hydrogen donor, such as its own reaction product L-DOPA, as cofactor [34]. Tyrosinase, also known as polyphenol oxidase, is expressed in bacteria, fungi, plants, and animals including human pigment-producing melanocytes in the skin. It is important for the production of melanin as it catalyzes both the first and second steps (hydroxylation of L-Tyr and of L-DOPA) in the melanin synthesis [35]. TH also has L-DOPA oxidase activity that is 2- to 8-fold lower than its TH activity, depending on the isoform and substate concentration [36].

In the presence of thiols such as dithiothreitol, the reaction product of the L-DOPA oxidase activity of TH is identical to that of tyrosinase and thought to be a thioether derivative of L-DOPA [36].

TH expression and activity are tightly regulated to control catecholamine homeostasis [37]. Long-term regulation of TH gene expression and protein levels is controlled by transcription regulators, alternative splicing and mRNA stability, whereas TH activity is short-term regulated by post-translational modifications and catecholamine end-product feedback inhibition [13, 38]. All catecholamines bind and inhibit TH competitively with BH_4, and it is suggested that most TH is found in the inhibited resting state ready to be activated upon need for catecholamine production [37]. Also, TH is phosphorylated at Thr8, Ser19, Ser31 and Ser40 by a range of protein kinases [24, 39]. The role of Thr8 phosphorylation has not yet been clarified, whereas the phosphorylation at Ser19 is associated with nuclear localization, degradation, binding to 14-3-3 proteins and hierarchical phosphorylation [16, 40, 41]. Phosphorylation at Ser31 is associated with hierarchical phosphorylation, vesicular transport and increased stability [17, 42, 43], and at Ser40 with alleviation of the binding and inhibition by catecholamines and increased activity [44]. Another, less-studied post-translational modification is nitric oxide-mediated S-nitrosylation, which can both enhance and inhibit TH activity depending on which amino acid is nitrosylated [45].

TH has several protein regulators that affect its expression and enzymatic activity. Ser19-phosphorylated TH binds to 14-3-3 proteins, which are regulatory proteins abundant in neuronal cells of the brain, and activators of TH activity [46, 47]. All 14-3-3 protein isoforms bind to the Ser-19 phosphorylated N-terminal of TH, and thereby activate TH and prevent dephosphorylation and proteolytic cleavage of this flexible tail [48, 49]. NT5DC2, which also is a binding partner of TH, inhibits TH activity [50]. DJ-1, a protein regulating oxidative stress, also binds TH and stimulates its activity by a direct protein-protein interaction which does not include a post-translational modification of TH [51]. In addition, DJ-1 up-regulates *TH* gene transcription by histone modification [52] and by activating the positive transcription factor nuclear receptor related-1 [53]. α-Synuclein, a protein regulating membrane

curvature, associated to synaptic vesicles and largely expressed in presynaptic nerve terminals [54], also binds TH and inhibits its activity by reducing phosphorylation suggesting that α-synuclein might have a regulatory function [55]. All in all, TH expression, location and activity, are thus tightly regulated for a controlled synthesis of catecholamines.

1.1.2 Structure and stability of TH

Historically, TH was purified for *in vitro* studies from natural sources, such as bovine adrenal glands and cell cultures of PC12 cells, which were originally derived from rat pheochromocytoma, a tumor of the adrenal gland. TH was often purified in a truncated form containing only the catalytic core [56] or co-purified with catecholamines resulting in an inhibited enzyme [57]. Later, through recombinant expression in *E. coli* and subsequent purification using chromatography an apo-enzyme of TH was prepared [58] and could easily be reconstituted with iron for functional studies [59].

Structurally, TH is a homo-tetramer with a monomeric size of 55.6 kDa and 497 amino acids for the smallest isoform (Fig. 3). Each identical subunit consists of a N-terminal regulatory domain (residues 1-156), a catalytic domain (164-456) and a C-terminal tetramerization domain (457-497). The crystal structure of the catalytic and tetramerization domains of rat TH with the active site iron was solved by Goodwill and colleagues (PDB ID 1TOH, [60]), and later with additionally bound BH_2, a cofactor analog (PDB ID 2TOH, [61]). The structure of the same regions for human TH has also been solved by Muniz and colleagues (Fig. 3B, PDB ID 2XSN, not published). A large part of the regulatory domain (residues 65–159) was solved by nuclear magnetic resonance (NMR, PDB ID 2MDA, [62]) and identified as a dimerized ACT-domain fold (Fig. 3A), which is a structural motif named after the first three proteins found with this domain: aspartate kinase, chorismate mutase, and tyrA (prephenate dehydrogenase) [63]. The structural work in this thesis has been performed based on these truncated structures, as a full-length structure of tetrameric human TH was first published in January 2022 [64].

The highly conserved catalytic domain contains the active site with a non-heme iron atom, to which the substrate L-Tyr and cofactor BH_4 bind prior catalysis. The active site is located in a 30 Å deep and 15 Å wide cleft with iron coordinated by three conserved residues in a 2-His-1-carboxylate triad 10 Å below the enzyme surface [60, 65]. BH_4 binds to one face of the large active-site cleft interacting with several residues and iron [61, 66]. The regulatory domain consists of an unstructured N-terminal tail important for binding to protein partners and membranes [21] and a the more structured ACT-domain [62].

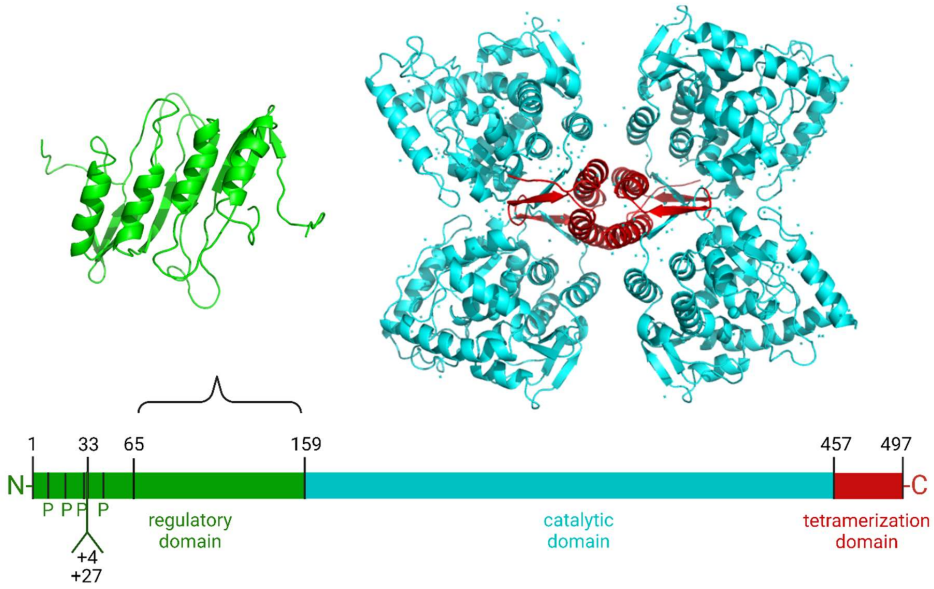

Figure 3: Available structures of TH. The NMR-derived structure of the ACT-domain of TH showing a dimerized arrangement (PDB ID 2MDA), is shown in green ribbon. The crystal structure of the catalytic and tetramerization domains with PDB ID 2XSN, determined by X-ray crystallography, shows a butterfly-like arrangement in light blue and red ribbons. The sequence of TH with an unresolved flexible tail at the N-terminal with four phosphorylation sites (P), possible insertions (+4 amino acids, +27, or +both) for the different isoforms, an ACT-domain motif (green), a large catalytic domain in the middle (light blue) and a tetramerization domain (red) at the C-terminus. Figure adapted from [67].

TH is part of an enzyme family called the aromatic amino acid hydroxylases (AAAHs) [68], which are similar in sequence, structure and function [32]. The other

members are phenylalanine hydroxylase (PAH) and the two tryptophan hydroxylases (TPH1 and TPH2), which hydroxylate L-phenylalanine (L-Phe) to L-Tyr and L-tryptophan (L-Trp) to 5-OH-L-tryptophan, respectively. The substrate specificity is not absolute and all AAAHs hydroxylate L-Phe and L-Trp to some extent, in addition to several analogs and other amino acids, but only TH hydroxylates L-Tyr [66]. The catalytic and oligomerization domains show high amino acid similarity across the AAAHs, whereas the largest differences are found in the N-terminal regulatory domains. All four enzymes form homo-tetramers, although PAH can also exist as a dimer-tetramer in equilibrium. The crystal structure of full-length human PAH with BH4 bound was solved and found to be tetrameric with separated (monomeric) ACT-domains (PDB ID 6HYC, [69]), similar to the structure of the rat enzyme in the absence of cofactor (PDB ID 5DEN, [70]). PAH is important for the metabolism of L-Phe, whereas the TPHs are essential for the production of serotonin, an important neurotransmitter and signal mediator in peripheral tissues. Mutations in PAH and TPHs can cause severe diseases such as phenylketonuria (PKU) and neuropsychiatric disorders, respectively [71, 72].

Human TH exists as four isoforms (hTH1-4) [73], whereas non-human primates have two isoforms, and only one is present throughout the remaining animal kingdom [74]. The human isoforms vary in length of their N-terminal regulatory domains as a result of alternative splicing (Fig. 3C) [75]), and their physiological location, with hTH1 and hTH2 being the most abundant in brain [76, 77]. hTH1 is the shortest isoform showing the highest sequence similarity to TH from other species [42] and it is the most well-studied isoform. In this work hTH1 was used and is just referred to as TH for most instances.

TH is a complex protein with an intrinsic structural instability, especially at the N-terminal, and is prone to aggregation [21, 78-81]. TH stability seems to be enhanced by the co-chaperone protein DNAJC12, which could play a key role in proper folding of TH and the other AAAHs [82] as DNAJC12 variants lead to a reduction in TH levels [83]. Also, deletion of the N-terminal region enhances TH stability in PD12D cells [81]. The tendency of TH to aggregate, complicated the purification of TH from

natural sources [15, 80]. TH seems to be degraded through the ubiquitin-dependent proteasome system [84-86] mediated through phosphorylation [23, 87].

TH is conformationally stabilized by inhibition of catecholamines and phenols that bind to the active site non-competitively towards L-Tyr and competitively towards BH_4 [88]. A small phenol molecule, levalbuterol, was found to stabilize TH, reduce its aggregation and sensitivity to dopamine inhibition without significantly affecting TH activity [89]. Other small molecules have been found in the search for pharmacological chaperones and show binding and stabilization of TH either with or without inhibitory effect [90, 91]. In addition, the cofactor BH_4 can have a chaperone-like stabilization effect on TH at physiological and supra-physiological concentrations [92], although an aggregation inducing effect on TH at BH_4 concentrations below its K_m in the TH reaction has been reported [78].

1.1.3 TH in disease

TH is involved in several pathological conditions. Although lack of, or deficient TH activity is usually not compatible with life [7, 8], mutations in TH occur and result in the autosomal recessive disorder TH deficiency (THD) [93]. THD causes symptoms ranging from DOPA-responsive dystonia (DRD) and infantile parkinsonism to severe encephalopathy [67, 93, 94]. A decrease in TH and DA is also associated with Parkinson's disease (PD) [95], and neuropsychiatric disorders such as schizophrenia [96] and depression [97, 98]. How TH is implicated in THD and PD, will be elaborated below.

THD is a rare monogenic disorder with 59 different THD mutations known to date [67]. Most mutations are missense point mutations resulting in amino acid substitution in regions of the catalytic domain that are well conserved across various species, although some are deleterious in one allele or located in the promotor region of TH [93, 99]. Patients can be homozygous with the same variant or compound heterozygous with two different variants, one for each allele. Genotype-phenotype correlations have not been established as there are considerable individual differences in symptom severity, even with the same combination of mutations, which indicates a demand for more personalized treatment [67]. However, mutant TH shows reduced

stability and/or reduced activity and/or substrate specificity shifting most often from L-Tyr towards L-Phe or L-DOPA, when studied *in vitro* [99]. For instance, mutations associated with severe THD phenotype have significantly less residual TH activity [99]. TH mutant R202H (numeration for hTH1) is the most common mutation for severe THD, often unresponsive to L-DOPA treatment (Korner 2015), and patients with this mutation need treatment alternatives.

THD is classified as a subgroup of DRD, which is a collective description for disorders of malfunctioning dopamine biosynthesis [100]. DRD is defined as selective nigrostriatal dopamine deficiency caused by genetic defects without neuronal degeneration, and includes mutations in the genes for the enzymes involved in the dopamine synthesis, BH_4 synthesis and BH_4 recycling [101]. Another more common subgroup of DRD is called Segawa syndrome after the first descriptor of this disorder [102]. It is caused by mutations in GTP cyclohydrolase I, which is the rate-limiting enzyme in the *de novo* synthesis of the cofactor BH_4 [103]. Segawa syndrome presents many of the same symptoms and can clinically be confused with THD.

It has been speculated that aberrancies in the regulation of TH could play a role in the development of PD and TH could therefore be a potential therapeutic target in this disease [95]. More details on PD itself are given in the next section, whereas possible roles of TH in the etiology or modulation of the disease are described below.

First of all, PD is a neurodegenerative disease with a gradual loss of dopaminergic neurons especially in the brain area called substantia nigra. These cells express large amounts of TH and as the cell death progresses TH levels and dopamine production drop. The neurodegeneration in PD leads to a selective loss of the TH1 isoform and a relative sparing of isoform 2 for some unknown reason [76]. Sympathetic nerve fibers in the heart also show a diminution of TH staining in PD compared to healthy controls, implying that the loss of TH is not restricted to the brain [104]. This indicates a possible correlation between TH and some of the non-motor symptoms such as the orthostatic hypotension seen in 40-60% of PD patients [105]. There is also evidence that protein levels of TH in different brain areas decrease before the

typical motor symptoms of PD occur [106, 107]. TH is expressed in other neurons than solely dopaminergic neurons [14] suggesting that dopamine production is not completely lost with the death of the dopaminergic neurons in PD.

Second, TH is found in Lewy bodies and Lewy neurites [108] which are protein inclusions and a hallmark of PD used as a final diagnosis *post mortem*. Similar inclusions of insoluble protein aggregates induced by proteasomal dysfunction in a rat cell model were found to be especially rich in TH phosphorylated at Ser40 [109]. Low levels of dopamine seem to accelerate TH phosphorylation and subsequent ubiquitination and degradation [110]. This vicious cycle leading to decline in TH levels and dopamine production, has therefore been proposed to lead to the negative spiral aggravating the symptoms of PD [86]. Precisely how and why Lewy pathologies occur is not known, but it is suggested that TH aggregation induced by low levels of BH_4, might act as a trigger of the formation of Lewy bodies in PD [78]. These results all indicate that accumulation of aggregated TH can have a pathological role in the development and progression of PD.

Third, alterations in the regulation of TH expression and activity are seen in PD and contribute to oxidative stress. A compensatory upregulation of nigral TH expression upon the release of high-mobility group box 1 (HMGB1) from astrocytes, is seen in a toxin-induced parkinsonian mouse model [111]. HMGB1 is an archetypical alarmin, an endogenous protein that is released from immune cells in inflammatory response to infections and injury to mediate cell proliferation and tissue regeneration [112]. This upregulation through HMGB1 release compensates for the reduced TH levels and thereby tends to maintain neuronal function of the affected dopaminergic pathways [111]. A persistent upregulation of TH activity by increased phosphorylation has been seen in the substantia nigra of rats after peritoneal injection of lipopolysaccharide to induce inflammation [113]. A reduction in soluble and well-functioning α-synuclein, through aggregation and subsequent formation of Lewy bodies, upregulates TH activity and thereby dopamine synthesis resulting in an increase of reactive dopamine metabolites [55]. TH itself can also increase oxidative stress as the TH reaction can become uncoupled and generate ROS [29, 30, 66]. In

this way, upregulation of both the expression and activity of TH and uncoupling of the TH reaction can contribute to increased oxidative stress which in turn might cause or accelerate neuronal cell death [95].

1.2 Parkinson's disease and its treatment options

Parkinson's disease (PD) was first described by James Parkinson in *An Essay on the Shaking Palsy* in 1817 and is characterized clinically by the typical motor features such as resting tremor, rigidity, postural imbalance, and bradykinesia, which are frequently accompanied by changes in sleep, mood, cognition and behavior [114]. As mentioned above, PD is a progressive neurodegenerative disorder with a gradual loss of dopaminergic neurons in the substantia nigra leading to reduced levels of dopamine in the striatum, and thus appears with subtle onset and gradual worsening of symptoms, occurring mainly in the elderly.

1.2.1 Pathology and disease progression

Pathologically, PD is defined by dopaminergic cell death and the presence of Lewy bodies in the brain stem [115]. Since various other conditions than PD can lead to the same motor symptoms, the collective set of these signs are considered a clinical syndrome called parkinsonism [116, 117]. Several of these parkinsonian conditions have been called familial forms of PD, such as infantile and juvenile PD and cause early-onset and usually have a clear genetic cause of which 70 different genes have been identified [118]. Among one of the most common forms is autosomal recessive juvenile parkinsonism, which has mutations in the *PARK2* gene encoding for parkin – a ubiquitin-protein ligase [119]. Lewy bodies are intracellular inclusions of protein aggregates where α-synuclein is the main component [120]. Many of the proteins associated with genetic forms of PD are also present in Lewy bodies [121]. Lewy bodies and associated pathologies are found in both the cell body and neurites and not only in dopaminergic neurons of the central nervous system, but also in the enteric nervous system indicating the importance of the gut-brain axis in this pathological progress [122].

Although formation of Lewy bodies and the spreading of α-synuclein aggregates are believed to play a major role in the neurodegenerative process [123], the etiology of PD is not known. Both genetic and environmental factors seem to affect the onset and progress of neurodegeneration in PD [124, 125]. Typically, monogenetic forms of PD occur more often in early-onset (in around 20% of cases <40 years) than in late-onset (no more than 3% of cases >40 years) [126]. For idiopathic PD the genetic factors are less clear, contain both rare and common variants and are rather considered risk factors [127]. Infections, neuroinflammation, oxidative stress, protein malfunction and exposure to toxins can induce the lysosomal and mitochondrial dysfunction and protein aggregation that lead to neurodegeneration [107, 128-131]. Surrounding non-dopaminergic neurons compensate for the degeneration of dopaminergic neurons by increasing TH expression and dopamine production and thereby delaying symptoms, which can mask the disease and lead to late diagnosis [132, 133].

PD is a progressive disorder that starts with slight signs aggravating over years and decades in both severity and number and ends with debilitation and severe disability [134]. The neurodegeneration precedes the clinical phase of PD and the non-motor symptoms, typically impaired rapid eye movement sleep, constipation and loss of olfactory function commence in this prodromal phase [135]. The dopaminergic neurons that degenerate in PD are part of the nigrostriatal pathway with nerve terminals in the striatum. Here dopamine would normally act in an inhibitory manner on the motor functions exhibited by excitatory GABAergic neurons in the different parts of the striatum [136]. Lack of dopamine results in an overactivity of the motor neurons in the striatum explaining at least the occurrence of tremor and rigidity which are part of the motor features in PD. PD is clinically diagnosed with the onset of motor manifestations such as tremor, rigidity, akinesia, postural imbalance, and gait impairment. The progressive nature was classified into five stages by Hoehn and Yahr, where patients in stage I-III have mild to moderate motor symptoms able to live an independent and relatively active life, whereas patients in stage IV-V are severely disabled [134].

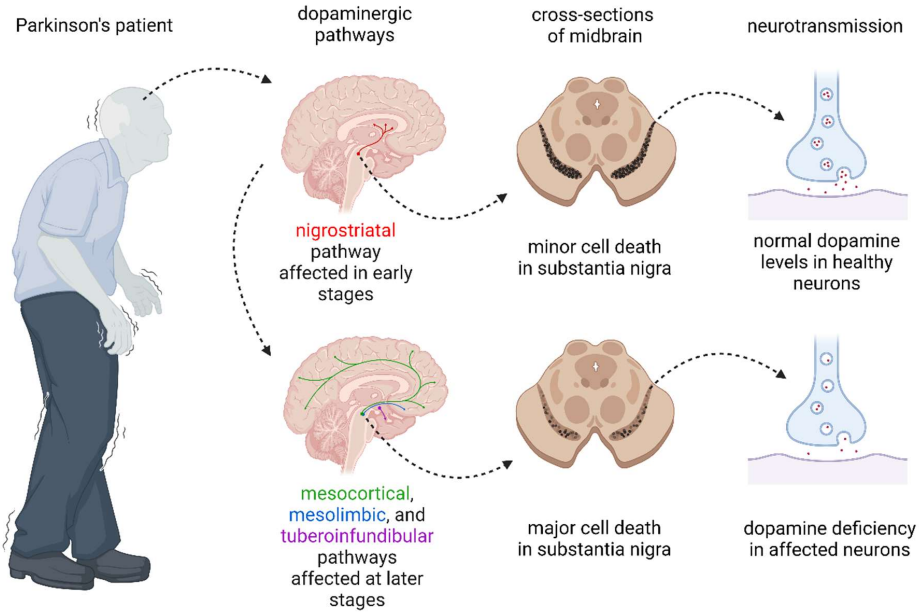

Figure 4: Alterations in brain function and structure due to neurodegeneration in Parkinson's disease. Motor symptoms such as tremor and rigid posture occur with the loss of dopaminergic neurotransmission in the substantia nigra and worsen along the progression of the disease.

Clinical heterogeneity, such as the variety and rate of progression of symptoms, and different age-of-onset between patient populations, have led to classification of parkinsonism and PD into subcategories [124]. In general, two major subtypes of idiopathic PD exist: a tremor-dominant form seen in younger patients and a postural imbalance and gait disorder type in older patients [137]. The former has usually a slower disease progression and little cognitive decline; the latter progresses faster and is often observed with the occurrence of dementia. This heterogeneity, together with the progressive nature and the unknown cause of PD, complicates the treatment of PD.

1.2.2 Treatments in use and under development

The most remarkable signs of PD can be assigned to the dopamine deficiency in the striatum. Treatment has therefore been directed to increase the supply and effect of dopamine. The most potent drug is regular oral supplement of the precursor of dopamine: L-DOPA also called levodopa, which was the first available treatment of

PD after its discovery in the 1960s [138, 139]. Typically, all PD patients will at some point be treated with levodopa. Oral supply of levodopa immediately relieves motor deficits as it readily crosses the blood-brain barrier (BBB) and is converted into dopamine, whereas dopamine itself would be retained in the blood stream. However, levodopa treatment has its price: most patients develop serious side effects such as dyskinesia and its pharmaceutical effect wears off due to pathological changes [140]. Therefore, treatment with levodopa is nowadays postponed for as long as possible.

Mild symptoms at early stages of PD are treated with other dopaminergic drugs such as dopamine receptor agonists and inhibitors of dopamine re-uptake. In addition, levodopa is usually given with carbidopa, an inhibitor of dopa decarboxylase (DDC) (Fig. 1), that reduces the peripheral conversion of levodopa and increases its circulation time and thereby reduces the fluctuations in drug levels, which seem to be responsible for the levodopa-induced dyskinesia [140]. Substantial research is done on improving the formulation of levodopa such that it can be delivered in a more continuous manner and that the plasma concentration is stabilized [141]. Enteral delivery of levodopa-carbidopa intestinal gel seems to give promising results compared to the usual oral administration, but the intestinal infusion system needs to be further improved to avoid mild to moderate adverse effects [142]. Drugs inhibiting the enzymes participating in dopamine degradation (such as catechol-O-methyltransferase and monoamine oxidase aldehyde dehydrogenase B) can also enhance the effect from levodopa. All pharmaceutical treatments directed at the dopaminergic system, solely offer symptomatic relief of the motor features in PD, since none reverses the disease progression.

Deep brain stimulation (DBS) is a treatment option in advanced stages of PD, where many patients experience troublesome levodopa-induced motor fluctuations that can no longer be maintained with medication adjustments [143]. This electrical stimulation interferes with the motor features that are caused by overactivity of some parts of the striatum (subthalamic nucleus and globus pallidus pars interna) that would normally be regulated by inhibitory nerve terminals coming from the dopaminergic nigrostriatal pathway which are diminished in PD [144]. DBS is done

by implanting electrodes unilaterally or bilaterally, into either the subthalamic nuclei or globus pallidus pars interna, which are specific parts of the striatum, and connecting them to a pulse generator implanted under the skin. The parameters of electrical stimulation need to be optimized, and to maximize clinical benefits, the physiological response during reprogramming can be monitored using functional magnetic resonance [145]. There is an expert consensus that DBS can improve tremor and reduce dyskinesia and thereby enhance the quality of life in patients with little or no cognitive or psychiatric problems [143]. However, the risk of surgical complications needs to be weighed against the prospects of improved quality of life for each individual candidate as DBS can have serious adverse effects such as post-operation infection and fatal intracerebral hemorrhage [143, 146].

Throughout all stages of PD, rehabilitative therapies such as physical exercise and focused training to improve balance or speech complement pharmacological treatment as they reduce the decline in abilities [140]. Especially a reduction in falls improves the patients' quality of life, as falls often lead to hospitalization or admittance to nursing homes. Exercise as early intervention [147] and a diet rich in antioxidants [136] can have neuroprotective effects. Nutritional interventions can improve levodopa uptake and reduce its side effects [148]. Also, the recognition of the non-motor signs and symptoms in PD has led to better treatment of these comorbidities [140].

There is currently much research into the development of novel or disease-modifying therapies and repurposing of existing drugs, and many treatment options with potential neuroprotective effects are in the pipeline [149]. Different treatment strategies exist and range from small pharmaceuticals to gene therapy, immunotherapy, and cell transplantation.

The small pharmaceutical agents attempt to address the pathophysiological pathways affected in PD: α-syn aggregation, elevated oxidative stress, mitochondrial dysfunction and neuroinflammation [149]. Several of these show promising neuroprotective effects in preclinical models. Among them are the recent discoveries of the anti-epileptic drug perampanel which blocked the cellular uptake of preformed

α-syn fibrils [150], and beta-methylphenylalanine which increased mitochondrial membrane potential and thereby recovered mitochondrial damage and protected against TH depletion [151]. However, none of the earlier so-promising drug candidates (nilotinib that inhibits α-syn aggregation through inhibition of autophagy and inosine that restores mitochondrial function by increasing urate levels) have hitherto been clinically proven to have a disease-modifying effect [152]. Several general challenges in the design of clinical trials have been identified including the lack of objective biomarkers for disease progression and target engagement, too short follow-up time to detect any long-term effects, and insufficient selection of patient subpopulation [152].

Advanced therapies such as gene delivery and cell replacement have evolved from being experimental tools in preclinical research towards becoming treatment options. These approaches have rapidly taken a substantial role in clinical research in PD and constitute more than a quarter of all new phase I clinical trials [153].

Gene delivery is mediated through intracerebral injection of non-replicating viral vectors containing genes to restore dopamine production, modify the basal ganglia network, improve lysosomal function, or enhance production of neurotrophic factors [154]. Limited but persistent transgene expression was observed *post mortem* as late as 10 years post-surgery of a gene therapy with neurturin, a neurotrophic factor, but unfortunately no reduction of the pathological Lewy bodies was seen [155].

Cell replacement is a form of tissue transplantation where healthy developing cells are placed into the putamen or other striatal parts of PD patients. Substantial efforts have led to procedures of inducing the graft cells towards differentiation into dopaminergic neurons, so that they integrate into the neuronal networks in the striatum to compensate for the lost dopamine innervation [156]. The cells used can be fetal mesencephalic cells or pluripotent stem cells, with the latter being either allogenic when derived from embryonic stem cells or autologous if induced from the patient's own pluripotent stem cells [149, 153]. *Post mortem* analysis of the brain of a patient that had received cell replacement 24 years earlier showed extensive dopaminergic innervation by the engrafted cells giving the patient 18 years of motor

improvements post-transplantation, before the graft lost its efficacy probably due to widespread α -synuclein pathology in the host brain [157].

In fact, many of the investigations into novel treatments of PD aim at targeting TH, which is integrated in different treatment strategies [158]. TH is included in several gene delivery studies [159-161] and in the development of cell replacement therapies [157, 162, 163]. These efforts indicate the importance of a well-functioning TH to restore dopamine production and provide symptomatic relief. In this work, we have envisioned a hitherto unexplored treatment option: an enzyme replacement therapy (ERT) with highly functional TH. With this strategy, we seek to develop a biologic that restores local dopamine production in a fashion that imposes few or little side effects to the patient.

1.3 Biologics – an emerging type of therapeutics

Biologics, also called biological drugs or biopharmaceutics, are manufactured through a biological process. This is in contrast to small pharmaceutical compounds, also called molecular drugs, which are usually produced by chemical synthesis. Biologics can be biochemical macromolecules or mixtures of components derived from biological sources, such as blood, cells or tissues, or from biotechnological origin. Although the definition of biologics includes vaccines [164], organ transplants, blood transfusions and derivatives [165], native proteins and gene therapies, most biologics are nowadays proteins produced with recombinant DNA technology in a wide range of microorganisms, such as *E. coli* or yeast [166].

Although biologics is a relatively new term, some biologics have been used in medical treatment for a long time. Heparin is a mucopolysaccharide isolated from animal liver or gut mucosa and used as a blood anti-coagulant for treatment of thrombosis since the 1930s [167]. Aprotinin is a peptide inhibitor of several proteases including plasmin that is important for fibrinolysis, the disintegration of blood clots. It can be isolated from bovine pancreas, and has been used as an antifibrinolytic molecule to reduce post-operative bleeding since the 1980s [168]. Insulin is a peptide hormone regulating blood sugar levels which can be isolated from the pancreas.

Already in 1922, concentrated pancreatic extract from bovine could successfully treat diabetes mellitus [169]. After further isolation, this effect was assigned to the peptide insulin and animal insulin has been used to treat diabetes until the first synthetic insulin entered the market in 1982 [170]. This insulin was produced through recombinant expression of the A and B peptide chains in two separate *E. coli* cultures, whereas later production was in one fermentation, and now many refined analogs, with either longer or shorter acting properties, are available [171]. Another peptide hormone that works opposite to insulin, but can also be isolated from animal pancreas, is glucagon. Its medical use is mainly in first aid to raise severely low blood sugar levels [172] and it has been used since 1960 [173].

Since biologics are much larger and more complex than small molecular drugs, they differ from their small pharmaceutical counterparts in several ways: first, by route of administration, as biologics are susceptible to degradation in the gut and too large to be taken up by the gut epithelium, they can usually not be taken orally but require parenteral delivery [166]; second, in pharmacological effects, as biologics are typically more specific as they are identical or very similar to the human body's own components and therefore they often have better specificity and biocompatibility with regards to toxicity and degradability [174]; third, in production-dependent uniqueness, as biologics can vary from batch to batch [175] and are more difficult to be prepared as an identical product by a different manufacturer, and off-label products of biologics are therefore called biosimilars instead of generic drugs [176]; and lastly, in production costs, as the development and manufacturing process is more complex and costly.

Biologics are expensive drugs, but they are used more and more extensively. They are highly effective in autoimmune diseases where other cheaper treatments have less effect. The societal benefits in terms of patients' reduced need for care and increased possibility to function in daily life and work, often outweighs the high prices. In an Italian study of patients with psoriasis, the non-medical and indirect costs were reduced by more than 70% upon starting biologics [177]. A German study also concluded that the overall costs did not increase despite an increase of directs costs

from increased prescription of biologics, since this was accompanied by a decrease in indirect costs due to less sick leave and less work disability [178]. In 2018, biologics accounted for 8 of the 10 best-selling medicines globally when comparing total revenue [179]. Since they are mainly prescribed by specialists and often first used in hospitals [176], most of them are not as widely available as small molecular drugs that can be taken orally. The use of biosimilars that are cheaper than the original (so-called reference) product, can be beneficial by increasing the availability of biologics, anticipating that the quality, safety, and efficacy of a biosimilar is not compromised [180, 181]. This would ensure that more patients could benefit from these modern and highly specialized treatments.

1.3.1 Therapeutic proteins

Most biologics are therapeutic proteins and these have been classified into those that have an enzymatic or regulatory activity (group I), a special targeting ability such as antibodies (group II), or that work as vaccines (group III) or diagnostic tools (group IV) [174]. Proteins in group I can either replace, augment, or add a function. Group II is by far the largest group, as it includes all monoclonal antibodies that are used in treatment of autoimmune diseases, cancer, or infections, and work through suppression or stimulation of the immune system [179]. Group II, III and IV are beyond the scope of this thesis.

Here, I focus on the therapeutic proteins that are collectively called protein replacement therapies and mostly developed to target rare monogenic diseases [174]. These includes coagulation factors such as factor VIII and IX to treat their respective genetic deficiencies called hemophilia A and B [182, 183], and enzymes such as acid α-alglucosidase and idursulfase to treat Pompe disease and Hunter syndrome, respectively [184, 185]. (For more details on enzyme replacement therapies, see next section). Development of treatments for such rare diseases is expensive, but is stimulated by the orphan drug act that came in 1983 in the U.S. and similar legislation in 2000 in the E.U. [186].

A common challenge with therapeutic proteins is that they often trigger an immunogenic response in the patient, which depends on the structure and sequence of

the protein [187]. There are several strategies to overcome this in order to better tolerate the medication: A strategy that has been developed for therapeutic antibodies is the humanization of murine antibodies or the production of fully human antibodies using transgenic mice or phage display technology [179]. A second general approach is to coat the protein with a hydrophilic polymer typically polyethylene glycol (PEG) through a process called PEGylation which masks the protein and also increases its hydrodynamic diameter and thereby decreases its renal clearance and prolongs circulation time [188]. The first polymer-conjugated biological drug to receive approval from the U.S. food and drug administration (FDA) in 1994 was the enzyme L-asparaginase coated with PEG for the treatment of acute myeloid leukemia [189]. A third way is the use of nanocarriers that prevents macrophage recognition and degradation of the therapeutic protein (see next chapter). Which strategy is best suited, depends on the type of protein, target site, route of administration, and disease.

1.3.2 Enzyme replacement therapy

ERT is the administration of a therapeutic enzyme to substitute a defect or deficient enzyme. This type of treatment was first suggested as a visionary idea in the 1960s by Christian de Duve, who discovered the lysosome [190] and the process of endocytosis [191], and Roscoe Brady, who discovered specific enzyme deficiencies for several of the lysosomal storage disorders (LSDs) [192]. Three decades after, β-glucocerebrosidase derived from human placentas came on the market in 1991 as a treatment for Gaucher's disease [193], which is one of the more common LSDs and also a known risk factor for PD [194]. This was the first ERT for a LSD that was approved by the US FDA [195] and was later substituted by recombinantly expressed enzyme [196]. ERT has expanded as a treatment for other metabolic, immunodeficient, and gastrointestinal diseases such as Fabry's disease [197], adenosine deaminase enzyme deficiency [198], and lactose intolerance [199], respectively.

Usually, the mutant enzyme that is malfunctioning or deficient, is replaced by a healthy variant of its own. In some diseases, it is also possible to substitute the mutant enzyme with a completely different enzyme that can carry out the same or a similar

function. This is for instance the case in PKU, where Patients have mutations in the gene for PAH, an AAAH, as TH (see section 1.1.2), which leads to the accumulation of L-Phe in blood. Although there have been efforts to use human PAH as an ERT for PKU [200], PAH was rather substituted with PEGylated cyanobacterial phenylalanine ammonia lyase (PAL), which also degrades L-Phe and is commercially known as Pegvaliase (Palynziq®) [201-203].

An ERT with TH for PD and related disorders would require delivery of TH in a functional form to the brain. It is generally regarded as challenging to deliver large macromolecular drugs as they are especially susceptible to degradation [204]. In addition, it is even more challenging for drugs to reach the brain [205] as it is well-protected by biological barriers that need to be overcome [206]. One approach would be to load TH into a nanoparticle (NP) to protect from degradation, maintain enzymatic activity, and for precise delivery to the target cells, the dopaminergic neurons of the substantia nigra and ventral tegmental area and compensating cells in the surroundings.

1.4 Nanoparticles for drug delivery

NPs and their therapeutic applications in drug delivery are a central part of research in the field of nano science and technology, as well as in pharmaceutical research. This area of interest emerged after the famous talk by Richard Feynman in 1959, who said that “there is plenty of room at the bottom” for groundbreaking discoveries at small size scale [207]. Feynman anticipated the large impact that improved knowledge of the microscopic scale, and manipulation thereof, would have on the synthesis of new material and their macroscopic properties. A short history of the field is given before a more detailed description of NPs, their classification, characteristics, and potential to revolutionize medical treatment.

1.4.1 History of nanotechnology

The development of modern microscopy techniques, such as the electron microscope by Ruska in the 1930s [208] and scanning tunneling microscopy by Binnig and

Rohrer in the 1980s [209, 210] revealed processes and structures at a scale much smaller than had previously been possible to observe: the nanoscale. The nanoscale is usually defined as a size range from one to some hundred nanometers, with one nanometer being a millionth millimeter (1 nm = 10^{-6} mm = 10^{-9} m). Fascinating observations at the nanoscale include resolving protein structures at atomic resolution through further development of electron microscopy by freezing samples to cryogenic temperatures (cryo-EM) and subsequent single particle analysis [211, 212]. The use of scanning tunneling microscopy not only allowed Eigler and Schweizer to image, but also to manipulate individual atoms [213] and, in a similar way, allowed Severin and coworkers to write using double stranded DNA with atomic force microscopy (AFM) [214]. Advances in super-resolution and live-imaging have revealed the nano-architecture of the cytoskeleton in neuronal axons [215]. These are all wonderful examples of observable biological features at the nanoscale, also called nanostructures.

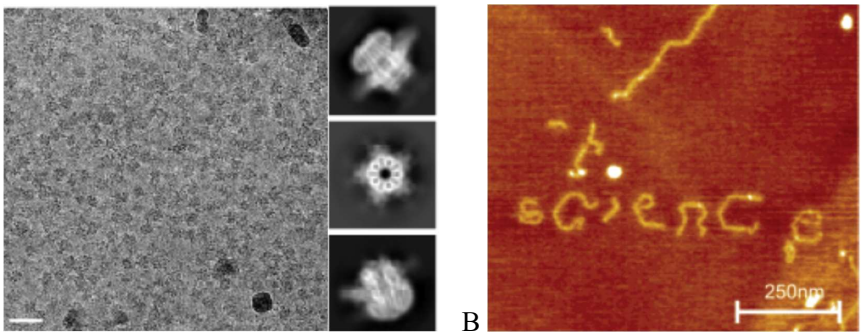

Figure 5: Organic nanostructures visualized with advanced microscopy. A) cryo-EM image including single particle analysis of the protein $GABA_A$ receptor [212]. B) AFM image of double stranded DNA formed into letters [214].

In a broad perspective, one can say that the living world is organized in nanostructures. Although vital processes are based on chemical reactions and physical interactions at sub-nanoscale, most of them depend on the structural organization at the nanoscale. Examples are assemblies of large protein complexes such as ribosomes [216], formation of tunneling nanotubes for cell-to-cell communication [217] and transmission of signals at neuronal interfaces [218]. In fact, the nanostructural components of cells and tissue often account for the macroscopic

properties of the organism. For instance, the mechanical elasticity of adipose tissue [219], the strength of bone tissue [220-222] and diffusion rates in the extracellular space of the brain [223] all depend on the nanoscale organization which is often altered in disease states.

Unique nanostructures can differ greatly in their properties compared to the same material in bulk. This remarkable difference has led to the field of nanotechnology with a whole range of applications. Material with specifically designed nanostructures can be found in industrial processes (as catalysts or construction material), in many common everyday products such as clothes, electronics, sun lotion and painting [224], but only those in medicine (as drug carriers and diagnostic tools) will be described in this thesis.

Nanomaterials can be broadly defined as materials that have features at the nanoscale. According to the European Union's legislative definition of nanomaterial, this would mean material containing particles, either unbound or in aggregates/agglomerates, where 50% or more of the particles have at least one dimension in the size range of 1-100 nm [225]. Examples of nanomaterials are nanolayers (one-dimension) such as graphene, nanotubes (two dimensions) such as carbontubes, or NPs (three dimensions). Material with a certain structures at the nanoscale (nanostructures) that gives it features that distinguishes it from its bulk counterpart, such as porous materials with pore dimensions in the size range of 1-100 nm such as metal-organic frameworks, has also been considered for inclusion in the definition of nanomaterials [225].

Several nanomaterials have been used in medicine as diagnostic tools and for therapeutic applications since the 1990s. Contrast medium for enhancing imaging techniques often contains colloidal suspensions, which are ensembles of nanoparticles in solution. For instance, iron oxide NPs are used for magnetic resonance imaging [226] and gold NPs for X-ray imaging and computer tomography [227, 228]. In addition, liposomes which are nanosized vesicles with a lipid bilayer and an aqueous interior compartment, have been used for anti-cancer drug delivery to reduce harmful

off-target effects from the drugs [229, 230]. NPs designed for drug delivery, also called therapeutic NPs or nanocarriers are a focus of this thesis.

1.4.2 Therapeutic nanoparticles

The development of therapeutic NPs came with the need for improving drug formulation. Low stability or solubility, large susceptibility to degradation, or high systemic toxicity of small molecular drugs led to redefining the concept of drugs being “magic bullets” by dividing drug properties into those related to its delivery and those to its therapeutic action [231]. This separation led to the investigation of NPs as delivery systems of pharmaceutical compounds and opened new possibilities for drug design. A successful nanocarrier would stabilize, solubilize, and protect its loaded drug (magic bullet design) while crossing biological barriers to the site of action (magic bullet flies) and where it releases its load (magic bullet explodes) without affecting healthy cells and tissue. As a result of this development, most of the current NPs used in the clinic or in clinical trials, are in fact liposomes containing small molecular drugs for treatment of cancer or various infections [232, 233]. The liposomal formulation improves the pharmacokinetic properties of the payload drug and increases delivery to the target site in this “magical” way, such that both toxicity and required dose for therapeutic effect, are reduced [232, 233].

NPs are usually classified by the type of material they are made of, and often divided into three major classes: inorganic, lipid-based, and polymeric types [230], although hybrid materials also exist. Inorganic nanoparticles are usually metallic, metal oxides or of semiconductor material. They can be made of elements such as iron (Fe), gold (Au), silver (Ag), copper (Cu), carbon (C), silicon (Si) or a combination of them, and include both solid and porous forms [234, 235]. Those that are approved for clinical use are mainly various types of polymer-coated iron NPs for iron replacement therapies [232]. Lipid-based nanocarriers [236] such as liposomes and solid lipid nanoparticles have so far had the most success. Doxil®, which is liposome-encapsulated doxorubicin was the first to get approval from the FDA in 1995 for cancer treatment [237] and many other liposomal formulations of chemotherapeutic cancer drugs have followed [232, 233]. In 2018, FDA approved the first lipid NPs

with RNA as payload [238]: patisiran, a short interfering RNA in lipid complex for knocking out the gene that causes pathogenic levels of transthyretin entered the market as treatment for transthyretin-mediated amyloidosis [239]. Two of the vaccines against the ongoing COVID-19 pandemic developed by Moderna and Pfizer-BioNTech, are also lipid NPs, carrying the mRNA of the viral spike protein [238]. Polymeric nanoparticles are made of synthetic or naturally derived polymers such as poly(lactic-co-glycolic acid) (PLGA), alginate or chitosan [240, 241]. Moreover, viral particles, extracellular vesicles [242], proteins (typically albumin) and certain protein aggregates [243] can also be regarded as nanocarriers of organic origin, of which some are FDA-approved for use in the clinic [232]. One of these latter types, Abraxane®, is a 130 nm protein cluster of human serum albumin approved for the delivery of the water-insoluble chemotherapeutic paclitaxel which has greater efficacy and fewer adverse effects than earlier formulations like Cremophor EL [243, 244].

The physicochemical properties of therapeutic NPs determine how they will fulfil their role as drug delivery devices (Fig. 6). The size influences the drug loading capacity and biodistribution. Circulating NPs smaller than 6 nm, such as zwitterionic quantum dots and cyclodextrins, will be removed from the bloodstream by renal clearance [245-247], whereas the upper size limit of NPs depends on which biological barriers the NPs need to cross. The overall shape of NPs affects bioadhesion and cellular uptake. Rod- and disc-shaped NPs attach stronger to cell surfaces than their spherical counterparts, which leads to more specific accumulation and better cell internalization [248, 249]. Elasticity is also an important factor that influences the biodistribution of the NPs, where soft NPs have longer circulation time and less cellular uptake than hard NPs [250]. Porosity and pore size are other characteristics of NP materials that have large effects on the process and capacity of drug loading. Larger pores can contain larger drug molecules, and a highly porous matrix can absorb larger amounts of drugs than a NP with low or no porosity. The inner structure of the NPs, whether it is a dense core or a compartment where the drug can be easily dissolved, also influences the drug loading capacity. For instance, hollow mesoporous silica NPs have higher loading capacity than their non-hollow

counterparts [251]. Some NPs, due to the porous structure or material they are made of, have optical properties that can be used for imaging purposes and as diagnostic tools [252, 253].

The surface properties determine the interactions with both drugs and the biological environment (Fig. 6). Surface charge plays a role in cell surface adhesion and subsequent cellular uptake. Highly charged, both positively and negatively, NPs are quickly opsonized and taken up by macrophages, whereas slightly negatively charged NPs have been demonstrated to best avoid this type of clearance and thereby had the longest circulation time [254]. Chemical groups exposed on the surface of the NPs and along the eventual pore walls, affect the binding affinity of drugs and biomolecules. For instance, many NPs are composed of organic or silicon-based material due to the versatile chemistry of carbon and silicon that allows modification reactions and conjugation of various biomolecules [255, 256]. The surface chemistry influences the hydrophobicity of the surface of the NPs, and hydrophobic surfaces absorb blood proteins such as opsonins and albumins, in the bloodstream [257]. This formation of a protein corona, also called opsonization, is the first step in the clearance of foreign intruders by the mononuclear phagocytic system (MPS; earlier called the reticular endothelial system), which must be by-passed or delayed to prevent rapid clearance of the therapeutic NPs [258]. By masking hydrophobic NPs with a coating of hydrophilic polymers, less opsonization occurs and circulation time increases [259]. Other modifications can be used to promote binding to certain receptors or markers to ensure targeted delivery to a specific tissue, cell type or intracellular location. These surface decorations can range from small ligands to peptides and antibodies (Fig. 6). For instance, cell-penetrating peptides are small sequences of positively charged amino acids similar to those protein domains that ensure membrane translocation, which can be attached to the surface of NPs for intracellular drug delivery [260]. Since the BBB expresses transferrin receptors to ensure sufficient iron transport into the brain, NPs with anti-transferrin antibodies on their surface bind to the BBB and thereby enhance uptake of the payload drug in the brain [261].

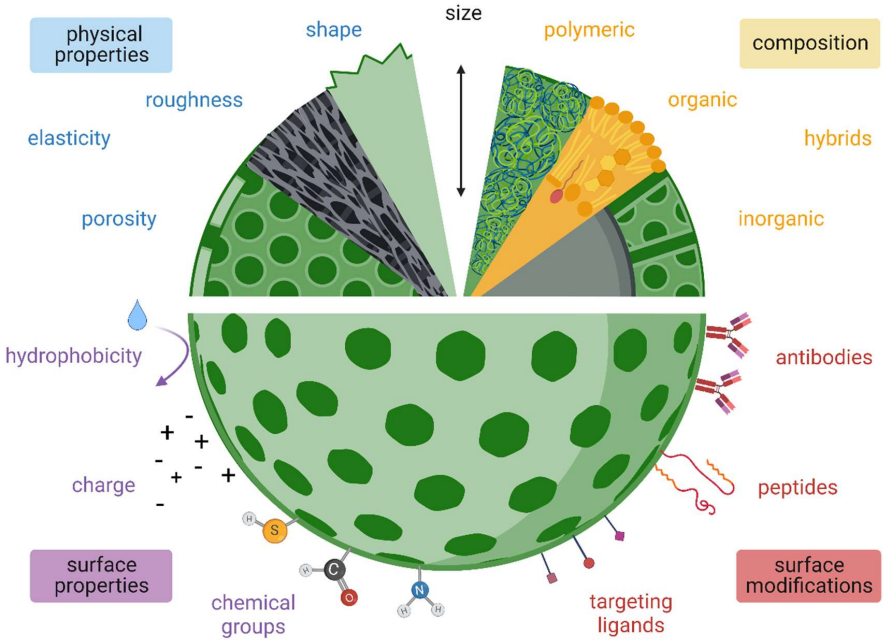

Figure 6: Illustration of a nanoparticle with different physiochemical properties. It is the combination of the material composition and physical properties together with the surface chemistry and modifications thereof that make the nanoparticle suitable for drug delivery. Figure inspired by [262].

Therapeutic NPs need to be of biocompatible and biodegradable material to avoid toxic effects and for easy removal or degradation by the clearance systems of the human body. The fate of NPs *in vivo* depends on both their material composition, structural features, surface properties and possible modifications thereof. All these properties are intertangled and their sum influences the suitability of the NPs for drug delivery purposes (Fig. 6). By tuning or selecting these properties, the NPs can be tailored for specific needs.

The success of drug delivery by therapeutic NPs depends on the ability to cross the biological barriers they encounter. Almost all approved therapeutic NPs are administered through intravenous injection [232]. Alternative routes, such as oral, pulmonary and topical administration, are under extensive investigations in preclinical research [263-265]. Recently, Hensify, which are hafnium oxide NPs for

enhancement of radiation therapy in cancer, was approved for intratumoral injection [233], and the COVID-19 vaccines are administered by intramuscular injection [238]. The main advantage of Intravenous administration is that it ensures quick and easy systemic delivery through blood circulation. However, hemorheological limitations, with regards to how fluid dynamics influences the adhesion to the vascular endothelium, can hinder necessary cellular uptake [258]. Next, for the drug to reach the site of interest, subsequent barriers are disease- and organ-specific. Intratumoral pressure and multidrug resistance are challenges in cancer treatment [258]. Diseases of the CNS are especially challenging to treat as the brain is a well-protected organ, such that intravenously injected NPs need to deliver the drug across the BBB, a cellular barrier consisting of endothelial cells with tight junctions and astrocyte end feet and highly restrictive transport pathways [205, 266]. NPs can use these pathways for transcytosis into the brain or by-pass this barrier through temporary disruption of the BBB, with for instance microbubbles and focussed ultrasound waves [267]. Many drugs also need intracellular location for being effective. Cellular uptake of NPs is mainly mediated through endocytosis, which entraps NPs in acidic compartments [268]. Extensive research is done in the design and development of NPs that escape these endosomal/lysosomal pathways through disruption of the vesicular membrane for release into the cytosol [268]. In addition, gene therapies also need to access the nucleus.

The advantages of using therapeutic NPs as drug carriers are many, especially for biologics where there are challenges with regards to formulation and administration, because of their intrinsic instability and limited permeability across biological barriers [262]. Biologics could also be administered by competing delivery technologies, such as pumps and depots, or through direct modification of the biological drug [204], but NPs are small enough for injection. In addition, NPs provide a structural environment that conserves the conformation of a protein drug enhancing its stability with regards to temperature, pH, agitation etc., protection against proteolytic degradation and immunological clearance, alter the biodistribution, and thereby reduce or prevent adverse effects and toxicity [262]. In this way, the NPs protect the sensitive cargo and delivers it to the site of action.

Many of the NPs described above may be suitable for TH delivery, since it is known that TH binds a variety of tissue components and large macromolecules. TH interacts with polyanions such as the mucopolysaccharide heparin [269]; poly acrylic acid (synthetic) and poly glutamic acid (biological) [270] and nucleic acids [271]; melanin [272]; and other biological anions such as phospholipids [273, 274]. The binding of TH to these molecules seems to occur through electrostatic interactions as binding can be prevented by high salt concentration [275]. The tendency of TH to bind these polyanionic macromolecules has been applied in research, as heparin-sepharose has long been used as column material in affinity chromatography in the purification of TH [276], and can also be exploited to ensure binding of TH to nanomaterials without compromising its enzymatic activity.

In this work, the focus has been on two types of NPs, which are very different from each other: the hard, inorganic and luminescent porous silicon NPs (pSiNPs) and the flexible, polymeric and stealth maltodextrin NPs with lipid core (MDNPs). These NPs were selected because they both showed promising abilities for protein drug delivery despite their remarkable difference with regards to material and structure. pSiNPs protect protein payload from harsh conditions [277] and are suitable for *in vivo* drug delivery [278]. MDNPs absorb large amount of protein and behave as stealth NPs [279]. Both selected NPs have advantageous properties with regards to loading capacity, biocompatibility, potential targeting and protein delivery as I will describe in detail below.

1.4.3 Porous silicon nanoparticles

Porous silicon is an exceptional material with a range of applications. It has a mechanically durable structure, versatile surface chemistry, and optical properties, which makes it a suitable substrate for cell culture [280] or an appropriate sensor component for the detection of chemical compounds [281] or biomolecular interactions [282].

Porous silicon is made through electrochemical etching of a silicon wafer using hydrofluoric acid in ethanol as electrolyte [283]. It can either remain as a porous layer on bulk silicon, be lifted-off into a free-standing film or fractured into particles [284].

The pore size, classified into micropores < 2 nm, mesopores 2-50 nm or macropores > 50 nm, and the degree of porosity can vary depending on many electronic and chemical factors, such as the presence of dopants in the silicon wafer, the concentration of hydrofluoric acid in the electrolyte and the current density used in the etch [285]. By applying high-current density pulses at regular intervals during the etching process, a multilayer of alternating porosity is obtained. Ultrasonic fracture cleaves the porous silicon predominantly at these high-porosity perforations, giving pSiNPs of controlled size and narrow size distribution [286]. In this way, pSiNPs are synthesized in a top-down fashion.

Surface modifications can improve *in vitro* and *in vivo* stability of freshly etched pSiNPs, enhance drug loading and facilitate targeted delivery [256]. Modifications specific to silicon include surface treatments such as oxidation, carbonization, and silanization to introduce covalent bonds between the silicon atoms and oxygen and carbon atoms and organic compounds, respectively [287]. Precipitation of a mineral, such as calcium which forms an insoluble calcium silicate shell, encloses the porous silicon structure, and thereby entraps the payload drug [288]. Chemical conjugation of targeting moieties and coating of polymers such as PEG, can be obtained after oxidation and a subsequent hydrolytic condensation reaction with silanol reagents that contain a thiol or amide group available for coupling chemistry [289].

Silicon oxidizes spontaneously in air or water, and the silicon oxide layer, which is mainly silicon dioxide (SiO_2) although nonstoichiometric and hydrated forms also exist, protects silicon from further corrosion [285]. However, SiO_2 dissolves in aqueous solutions above pH 7 into silicic acid, which is a family of chemical compounds of silicon, hydrogen and oxygen, where ortho-silicic acid, $Si(OH)_4$, is the predominant bioavailable form [290].

Silicon is regarded as a dietary trace element consumed mainly through cereal-based food at 25-30 mg/day, resulting in an average serum concentration of 8 µmol/l [291]. It is important for connective tissues, such as bone and cartilage [292], both during growth and development [293], and in adults to achieve a sufficiently high bone marrow density to avoid osteoporosis [294]. Hence, silicon-based biomaterials

including pSiNPs, are regarded as biodegradable and beneficial silicon sources [295]. Intravenously injected pSiNPs show good *in vivo* compatibility and decompose into silicic acid within a few days [278]. Excess silicic acid is excreted in urine through renal clearance [296].

Protein loading into pSiNPs can be obtained through physical adsorption, immobilization, or entrapment. Physical adsorption depends on several factors, such as the chemical groups at the porous silicon surface, pore size, pH and ionic strength of the loading solution, protein charge etc. Adsorption to hydrogen-terminated surface of non-oxidized porous silicon occurs via hydrophobic interactions and thus results in structural rearrangement of the protein with subsequent loss of native structure and bioactivity, whereas oxidized porous silicon interacts with proteins through electrostatic interactions preserving protein structure and retaining bioactivity [297]. Proteins penetrate far into the pores of porous silicon (> 60 μm) [298] if the pores are larger than the protein itself [299]. Maximal adsorption of protein was found to be when the pH of the loading solution was at the isoelectric point (pI) of the protein, since this minimizes both the repulsion from negatively charged surface of oxidized silicon (if pH>pI, the protein is also negatively charged) and the protein-protein repulsion (if pH<pI, the protein is positively charged) [300].

pSiNPs are suitable carriers for protein drugs because of their advantageous properties. The adjustable, but well-defined pore size of silicon-based NPs allows for the loading of proteins of various sizes [301]. The rigid framework of the silicon matrix provides protection for protein drugs in harsh environments such as the acidic condition in gastric fluid [302] or against denaturation and subsequent loss of activity [303]. Surface modifications and loading approach also allow for controlled release of the protein, whether this is rapid, triggered or by sustained release [255, 304, 305]. Finally, the intrinsic photoluminescence of porous silicon has been shown to be a major advantage for imaging applications [278]. The luminescent features originate from quantum confinement in the nanometer thick pore walls consisting of crystalline silicon, which arise as free-standing wires orthogonal to the etched face of the silicon wafer when porosity is sufficiently high [306], and is preserved throughout particle

synthesis [307]. Oxidation creates a silicon oxide shell around the silicon skeleton which reduces the pore wall thickness and thereby increases the quantum yield of the photoluminescence [308]. The luminescence can be used to track the accumulation and degradation of pSiNPs *in vivo* [278], and it has a long emission lifetime which allows for complete elimination of the shorter lived autofluorescence when imaging with a time-gated set-up [309]. In this way, pSiNPs can be regarded as non-toxic and biodegradable quantum dots that show great potential to combine drug delivery with imaging and tracking.

1.4.4 Maltodextrin nanoparticles

Maltodextrins are small polysaccharides derived from partial hydrolysis of starch and are used as additives in many food products. They consist of 3 to 17 glucose molecules mainly linked through the linear α-1,4 glycosidic bond and to some extent through the branched α-1,6 glycosidic bond [310]. The physicochemical properties of maltodextrins such as sweetness and viscosity, vary with the length of the oligomer and the degree of branching, and are also related to the content of reducing end-sugars [310].

MDNPs can be synthesized in a bottom-up fashion by different methods. The long-established synthesis through polymerization is obtained by crosslinking and was patented in the 1990s by Biovector Therapeutics [311, 312]. Crosslinking results in a gel that is subsequently sheared under high pressure in a homogenizer and ultrafiltrated to obtain MDNPs [311]. Other methods to synthesize MDNPs have recently appeared in the literature and include anti-solvent nanoprecipitation [313], the double emulsion method [314] and nanoencapsulation [315].

Many properties of the MDNPs can be modified at different stages of their synthesis. Modification of the maltodextrin oligomer can be done at the reactive hydroxyl groups that is present on each glucose monomer and facilitates both crosslinking and chemical derivatization [316]. Fluorescent dyes and H_2O_2-activatable molecules can be attached to the hydroxyl groups before synthesis of therapeutic and diagnostic MDNPs [314, 317]. The most used crosslinker for starch-based polymers is epichlorohydrin, which is also employed in the preparation of Sephadex. It produces

a neutral polymeric matrix of maltodextrin that can be acetylated with $POCl_3$ and NaOH for further functionalization such as the incorporation of ionic compounds [316]. The number of points of crosslinking and polymer length define the mesh size [318]. Charge can also be introduced directly into the polymeric matrix of MDNPs during synthesis by changing the type of crosslinker to for instance the cationic glycidyltrimethylammonium chloride or the anionic phosphoryl chloride [311]. Post-synthesis, the MDNPs can be modified in many ways, such as through the incorporation of lipids which gives the NPs amphiphilic properties that allow for the loading of both hydrophilic and hydrophobic drugs and improved cellular uptake [312, 319].

MDNPs seem good drug delivery devices as they have high biocompatibility. Maltodextrins are biodegradable polysaccharides and a nutritious source of carbohydrates, and depending on the type of crosslinker used, the MDNPs can be disassembled by enzymatic hydrolysis of the crosslinking bonds [316]. MDNPs have an extremely good stability during storage (> 12 months) [320] and can be sterilized by filtration through a 0.22 µm filter [316]. Cationic MDNPs with lipids incorporated into their core behave as stealth NPs that do not induce complement activation in an *in vitro* test of the hemolytic activity of human serum [279]. The same MDNPs were shown to have no cytotoxicity or ROS induction *in vitro* and good *in vivo* tolerability, since no genotoxicity was seen in rats after nasal administration, even at 1000 fold the expected human dose [321]. These NPs have been shown to enter airway epithelial cells by clathrin-dependent endocytosis and are exocytosed in a cholesterol-dependent manner [322]. Both neutral and cationic MDNPs were shown to transcytose across a cellular model of the BBB and could thus deliver drugs to the brain after intravenous injection [323].

The potential of MDNPs to deliver therapeutic proteins has been demonstrated in several preclinical studies. First of all, MDNPs behave as sponges and can absorb large amount of protein without drastic changes in their physicochemical properties [279]. Just by gently mixing the MDNPs with the protein of interest, a high yield of loading is obtained post-synthesis [320]. MDNPs loaded with ovalbumin, a model

protein drug, are taken up by different types of mucosal cells, to at least twice the extent of uptake compared to PLGA NPs or liposomes [324]. Also, more complex mixtures of proteins, such as heterogenous antigens from a parasite, have been loaded in MDNPs and delivered to a bronchial epithelial cell line [325]. This MDNPs-mediated delivery of parasitic antigens shows promising effect as vaccine against the infection in a mouse model [325]. MDNPs loaded with interleukin-2, an immunostimulating protein with therapeutic potential in cancer, infections, and immunodeficiency, have been shown to stabilize and enhance the proliferative activity of interleukin-2 and facilitate its uptake by B-cells [326].

2. Aims

The overall aim of this work was to improve the treatment of diseases where TH function is lacking or impaired. TH itself is a potential therapeutic protein in ERT for TH deficiencies, but its intrinsic instability makes its study and pharmacological development difficult. The main goal of this work has therefore been to investigate how NPs can stabilize and eventually deliver TH intracellularly. For this, it was necessary to identify key factors that determine the stabilization of TH and how these can be improved for technological and therapeutic applications. The work was divided in subprojects with the following specific objectives:

1. Obtain a recombinantly expressed and purified human TH that is stable and functional, and find structure-stability determinants of TH.

2. Develop catalytic NPs showing high TH activity, low proteolytic susceptibility, and low toxicity, by investigating NPs for TH binding, stabilization, and functional delivery.

3. *In vitro*, *in cellulo* and *in vivo* evaluation of the potential of catalytic nanoparticles for ERT, with therapeutic potential in disorders associated with a reduction of TH activity, such as THD and PD.

3. Summary of results

3.1 Optimization and structural characterization of TH preparation (Paper I)

Prior to this work, our lab had expressed recombinant TH in *E. coli* and purified it by affinity chromatography on Heparin Sepharose for decades, where little had changed in the protocol. There had been some reports on the use of fusion tags in the preparation of TH, which resulted in unspecific cleavage within the N-terminal [327] and low activity [328], which prevented us from transitioning to those expression and purification approaches. We needed a preparation procedure that ensured a large yield of high-quality protein: a homogeneous sample of highly active and conformationally stable TH.

We searched for the best fusion tags and found that the His-tagged ZZ fusion partner improved the stability of TH by increasing the melting temperature with 3 °C. The resulting cobalt-bound and partially inhibited TH gave a protein sample with high conformational stability and an integral N-terminus, which allowed good data acquisition by small angle X-ray scattering (SAXS). Together with molecular dynamics simulations, a SAXS-based modeled solution structure of TH was obtained, which was a fascinating discovery: (i) it showed a twisted out-of-plane orientation of the four catalytic domains in the quaternary structure, (ii) confirmed the proposed dimerization of the regulatory ACT domains, and (iii) revealed an elongated shape positioning one dimer of ACT domains on each side of the equatorial plane, with N-terminal tails protruding from the global core. TH obtained from the fusion protein with His-tagged ZZ, was thus well-suited for structural analysis but unfortunately, it lacked a proper function as it contained Co^{2+} in the active site instead of Fe^{2+}.

For functional studies, we required a TH that was not only homogenous and stable, but also had all the physiologically relevant features, including standard catalytic activity and feed-back inhibition and stabilization by dopamine. We found that the His-tagged maltose binding protein (MBP) fusion partner preserved the greatest catalytic activity, still maintaining a conformational stability rather close to the His-

tagged ZZ-derived Co^{2+}-bound TH and resulted in a well-functioning enzyme: a protein which could be activated by Fe^{2+} and stabilized by regulatory dopamine. We therefore chose the His-tagged MBP-derived TH for all proceeding work.

3.2 Characterization of photoluminescent porous silicon (Paper II)

In Paper II, we have explored the intrinsic photoluminescent properties of porous silicon microparticles in relation to the release of a model protein payload, i.e., bovine serum albumin (BSA). We varied factors such as oxidation time, loading method and release conditions, to find how this influenced the correlation between the luminescence wavelength and intensity, and protein release. We searched for correlations that would be useful with regards to self-reporting of drug delivery, which correlated with release of the payload either linearly, or by a rapid change when most of the payload was released.

Oxidation creates a silicon oxide shell on the pore walls of the silicon matrix delaying the dissolution of the silicon core that is responsible for the luminescence. Besides altering the initial characteristics of the luminescent properties (quantum yield, maximum wavelength, and visual appearance), we also found that oxidation delayed the changes in luminescence that occur during BSA release. The longer the oxidation, the thicker the silicon oxide shell, the more the blue shift and intensity decline was delayed. This result was independent of the loading method and indicates that oxidation time can be used to tune the diminishing of photoluminescent features during release.

How BSA was loaded, influenced how the protein was attached in the pores and therefore also how it was released. The trapping of BSA by local precipitation of magnesium silicate gave the highest mass loading and prevented the burst release that was seen when BSA was loaded through electrostatic adsorption. Since BSA was trapped in the precipitated magnesium silicate, its release was also more closely tied to silicon dissolution and the subsequent decline of photoluminescence. The

magnesium silicate coating delayed not only the BSA release, but also the degradation of the pure silicon matrix and the silicon oxide shell.

When release was studied under accelerated conditions, silicon dissolution was constant throughout release and was not affected by loading method or oxidation time indicating that the silicon oxide shell protects the silicon matrix from degradation by dissolving first. The long-term release study with physiological conditions confirmed this for those samples where BSA was adsorbed electrostatically. However, it also revealed that the magnesium silicate-trapped samples with a thin oxide shell were less stable than those with thicker oxide shells; they dissolved more rapidly and released BSA faster.

For clinical applications, it is necessary that the changes in photoluminescence are easy to check. Therefore, we tested if the loss of photoluminescent intensity could also be captured by a low-cost camera. We demonstrated this and the measurements show the same tendency of decrease as with more precise detection.

We also described how the near-infrared photoluminescence could be tuned by oxidation time and that the preferred loading method is magnesium silicate trapping. Longer oxidations show that the photoluminescence intensity scales with the payload release, resulting in the ability to report a predetermined level. Short oxidation (or adsorption loading) makes the photoluminescence change rapidly indicating the ability to report the end of the functional life of the nanocarrier. We also showed how these changes can be monitored in a clinical setting. Consequently, Paper II shows a proof-of-concept on the use of porous silicon photoluminescent properties to self-report on drug delivery.

3.3 Electrostatic interaction of TH with pSiNPs (Paper III)

With the acquired knowledge on the usefulness of the photoluminescent properties of porous silicon and the numerous reports on protein binding and release from this material, we wanted to investigate the ability of pSiNPs to load and stabilize TH. We

varied the pH to see how this affected loading, the propensity of TH to aggregate, and the catalytic activity of TH.

pH determines the surface charge of proteins as they contain many functional groups that can take up an H^+ ion. Proteins are neutral at their pI and porous silicon is known to adsorb large amounts of protein in the pores when pH is at the pI of the protein that is to be loaded [300]. However, aggregation can happen more easily at a protein pI-value because the lack of charge brings the protein molecules in close proximity, which can induce the formation of intermolecular interactions. At pH 6, which is close to the pI of TH, the size of the pSiNPs coincided with that of the aggregated form of TH and thus prevented us from evaluating if TH was loaded by DLS, which is a customary method in NP loading characterization. On the other hand, at pH 7, where TH is most active, we could observe a size increase in the pSiNPs, indicating that TH binds on the outer surface of the pSiNPs. To evaluate the extend of TH loading in the pores we took TEM images, but also here aggregation posed a challenge for taking good images at pH 6. Thioflavin-T fluorescence, which monitors the extend of cross-β interactions that occur during aggregation, confirmed the larger tendency of TH to aggregate at pH 6 and showed that the pSiNPs accelerated aggregation at both pH 6 and 7.

For ERT it is important that the enzyme retains its catalytic function upon loading into a nanocarrier. We found that TH activity was not significantly decreased by binding to pSiNPs. We also performed calculations of the electrostatic surface potential that revealed a large positive patch in the N-terminal regulatory domains, mainly formed by residues Arg89 to Lys102, that could bind to negatively charged surfaces such as in pSiNPs.

Thus, in this paper we described that TH could be loaded in pSiNPs through electrostatic adsorption. Our results also support that the interaction occurs through the regulatory domain, thereby avoiding structural changes to the catalytic site, as TH activity was not altered significantly by the interaction with pSiNPs. However, as TH propensity to aggregate was increased through the interaction with pSiNPs, additional experiments are necessary to choose the characteristics of the pSiNPs and the

conditions for loading active TH, and realize the potential of these promising and superior NPs with respect to imaging and tracking of cargo release for their use in ERT for TH deficiencies and PD.

3.4 Stabilization of TH in maltodextrin NPs (Paper IV)

In search for a nanocarrier that could both stabilize and deliver TH, we tested a type of polymeric NPs made of cross-linked maltodextrin with and without a lipidic core. The first results were promising, as these NPs could absorb large amount of TH into the porous structure. Preliminary titrations of NPs with increasing TH concentration showed no size increase of the lipid-core maltodextrin NPs while loading TH up to a 2:1 (w/w) ratio indicating that TH absorbed into the flexible porous matrix in a sponge-like fashion. The smaller non-lipid-filled maltodextrin NPs were saturated at lower TH concentration and thus we proceeded with the lipid-core maltodextrin NPs.

The maltodextrin NPs seemed to have several positive effects on the stability of TH. They prevented thermal-induced aggregation, preserved TH activity at 4 °C and kept TH functional with regards to enzymatic activity and amenability to phosphorylation after intracellular delivery to neuroblastoma cells. These favorable results encouraged us to assess the delivery more closely.

The intracellular location of TH after delivery by these NPs was imaged in relation to the plasma membrane, early endosomes, and lysosomes *in cellulo*. Co-localization studies revealed that although not all TH crossed the plasma membrane and some ended up in lysosomes after endosomal uptake, a substantial amount of TH could be found in the cytosol. We also showed that this TH was able to increase the level of L-DOPA produced in the cytosol significantly, which was measured by fluorescent detection through the conversion to dopachrome after cell lysis.

Assessment of *in vivo* delivery to neuronal tissue was done through intracranial injection into mouse brains. We did not observe any direct adverse effects on the mice after the procedure, indicating that the injection of TH-loaded NPs was well tolerated. After sacrifice, the brains were either sliced for imaging or homogenized

for activity assays. We mapped the biodistribution in the whole brain by fluorescent imaging and reported on the diffusion into the neuronal tissue around the injection site with more detailed confocal imaging. We measured the remaining catalytic activity of TH in the mouse brains after *in vivo* delivery and found significantly higher TH activity in brain lysates after injection of TH-loaded NPs. We were surprised to find that also delivery of empty NPs seemed to stimulate TH activity.

All in all, lipid-core maltodextrin NPs seem to be a good choice for maintaining TH stability and delivery of functional TH with the potential therapeutic goal of an ERT for diseases with TH and dopamine deficiency. Consequently, paper IV is a proof-of-concept of how catalytically active TH can be delivered to neuronal cells and tissue by NPs for ERT.

4. General discussion

To investigate if TH-functionalized NPs could have the potential to be developed into an ERT for diseases where dopamine supplement is needed, such as in PD, requires an interdisciplinary approach. Knowledge of the optimal conditions for reproducible production of both stable and active TH and low-cost, scalable, and suitable NPs, as well as the optimization of methods to evaluate the loading and delivery of active TH to the target site, is required. In this PhD project, I have tried to address most aspects of this endeavour and the techniques used spanning from protein chemistry and NP synthesis to biochemical assays, cell biology and animal experiments.

4.1 Conformational and functional stability of TH

Protein aggregation can be disastrous as it prevents not only the proper functioning of the affected protein, but also the viability of the cells containing such aggregates. In some diseases, such as Alzheimer's disease and PD, protein misfolding and aggregation are the hallmarks of pathophysiology. Signs and symptoms of misfolding diseases are often classified into those mainly related to the loss-of-function, where the reduction of correctly folded, functional protein is the cause of the disease, or to the gain-of-function, when the aggregated proteins induce negative effects on other biomolecules and compromise cell viability [329].

For PD, it is still discussed if the formation of inclusion bodies containing large fibrils of protein aggregates is a pathological feature or a cell-protective measure by removing the most damaging smaller oligomeric aggregates [121]. It is of uttermost importance that the enzyme delivered in ERT is conformationally and functionally stable, as in the case of TH, as supplementation with unstable or even misfolded TH, may enhance toxic intracellular protein aggregation [330]. As for any other biologics in the medicinal market, maintaining structural stability of the protein has a large impact on the biotechnological value of such therapeutical products. TH needs to fold correctly during expression and stay in a stable and active conformation during

purification, NP loading, storage, and subsequent delivery. Thus, the recombinant expression and purification of TH were optimized during this PhD project (Paper I).

Recombinant proteins can be fused with a partner protein to improve solubility and yield during expression and purification by cloning both proteins into the same expression vector [331]. Some fusion partners also called tags, are specially designed (ZZ) or used (MBP) to promote folding of the target protein [332, 333], and we therefore selected these partners for TH expression and purification in Paper I. We positioned the fusion tag at the N-terminal of TH, instead of the C-terminal, as it has several advantages: (i) the fusion tag is translated before the TH fusion partner, and thereby promotes folding from the moment TH gets expressed; (ii) it prevents proteolytic degradation of the flexible N-terminal of TH, and (iii) ensures a location at the outer surface of the homo-tetramer of TH, without interfering with the tetramerization domain at the C-terminus (Fig. 3). The cleavage site determines which protease can remove the fusion tag and we selected the tobacco etch virus (TEV) protease cleavage site (Paper I) to minimize unspecific cleavage that can occur at the disordered N-terminal of TH [327], to ensure a pure sample of full-length protein.

The optimized purification of TH was of great importance as the structure of the full-length enzyme has been a long-awaited milestone in the field, and the improved homogeneity and stability of purified TH allowed us to determine the solution structure of TH by SAXS (Paper I), which is a powerful method in structural biology. SAXS does not give the exact position of each amino acid, which is provided by X-ray crystallography or NMR, but is a low-resolution method providing the size and shape of the protein. However, in combination with modelling techniques [334], it can be used to obtain reliable and useful structural models [335]. For instance, the TH model presented in Paper I has guided the predicted orientation of membrane-bound TH [79]. Earlier investigations of TH binding to lipid bilayers [26] did not have such a model available and had to rely on proteolyzed structures, predictive methods and circular dichroism to give the extent of α-helices and β-sheets in the secondary structure and identify interaction regions in TH. Another approach to deal with the

lacking full-length structure, is to work with the N-terminal peptide of TH [21], which provides information on interactions between specific amino acids of the flexible tail of TH and the lipid surface, but not in relation to the other protein domains. The full-length structure of TH obtained by SAXS complemented by molecular modeling (Paper I), also allowed the prediction of the residues on the outer surface of TH that attached to the surface of porous silicon characterized in Paper II, locating them to a positively charged patch of the regulatory domain (Paper III).

The position of the regulatory ACT domains in our SAXS-derived TH structure from Paper I, stands in contrast with the crystal structure of full-length human PAH which was found to have monomeric ACT domains [69]. A monomeric positioning of these domains was proposed in a later solution structure also derived by SAXS [336]. However, recent cryo-EM studies performed in collaboration with José Maria Valpuesta in Madrid have unequivocally confirmed the dimerization of the ACT regulatory domains in TH, both without and with dopamine bound, and the elongated form of tetrameric TH (Fig. 7) [64].

Enzymatic activity depends on the structural conformation of the enzyme, the influx of substrates and cofactors, and outflux of products from the active site. Upon binding to NPs, the active site can be altered or sterically hidden, resulting in a reduced enzyme activity compared to that of the free enzyme in solution, especially if the enzyme is loaded inside the NPs [337] or if the orientation is not specifically modulated [338]. However, NP-loading can also have advantageous effects on enzyme activity as such immobilization can increase enzyme reusability and improve thermal and storage stability [339, 340].

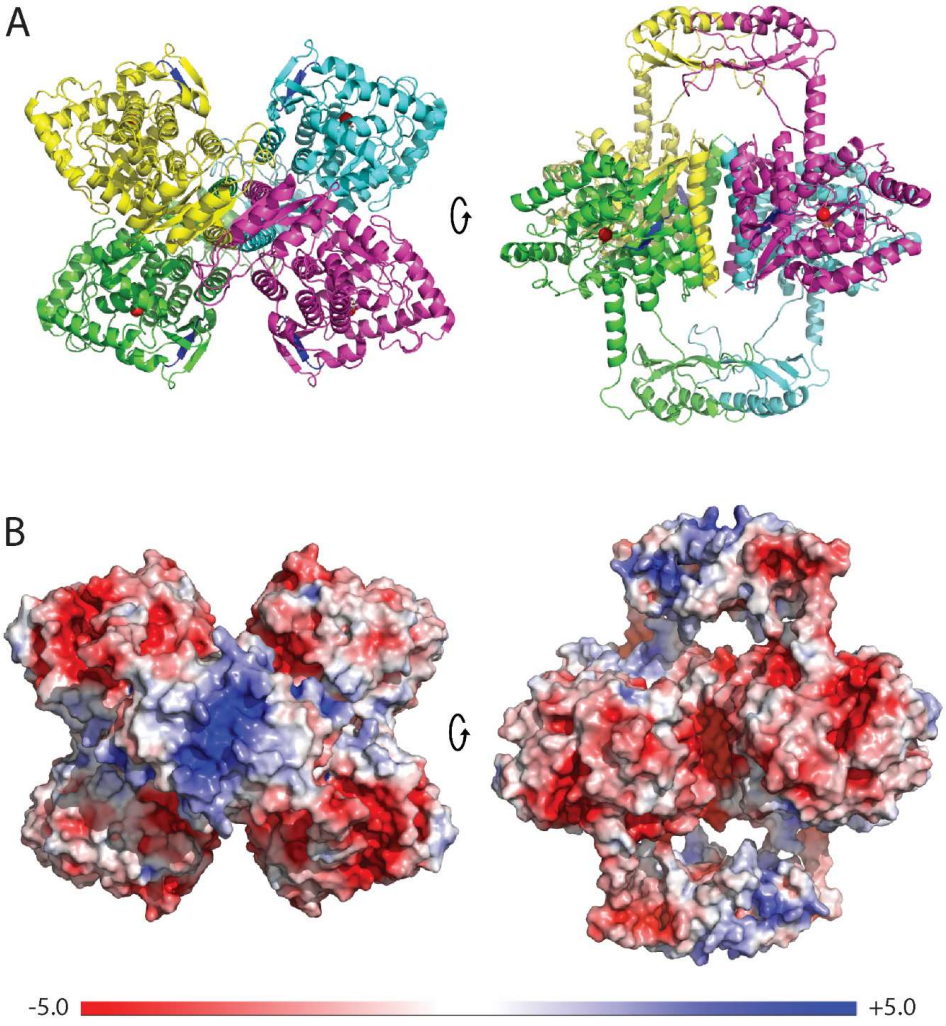

Figure 7: Structure of full-length TH in complex with dopamine. A) Ribbon representation of the structure of TH (colored by monomer with iron atom in red and dopamine in light grey and Ser429-Ser434 in dark blue) derived by cryo-EM with PDB ID 6ZVP [64]. B) Surface electrostatic potential of TH (PDB ID 6ZVP) calculated with the APBS Electrostatics plugin in PyMOL (Schrödinger LLC, version 2.3.4).

We have therefore monitored TH activity in different stages of this PhD project, which required the use of several L-DOPA measurement methods according to the type of sample. For *in vitro* assays of purified protein (Paper I, III and IV), activity measurements were based on quantification of L-DOPA by HPLC and fluorometric detection, a non-hazardous method based on the native fluorescence of L-DOPA

[341]. TH-binding to both pSiNPs and MDNPs did not significantly reduce the enzymatic activity of TH (Paper III and IV). HPLC-detection requires rather clean samples to prevent clogging in the chromatography column and is therefore not well suited for cell and tissue extracts. TH activity in neuronal cell lysates and crude extracts of mouse brain homogenates (Paper IV) was measured with a radioactive assay using tritium-labelled L-Tyr as substrate, where tritium, upon the conversion of L-Tyr to L-DOPA, is left in the water as a by-product of the reaction [342]. This method allowed precise detection in the picomolar range by a scintillator, showing a significant increase in TH activity in neuronal cell lysates and in brain homogenates upon treatments with TH-loaded MDNPs (Paper IV). Furthermore, the determination of intracellular accumulation of L-Dopa requires the inhibition of DDC, by benserazide and 3-hydroxybenzylhydrazine, and the measurement of intracellular TH activity by quantification of L-DOPA through oxidization to the chromophore dopachrome, which can be measured by fluorescence detection [343]. In this way, we were able to show significantly higher TH activity in cells treated with TH-loaded MDNPs compared to untreated cells (Paper IV).

4.2 TH in a pharmaceutical perspective

One could ask why we in the vision of developing an ERT, chose to use the human isoform 1 of TH, which is such a large, unstable protein with complex regulation instead of e.g., truncated forms just including the catalytic domain. In fact, isoform 1 is the most extensively studied isoform since it is homologous to TH from other mammals, such as rat, mouse and bovine, which express only one isoform [74]. It is also one of the most abundant isoforms in the brain [77] and the isoform that undergoes major loss in PD [76] and therefore is in the largest need of therapeutic replacement in PD. In addition, our lab has a well-established production of recombinant hTH1 and long-standing experience with its characterization and stabilization [59, 90-92, 344]. The use of full-length TH for ERT will prevent unregulated production of dopamine as a complete regulatory domain ensures feedback inhibition to avoid its over-production [64]. This is of uttermost importance

as an excess of dopamine in the cytoplasm, especially when not transported into vesicles, will lead to an increase of oxidative metabolites in the cytoplasm, which has been found to be one of the factors contributing to the neuronal cell death seen in PD [345].

Moreover, other enzymes with tyrosine hydroxylation abilities do exist: tyrosinases from a range of organisms that differ greatly in structure [346-348], and bacterial mono-oxygenases [349] can hydroxylate L-Tyr to form L-DOPA. The diverse class of tyrosinases also includes certain cytochrome P450 enzymes which are involved in the synthesis of betalain pigments in beets and other vegetative species [350]. The bacterial mono-oxygenases have a natural substrate selectivity for hydroxyphenylacetate [351], but can be genetically engineered in *E. coli* for L-DOPA production [352-355]. These enzymes are definitive worth considering as an alternative to TH, as many of them show better stability and activity than any human isoform of TH in its native form. However, they differ greatly from TH in both structure and catalytic mechanism, which implies that they work in different environments, with different cofactors, and that their activity is not regulated by the same mechanisms as for TH. Both tyrosinases and bacterial mono-oxygenases can hydroxylate a range of substrates, which increases the likelihood for off-target effects. In addition, substituting the lack of TH with a completely different enzyme, poses new challenges. For instance, biologics from microbial, plant or animal sources can give undesired immunological responses, as observed with pegvaliase (Palynziq®) for PKU [356].

There are many strategies for improved performance of TH to obtain high catalytic activity and stability, which might be a better option than investigating other enzymes. The search for pharmacological chaperones has shown that certain small molecules have a stabilizing effect on TH upon binding [90, 91]. The work done to establish a whole-cell lysate catalyst for tyrosine hydroxylation using mouse TH and an endogenous *E. coli* co-factor for bioproduction of the antioxidant hydroxytyrosol, shows the potential of switching cofactor [357]. Other possible strategies to find more stable and/or active mutants include structure-based redesign and directed evolution.

Structure-based redesign of a flavin-dependent mono-oxygenase where amino acids close to the active site were mutated, has shown to successfully enhance the substrate specificity for L-Tyr [355]. Directed evolution of the TEV protease was done by applying random mutagenesis to its gene with error-prone PCR, and subsequent screening of the mutants resulted in a top performing protease [358]. These strategies can be applied to hTH1 to find an optimized tyrosine-hydroxylating catalyst for the development of an ERT.

The aim of an ERT with a TH enzyme is ambitious, since it is not sufficient to metabolize L-Tyr, but also necessary to synthesize L-DOPA and/or dopamine. In the metabolic disorders where enzyme therapies exist, such as LSDs and PKU, the supplemented enzymes remove the accumulated metabolites [196, 197, 359], whereas for PD and THD, this would not be sufficient, as it is the lack of L-DOPA and subsequent low levels of dopamine which cause the symptoms. Although there are attempts of protein therapy reported for PD [360-362], this current PhD project is to our knowledge, the first investigation on the initial steps to develop an ERT with TH for PD and other related disorders with dopamine deficiency.

4.3 Enzyme replacement therapy for Parkinson's disease

It is difficult to find a curative therapy for PD without a complete understanding of its etiology. Most current treatments are symptomatic and focus on the dopaminergic system, but some of the treatments in the pipeline aim at halting or reversing the neurodegeneration in PD. A potential ERT for PD adds to the list of symptomatic treatments, although hopefully it works in a more sustainable manner. I will discuss the advantages and disadvantages of ERT in comparison with some of the other treatment options below.

The most effective drug against PD is levodopa – an oral supplement of L-DOPA that can enter the human brain where it is converted into dopamine. However, debilitating complications, such as levodopa-induced-dyskinesia, are experienced by almost all patients on long-term levodopa treatment [363]. They are, at least partly, caused by disturbance of the natural variation of dopamine concentration in the brain, which

come from fluctuations in blood level of L-DOPA due to oral dosage. ERT with TH can bypass this problem by providing more stable plasma L-DOPA levels, as L-DOPA can be produced continuously by TH, as long as TH is active and L-Tyr available. TH could be administered by intravenous injection, which is done weekly or biweekly for most existing ERTs [364]. However, it is more beneficial to replace TH at its target site: the nerve terminals of the nigrostriatal neurons since this will ensure local supply of L-DOPA to restore dopamine levels in the brain. TH replacement in the brain also avoids the side effects associated with the peripheral degradation of L-DOPA, which also occur with oral levodopa therapy and is related to the fact that only a small fraction (<5%) of levodopa enters the brain through the BBB [365].

ERT to the brain requires a formulation of TH suited for transport into neuronal tissue and a route of administration that ensures brain location, which is why we have studied different NPs as carriers of TH in Paper III and IV (see next section for detailed comparison). Regular intravenous injections are also a larger burden for the patient and society than oral treatment, such as with levodopa therapy. Direct administration of ERT to the brain by intraparenchymal, intraventricular, intracisternal or intrathecal injection, is being investigated for delivery to the CNS [364]. A formulation of idursulfase that has been injected through an intrathecal catheter in monkeys for distribution through the cerebrospinal fluid and potential treatment of Hunter syndrome, showed good clinical effect in CNS tissues [366]. We performed a preliminary characterization of the biodistribution of TH in neuronal cells and tissue after direct administration by an injection that can be classified as intraparenchymal (Paper IV). Direct administration to the brain poses more risks and a higher treatment burden than intravenous injections, but not as high as other advanced treatments that require surgery to the brain, such as DBS and cell transplantation. If direct administration is necessary, reducing the number of injections would be beneficial for both risk minimization and treatment burden, which is why we suggest that a further improvement of ERT could include brain-implantable biodegradable hydrogels containing NPs with TH (Paper III and IV) and consider intraparenchymal injections a research tool for the initial proof-of-concept.

Several gene therapies are being developed for the treatment of PD, which address different aspects of the disease. Some include the *TH* gene [159-161], whereas others include genes important for α-syn clearance or neuroprotection [367, 368] [154]. Initial studies on a rat model of PD showed that the *TH* gene delivered by targeted liposomes after intravenous injection, normalized striatal TH activity [159, 369]. *TH* is included in two viral vectors that aim to replace dopamine levels locally with one single intervention [160, 161]. Delivery of *TH* and the gene for GTPCH1, *GCH1*, by an adeno-associated viral vector, reversed motor impairments in a preclinical primate model of PD [160]. Injection of ProSavin, a lentiviral vector containing *TH*, *GCH1* and *DDC*, resulted in improvement in motor behavior in early clinical trials with 15 PD patients [161]. Gene therapy and ERT will both have the best therapeutic effect with direct administration to the brain and benefit from technological advances in intracerebral drug delivery, such as the improvements in convection-enhanced infusion cannulas [370, 371]. Gene therapy and ERT vary in the required amount of therapeutical material that needs to be delivered. Only small amounts of gene delivered to cells for gene expression, will result in sufficient dopamine production, whereas delivery of TH protein by ERT requires larger amounts and might need multiple administrations. On the other hand, TH protein is ready for catalysis and can produce L-DOPA on site, also without cellular uptake, whereas gene therapy requires delivery to the nucleus of the host cells and depending on the type of vector, also subsequent integration of TH into the host genome [372], before TH is expressed and active.

Both vector-mediated gene therapy and ERT address only the loss-of-function, but often there is also a certain toxic gain-of-function due to aggregation of mutant protein. In PKU, the R261Q mutant of PAH has been found in amyloid-like aggregates in hepatic tissue in a knock-in mouse model showing traits such as altered lipid metabolism and oxidative stress, which provides a possible explanation of comorbid conditions that are not related to hyperphenylalaninemia [373]. Ideally, gene therapy should not only provide the non-mutated gene, but rather correct the mutated gene and disease phenotype, which has actually been achieved in a mouse

model of PKU with genome editing tools [374]. This seems a potential strategy to correct monogenetic disorders such as THD, but not for PD.

TH also plays a central role in attempts of cell transplantation that aim to restore the degenerated dopaminergic neurons in PD. TH is integrated in the development of cell replacement therapies through differentiation of embryonic cells into dopaminergic neurons that express TH or through transfection of the *TH* gene in cells prior to implantation into rat models of PD [157, 162, 163]. Cell transplantation requires surgical implantation of grafts with a large enough number of viable cells. *Post mortem* analysis of a patient brain 24 years after transplantation of embryonic cells shows that the grafted cells have continued to stain positive for TH and ensured an extensive reinnervation of the striatum [157]. In contrast to ERT, it is challenging to obtain sufficient therapeutic material. For instance, 87 out of 128 planned surgeries in a recent clinical trial with fetal dopamine cells, were canceled due to tissue supply [375]. At least three fetuses are needed for one unilateral surgery, and these cannot be stored longer than four days after dissection [375]. These practical challenges, together with the variability between samples, the large percentage of grafted cells that are not dopaminergic cells, and ethical concerns, militate for the use of stem cells in cell replacement [156]. Improvements in stem cell technology that allows induction of pluripotency in human fibroblasts [376], have led to the first implantation of patient-derived stem cells without the need for immunosuppression [377]. However, new challenges arise, as implanted stem cells should not be tumorigenic [156]. Cell transplantation poses also larger risks than ERT, as the grafting surgery must not lead to an infection, nor should the implanted cells be rejected. Although grafted cells can successfully integrate into the nigrostriatal circuit, degeneration continues to proceed, Lewy bodies eventually spread to the grafted cells and the dopaminergic graft loses its efficacy [157]. In that regard, cell replacement therapies are not a real cure for PD, but can, just like ERT, provide long-lasting symptomatic relief.

4.4 TH-loaded NPs as biovectors in ERT

For NPs to work as vectors for the delivery of TH as ERT for PD as envisioned in this thesis, the NPs need to be biocompatible, show good loading, preserve high catalytic activity, and efficiently deliver TH so that L-DOPA production in the dopaminergic nerve terminals of the striatum is enhanced. Delivery would in many therapeutic settings include both the administration, transport, and release of a drug. However, the concept for this thesis is that the TH-loaded NPs work as small L-DOPA factories, also called nanoreactors, which provide continued protection and stabilization of TH at the target site and thereby increase the functional lifetime of TH In the following paragraphs, I will compare the pSiNPs and MDNPs to each other and to other NPs with regards to TH loading, delivery and catalytic activity, as well as further modifications to reach their potential in ERT.

The loading of TH into pSiNPs and MDNPs was done post-synthesis by gentle mixing and incubation in a buffered solution containing TH and NPs. Loading occurred as physical adsorption dominated by electrostatic interaction in both pSiNPs and MDNPs. The interactions were predominantly between the positively charged patch in the regulatory domain of TH and the negatively charged surface of the pSiNPs (Paper III), whereas it is the overall negative charge of TH that ensures the adsorption of TH into the internal mesh of positively charged crosslinked polymer until a point of saturation, after which TH coated the surface and increased the hydrodynamic diameter of the MDNPs (Paper IV). The differences in loading can be partly explained by the properties and porous structure of the NPs material. The MDNPs are composed of flexible polymeric chains crosslinked into a mesh of unknown and probably dynamic pore sizes into which TH can diffuse freely and penetrate deep, whereas the pSiNPs are rigid with pores of average diameter of 12 nm [286], where it not clear if and how far TH can penetrate. Porous silicon microparticles can easily have pores of 60 nm [302] or 100 nm for porous silicon films [282]. pSiNPs can also be synthesized with larger pore size by increasing current density during the etch, but larger pores increase the overall porosity, which makes the pSiNPs more fragile resulting in a broadening of the size distribution [286]

which again might alter the biodistribution. In microparticles, the loading efficiency of BSA was much larger (20% instead of 3%) when the pore size was 20 nm instead of 10 nm (Paper II), but TH is about twice the size of dimeric BSA. To determine how large the pores need to be for good penetration of TH, the optical thickness of a porous silicon film can be monitored to see the extent of loading into the porous layer as has been done for the monoclonal antibody Bevacizumab (Avastin®) [305], BSA [300] and lysozyme during the initial characterization of porous silicon in this doctoral work (not published).

The oriented binding of TH onto pSiNPs preserved TH activity but unfortunately also promoted aggregation (Paper III). Similar aggregation of TH was seen after binding to negatively charged lipid bilayers and was proposed to be mediated through a motif included in a surface-exposed β-strand in the catalytic domain containing the residues Ser429 to Ser434 (Fig. 7A) [79]. In MDNPs, the TH orientation was not studied, and it may probably be random. The MDNPs prevented or delayed TH aggregation and significantly increased the TH activity after cellular uptake (Paper IV). Although the TH-loaded MDNPs were not tested for remaining activity for as long as for instance tyrosinase in chitosan NPs that retained 75% of its activity after 70 days [378], a 5-day storage at 4 °C did not significantly decrease the TH activity of TH-loaded MDNPs *in vitro* (Paper IV). We found this sufficient to proceed with testing of delivery in a biological setting.

There exist several animal models of PD where the symptomatic features of the disease are induced by the neurotoxin MPTP or by transgenic overexpression of α-synuclein [379]. However, such models deserve treatment options that are approaching clinical investigations. This project is at a more preliminary stage and the mice were used to evaluate the local distribution of the loaded NPs and confirm functional delivery. The mice were therefore wild-type black-6 mice. As an initial proof-of-concept of delivery into living neurons, we injected the TH-loaded MDNPs intraparenchymal. This allowed us to evaluate the physiological response and the biodistribution of TH delivered to neuronal tissue. TH-loaded MDNPs locally injected into mouse brains diffused into the surrounding neuronal tissue and

maintained TH activity when measured in lysates afterwards (Paper IV). Local injection of enzyme-loaded NPs is exploited as initial proof-of-concept in preclinical work on other enzyme deficiencies, such as proven for instance for the intra-articular administration of uricase-encapsulated NPs for the removal of uric acid in ankle joints in a murine gout model [380]. Other studies use intraperitoneal [381] or intravenous [382] injections of enzyme-loaded NPs and evaluate therapeutic efficacy in mouse models of diseases where the enzyme needs to reach the brain through the BBB. Although NPs are extensively explored for the delivery of biologics, only the so-called "single enzyme NPs" which are enzymes conjugated to a polymer or targeting moiety, are ERTs that have been FDA-approved [383], so there is not yet any ERT to learn from, that targets the brain and is in clinical use.

Several routes of administration in ERT have been discussed above (section 4.3), but the use of NPs as drug carriers opens for consideration of other routes as well, among which the direct nose-brain pathway is a promising one. Intranasal application of L-DOPA [384] or dopamine [385] alleviate symptoms in rat models of PD. Neuromelanin-inspired polymeric NPs efficiently delivered dopamine to the striatum after nasal administration and attenuated motor alterations in a rat model of PD [386]. The MDNPs have already been given intranasally to mice for delivery of influenza or toxoplasmosis antigens for vaccine development [387, 388]. It would therefore be interesting to test if the MDNPs could deliver TH through the nose-brain pathway after intranasal administration.

The concept of considering TH-loaded NPs as nanoreactors is not unique to this project. Similarly, uricase is encapsulated in a membrane-coated metal-organic framework [380] and thymidine phosphorylase in triblock polymeric NPs [337] which are both investigated for enzyme therapy without intended release of the enzyme. This approach requires that substrates and products diffuse freely through the porous material of the NPs. Since L-Tyr and L-DOPA are much smaller than TH, it can be assumed that they can diffuse freely in the porous matrix of pSiNPs and MDNPs. However, further functionalization might include a coating around the TH-loaded NPs, thus L-Tyr and L-DOPA must also penetrate such a coating.

Permeabilization of a coating can also be achieved through incorporation of a biological pore, as has been done with a nucleotide porin in the triblock polymer that forms a spherical bilayer around thymidine phosphorylase [337]. A major advantage of a coating is that it provides a barrier against proteases, as shown by a 2 h incubation with trypsin that did degrade free uricase but not the membrane-coated encapsulated uricase [380].

Altogether, TH loading into NPs was easier in MDNPs than in pSiNPs, which is why the pSiNPs have not been tested in any biological system yet. Further optimization of the loading in pSiNPs is needed to ensure infiltration of TH into the pores and avoid aggregation of TH. The intrinsic photoluminescence of porous silicon is however an advantage for visualization experiments in cells and animals. The functional delivery of TH by MDNPs was demonstrated in neuronal cells and tissue and serves as a proof-of-concept for ERT which is worth exploiting further.

5. Conclusions

In this thesis, we have investigated how TH could be pharmacologically developed into a potential biological drug. We have developed two different types of catalytic NPs and tested their stability, catalytic activity, and delivery of TH to cell and mouse brain, to evaluate their therapeutic potential as ERT for diseases where TH is deficient.

The inherent unstable nature of TH inquired detailed analysis of the structure-stability determinants. We tested various fusion tags in the purification of TH, which resulted in a stable enzyme preparation that allowed the determination of the full-length solution structure, aiding further investigations of TH stability and molecular interactions with NPs.

The first type of NPs was made of porous silicon, which has an intrinsic photoluminescence that allows tracking and imaging simultaneous to drug delivery. We found that this photoluminescence can be tuned to correlate with the release of a model protein and thereby work as a self-reporting drug delivery device. Furthermore, loading of TH into these inorganic pSiNPs occurred through electrostatic interactions orienting TH with its regulatory domain onto the oxidized silicon surface and preserving TH activity. However, the interactions with these NPs also promoted TH aggregation, preventing further studies.

The second type of NPs, the polymeric MDNPs absorbed large amounts of TH while preserving its activity and preventing or delaying its aggregation. These NPs delivered functional TH to neuronal cells and tissue and thereby significantly increased the intracellular TH activity. The TH-loaded MDNPs are ready to be functionalized with targeting molecules and tested with different routes of administration in relevant mouse models to evaluate their therapeutic effect as ERT for TH deficiencies.

Overall, this thesis has shown that recombinantly expressed and purified TH can be loaded into NPs and delivered functionally to neuronal cells and tissue. Detailed

analysis of its structure and stability has given insights into the mechanisms necessary to obtain and improve loading in NPs for therapeutic applications.

6. Future perspectives

All aspects of the envisioned ERT with TH-loaded NPs could benefit from improvements. First, further optimization by structure-based redesign, or directed evolution to find mutants of TH with higher stability and activity, may improve the formulation of therapeutic TH. Second, the stability of TH may also be increased by supplementation with pharmacological chaperones. Lastly, the efficacy of an ERT with TH-loaded NPs highly depends on the drug delivery properties of the NPs and the route of administration. Both can be improved and tailored to the needs of TH and the patients intended to treat.

When it comes to the pSiNPs, it is foremost that the loading must be further optimized. A first step would be to find out which pore size is necessary to improve the loading of TH by monitoring the optical thickness of porous silicon films to determine the infiltration. Subsequently, we could test if pSiNPs with such larger pore sizes can be synthesized or if they become too fragile with increased porosity. With optimized pore size, the pSiNPs can be tested for TH loading including an evaluation of its aggregation.

The MDNPs could be functionalized for delivery across the BBB after intravenous injection or through the nasal pathway. Both directions are worth exploring as they open for two non-invasive routes of administering TH-bound NPs. To enhance crossing of the BBB, the NPs can be decorated on their surface with various molecules targeting receptors that are highly expressed at the BBB, such as the transferrin or the insulin receptor, to increase the receptor-mediated transcytosis [389]. Although the MDNPs have been tested without further functionalization for nasal delivery [387], it would be necessary to test in animal models if they can get transported along the olfactory nerves to the brain as can dopamine-loaded chitosan NPs [390]. Alternatively, the MDNPs could be functionalized for delivery through the cerebrospinal fluid after intrathecal administration, which is a very effective, but more invasive route. If adequate TH-bound NPs are obtained, the functionalization and route of administration can be evaluated by testing TH delivery with these

functionalized MDNPs in a disease-relevant mouse model. This can be done in the knock-in mouse of THD with the mutation *Th-R203H*, associated with a severe THD phenotype in humans [94], or in the mouse model of PD induced by the neurotoxin 1-methyl-4-phenyl-1,2,3,6-tetrahydropyridine [391].

Other NPs both inorganic, lipid-based, polymeric and hybrid types, may be tested for suitability to deliver large biologics such as TH. Among the promising candidates are for instance the inorganic cerium oxide NPs that have shown to have antioxidant and antiapoptotic effects by themselves in a rat model of PD [392] and the nanostructured lipid carriers that have delivered a growth factor to the brain after intranasal administration [393]. There are also many promising polymeric NPs, such as the hyaluronate NPs that have been shown to cross the BBB with a neuroprotective protein after intravenous injection in rats [394], and the poly(lactic-co-glycolic acid) NPs conjugated with PEG and a lectin, that enhanced brain uptake of a therapeutic peptide after intranasal delivery [395]. At last, improvements in the encapsulation in metal organic frameworks by gentler methods that are better suited for biologics, indicate the potential of this hybrid material for protein drug delivery to the brain [396].

Finally, the increased knowledge of the determinants for the structural stability of TH obtained through the work of this PhD thesis provides the possibility to study the interaction between TH and NP surfaces by molecular dynamics simulations and docking. These virtual methods could provide further insight into the factors modulating the catalytic and structural stability of TH and guide the development of a more stable form of highly active TH, as well as the optimal NPs for TH loading and delivery.

Bibliography

1. Nagatsu, T., M. Levitt, and S. Udenfriend, *Tyrosine Hydroxylase. The Initial Step in Norepinephrine Biosynthesis.* J Biol Chem, 1964. **239**: p. 2910-7.

2. Fitzpatrick, P.F., *The metal requirement of rat tyrosine hydroxylase.* Biochemical and Biophysical Research Communications, 1989. **161**(1): p. 211-215.

3. Numata, Y., et al., *Effects of stereochemical structures of tetrahydropterins on tyrosine hydroxylase.* Biochemical Pharmacology, 1975. **24**(21): p. 1998-2000.

4. Bergquist, J., et al., *Catecholamines and methods for their identification and quantitation in biological tissues and fluids.* Journal of Neuroscience Methods, 2002. **113**(1): p. 1-13.

5. Peaston, R.T. and C. Weinkove, *Measurement of catecholamines and their metabolites.* Annals of Clinical Biochemistry, 2004. **41**(1): p. 17-38.

6. Zouhal, H., et al., *Catecholamines and the Effects of Exercise, Training and Gender.* Sports Medicine, 2008. **38**(5): p. 401-423.

7. Kobayashi, K., et al., *Targeted Disruption of the Tyrosine Hydroxylase Locus Results in Severe Catecholamine Depletion and Perinatal Lethality in Mice.* Journal of Biological Chemistry, 1995. **270**(45): p. 27235-27243.

8. Zhou, Q.Y., C.J. Quaife, and R.D. Palmiter, *Targeted disruption of the tyrosine hydroxylase gene reveals that catecholamines are required for mouse fetal development.* Nature, 1995. **374**(6523): p. 640-643.

9. Pickel, V.M., et al., *Cellular localization of Tyrosine Hydroxylase by immunohistochemistry.* The Journal of histochemistry and cytohistochemistry, 1975. **23**(1): p. 1-12.

10. Huang, M.H., et al., *Neuroendocrine properties of intrinsic cardiac adrenergic cells in fetal rat heart.* Am J Physiol Heart Circ Physiol, 2005. **288**(2): p. H497-503.

11. Witkovsky, P., et al., *Influence of light and neural circuitry on tyrosine hydroxylase phosphorylation in the rat retina.* Journal of Chemical Neuroanatomy, 2000. **19**(2): p. 105-116.

12. Zhou, M., H. Hank Simms, and P. Wang, *Increased gut-derived norepinephrine release in sepsis: up-regulation of intestinal tyrosine hydroxylase.* Biochimica et Biophysica Acta (BBA) - Molecular Basis of Disease, 2004. **1689**(3): p. 212-218.

13. White, R.B. and M.G. Thomas, *Moving beyond tyrosine hydroxylase to define dopaminergic neurons for use in cell replacement therapies for Parkinson's disease.* CNS Neurol Disord Drug Targets, 2012. **11**(4): p. 340-9.

14. Weihe, E., et al., *Three Types of Tyrosine Hydroxylase-Positive CNS Neurons Distinguished by Dopa Decarboxylase and VMAT2 Co-Expression.* Cellular and Molecular Neurobiology, 2006. **26**(4-6): p. 657-676.

15. Wurzburger, R.J. and J.M. Musacchio, *Subcellular distribution and aggregation of bovine adrenal tyrosine hydroxylase.* J Pharmacol Exp Ther, 1971. **177**(1): p. 155-68.

16. Nakashima, A., et al., *Phosphorylation of the N-terminal portion of tyrosine hydroxylase triggers proteasomal digestion of the enzyme.* Biochemical and Biophysical Research Communications, 2011. **407**(2): p. 343-347.

17. Jorge-Finnigan, A., et al., *Phosphorylation at serine 31 targets tyrosine hydroxylase to vesicles for transport along microtubules.* J Biol Chem, 2017. **292**(34): p. 14092-14107.

18. Kuczenski, R.T. and A.J. Mandell, *Regulatory Properties of Soluble and Particulate Rat Brain Tyrosine Hydroxylase.* Journal of Biological Chemistry, 1972. **247**(10): p. 3114-3122.

19. McGeer, E.G., P.L. McGeer, and J.A. Wada, *Distribution of tyrosine hydroxylase in human and animal brain.* Journal of Neurochemistry, 1971. **18**(9): p. 1647-1658.

20. Halskau, O., Jr., et al., *Three-way interaction between 14-3-3 proteins, the N-terminal region of tyrosine hydroxylase, and negatively charged membranes.* J Biol Chem, 2009. **284**(47): p. 32758-69.

21. Skjevik, A.A., et al., *The N-terminal sequence of tyrosine hydroxylase is a conformationally versatile motif that binds 14-3-3 proteins and membranes.* J Mol Biol, 2014. **426**(1): p. 150-68.

22. Morita, K., K. Teraoka, and M. Oka, *Interaction of cytoplasmic tyrosine hydroxylase with chromaffin granule. In vitro studies on association of soluble enzyme with granule membranes and alteration in enzyme activity.* Journal of Biological Chemistry, 1987. **262**(12): p. 5654-5658.

23. Nakashima, A., et al., *Proteasome-mediated degradation of tyrosine hydroxylase triggered by its phosphorylation: a new question as to the intracellular location at which the degradation occurs.* Journal of Neural Transmission, 2018. **125**(1): p. 9-15.

24. Daubner, S.C., T. Le, and S. Wang, *Tyrosine hydroxylase and regulation of dopamine synthesis.* Arch Biochem Biophys, 2011. **508**(1): p. 1-12.

25. Cartier, E.A., et al., *A Biochemical and Functional Protein Complex Involving Dopamine Synthesis and Transport into Synaptic Vesicles.* Journal of Biological Chemistry, 2010. **285**(3): p. 1957-1966.

26. Thórólfsson, M.a., et al., *The binding of tyrosine hydroxylase to negatively charged lipid bilayers involves the N-terminal region of the enzyme.* FEBS Letters, 2002. **519**(1-3): p. 221-226.

27. Olsson, E., et al., *Substrate Hydroxylation by the Oxido-Iron Intermediate in Aromatic Amino Acid Hydroxylases: A DFT Mechanistic Study.* European Journal of Inorganic Chemistry, 2011. **2011**(17): p. 2720-2732.

28. Werner, E.R., N. Blau, and B. Thöny, *Tetrahydrobiopterin: biochemistry and pathophysiology.* Biochemical Journal, 2011. **438**(3): p. 397-414.

29. Frantom, P.A., et al., *Reduction and Oxidation of the Active Site Iron in Tyrosine Hydroxylase: Kinetics and Specificity.* Biochemistry, 2006. **45**(7): p. 2372-2379.

30. Haavik, J., B. Almås, and T. Flatmark, *Generation of Reactive Oxygen Species by Tyrosine Hydroxylase: A Possible Contribution to the Degeneration of Dopaminergic Neurons?* Journal of Neurochemistry, 1997. **68**(1): p. 328-332.

31. Pong, K., S.R. Doctrow, and M. Baudry, *Prevention of 1-methyl-4-phenylpyridinium- and 6-hydroxydopamine-induced nitration of tyrosine hydroxylase and neurotoxicity by EUK-134, a superoxide dismutase and catalase mimetic, in cultured dopaminergic neurons.* Brain Research, 2000. **881**(2): p. 182-189.

32. Skjaerven, L., K. Teigen, and A. Martinez, *Structure-Function Relationships in the Aromatic Amino Acid Hydroxylases Enzyme Family: Evolutionary Insights*, in *eLS*. 2014.

33. Jung-Klawitter, S. and O. Kuseyri Hubschmann, *Analysis of Catecholamines and Pterins in Inborn Errors of Monoamine Neurotransmitter Metabolism-From Past to Future.* Cells, 2019. **8**(8).

34. Pomerantz, S.H., *Tyrosine hydroxylation catalyzed by mammalian tyrosinase: An improved method of assay.* Biochemical and Biophysical Research Communications, 1964. **16**(2): p. 188-194.

35. Sánchez-Ferrer, Á., et al., *Tyrosinase: a comprehensive review of its mechanism.* Biochimica et Biophysica Acta (BBA) - Protein Structure and Molecular Enzymology, 1995. **1247**(1): p. 1-11.

36. Haavik, J., *l -DOPA Is a Substrate for Tyrosine Hydroxylase.* Journal of Neurochemistry, 1997. **69**(4): p. 1720-1728.

37. Kumer, S.C. and K.E. Vrana, *Intricate Regulation of Tyrosine Hydroxylase Activity and Gene Expression.* Journal of Neurochemistry, 2002. **67**(2): p. 443-462.

38. Tekin, I., et al., *Complex molecular regulation of tyrosine hydroxylase.* J Neural Transm (Vienna), 2014. **121**(12): p. 1451-81.

39. Haycock, J.W., *Phosphorylation of Tyrosine-Hydroxylase Insitu at Serine-8, Serine-19, Serine-31, and Serine-40.* Journal of Biological Chemistry, 1990. **265**(20): p. 11682-11691.

40. Ghorbani, S., et al., *Serine 19 phosphorylation and 14-3-3 binding regulate phosphorylation and dephosphorylation of tyrosine hydroxylase on serine 31 and serine 40.* Journal of Neurochemistry, 2020. **152**(1): p. 29-47.

41. Kleppe, R., et al., *Phosphorylation dependence and stoichiometry of the complex formed by tyrosine hydroxylase and 14-3-3gamma.* Mol Cell Proteomics, 2014. **13**(8): p. 2017-30.

42. Lehmann, I.T., et al., *Differential Regulation of the Human Tyrosine Hydroxylase Isoforms via Hierarchical Phosphorylation.* Journal of Biological Chemistry, 2006. **281**(26): p. 17644-17651.

43. Moy, L.Y. and L.-H. Tsai, *Cyclin-dependent Kinase 5 Phosphorylates Serine 31 of Tyrosine Hydroxylase and Regulates Its Stability.* Journal of Biological Chemistry, 2004. **279**(52): p. 54487-54493.

44. Andersson, K.K., et al., *Purification and characterization of the blue-green rat phaeochromocytoma (PC12) tyrosine hydroxylase with a dopamine-Fe(III) complex. Reversal of the endogenous feedback inhibition by phosphorylation of serine-40.* Biochemical Journal, 1992. **284**(3): p. 687-695.

45. Wang, Y., C.C. Sung, and K.K. Chung, *Novel enhancement mechanism of tyrosine hydroxylase enzymatic activity by nitric oxide through S-nitrosylation.* Sci Rep, 2017. **7**: p. 44154.

46. Kleppe, R., et al., *Modelling cellular signal communication mediated by phosphorylation dependent interaction with 14-3-3 proteins.* FEBS Letters, 2014. **588**(1): p. 92-98.

47. Ichimura, T., et al., *Brain 14-3-3 protein is an activator protein that activates tryptophan 5-monooxygenase and tyrosine 3-monooxygenase in the presence of Ca2+,calmodulin-dependent protein kinase II.* FEBS Letters, 1987. **219**(1): p. 79-82.

48. Obsilova, V., et al., *14-3-3 proteins: a family of versatile molecular regulators.* Physiol Res, 2008. **57 Suppl 3**: p. S11-21.

49. Ghorbani, S., et al., *Regulation of tyrosine hydroxylase is preserved across different homo- and heterodimeric 14-3-3 proteins.* Amino Acids, 2016. **48**(5): p. 1221-9.

50. Nakashima, A., et al., *Identification by nano-LC-MS/MS of NT5DC2 as a protein binding to tyrosine hydroxylase: Down-regulation of NT5DC2 by siRNA increases catecholamine synthesis in PC12D cells.* Biochemical and Biophysical Research Communications, 2019. **516**(4): p. 1060-1065.

51. Ishikawa, S., et al., *Oxidative Status of DJ-1-dependent Activation of Dopamine Synthesis through Interaction of Tyrosine Hydroxylase and 4-Dihydroxy-l-phenylalanine (l-DOPA) Decarboxylase with DJ-1.* Journal of Biological Chemistry, 2009. **284**(42): p. 28832-28844.

52. Zhong, N., et al., *DJ-1 Transcriptionally Up-regulates the Human Tyrosine Hydroxylase by Inhibiting the Sumoylation of Pyrimidine Tract-binding Protein-associated Splicing Factor.* Journal of Biological Chemistry, 2006. **281**(30): p. 20940-20948.

53. Lu, L., et al., *DJ-1 upregulates tyrosine hydroxylase gene expression by activating its transcriptional factor Nurr1 via the ERK1/2 pathway.* The International Journal of Biochemistry & Cell Biology, 2012. **44**(1): p. 65-71.

54. Sulzer, D. and R.H. Edwards, *The physiological role of α-synuclein and its relationship to Parkinson's Disease.* Journal of Neurochemistry, 2019. **150**(5): p. 475-486.

55. Perez, R.G., et al., *A Role for α-Synuclein in the Regulation of Dopamine Biosynthesis.* The Journal of Neuroscience, 2002. **22**(8): p. 3090-3099.

56. Shiman, R., M. Akino, and S. Kaufman, *Solubilization and Partial Purification of Tyrosine Hydroxylase from Bovine Adrenal Medulla.* Journal of Biological Chemistry, 1971. **246**(5): p. 1330-1340.

57. Haavik, J., A. Martinez, and T. Flatmark, *pH-dependent release of catecholamines from tyrosine hydroxylase and the effect of phosphorylation of Ser-40.* FEBS Lett, 1990. **262**(2): p. 363-5.

58. Le Bourdelles, B., et al., *Phosphorylation of human recombinant tyrosine hydroxylase isoforms 1 and 2: an additional phosphorylated residue in isoform 2, generated through alternative splicing.* J Biol Chem, 1991. **266**(26): p. 17124-30.

59. Haavik, J., et al., *Recombinant human tyrosine hydroxylase isozymes. Reconstitution with iron and inhibitory effect of other metal ions.* European Journal of Biochemistry, 1991. **199**(2): p. 371-378.

60. Goodwill, K.E., et al., *Crystal structure of tyrosine hydroxylase at 2.3 A and its implications for inherited neurodegenerative diseases.* Nat Struct Biol, 1997. **4**(7): p. 578-85.

61. Goodwill, K.E., C. Sabatier, and R.C. Stevens, *Crystal structure of tyrosine hydroxylase with bound cofactor analogue and iron at 2.3 A resolution: self-hydroxylation of Phe300 and the pterin-binding site.* Biochemistry, 1998. **37**(39): p. 13437-45.

62. Zhang, S., et al., *The solution structure of the regulatory domain of tyrosine hydroxylase.* J Mol Biol, 2014. **426**(7): p. 1483-97.

63. Grant, G.A., *The ACT Domain: A Small Molecule Binding Domain and Its Role as a Common Regulatory Element.* Journal of Biological Chemistry, 2006. **281**(45): p. 33825-33829.

64. Bueno-Carrasco, M.T., et al., *Structural mechanism for tyrosine hydroxylase inhibition by dopamine and reactivation by Ser40 phosphorylation.* Nature Communications, 2022. **13**(1).

65. Ramsey, A.J., et al., *Identification of iron ligands in tyrosine hydroxylase by mutagenesis of conserved histidinyl residues.* Protein Science, 1995. **4**(10): p. 2082-2086.

66. Teigen, K., et al., *Selectivity and affinity determinants for ligand binding to the aromatic amino acid hydroxylases.* Curr Med Chem, 2007. **14**(4): p. 455-67.

67. Nygaard, G., et al., *Personalized Medicine to Improve Treatment of Dopa-Responsive Dystonia—A Focus on Tyrosine Hydroxylase Deficiency.* Journal of Personalized Medicine, 2021. **11**(11): p. 1186.

68. Counsell, R.E., et al., *Aromatic amino acid hydroxylase inhibitors. I. Halogenated phenylalanines.* Journal of Medicinal Chemistry, 1970. **13**(6): p. 1040-1042.

69. Flydal, M.I., et al., *Structure of full-length human phenylalanine hydroxylase in complex with tetrahydrobiopterin.* Proceedings of the National Academy of Sciences, 2019. **116**(23): p. 11229-11234.

70. Arturo, E.C., et al., *First structure of full-length mammalian phenylalanine hydroxylase reveals the architecture of an autoinhibited tetramer.* Proceedings of the National Academy of Sciences, 2016. **113**(9): p. 2394-2399.

71. Følling, I., *The discovery of phenylketonuria.* Acta Paediatrica, 1994. **83**(s407): p. 4-10.

72. McKinney, J.A., et al., *Functional properties of missense variants of human tryptophan hydroxylase 2.* Human Mutation, 2009. **30**(5): p. 787-794.

73. Le Bourdelles, B., et al., *Analysis of the 5' region of the human tyrosine hydroxylase gene: combinatorial patterns of exon splicing generate multiple regulated tyrosine hydroxylase isoforms.* J Neurochem, 1988. **50**(3): p. 988-91.

74. Haycock, J.W., *Species differences in the expression of multiple tyrosine hydroxylase protein isoforms.* Journal of Neurochemistry, 2002. **81**(5): p. 947-953.

75. O'Malley, K.L., et al., *Isolation and characterization of the human tyrosine hydroxylase gene: identification of 5' alternative splice sites responsible for multiple mRNAs.* Biochemistry, 1987. **26**(22): p. 6910-6914.

76. Shehadeh, J., et al., *Expression of tyrosine hydroxylase isoforms and phosphorylation at serine 40 in the human nigrostriatal system in Parkinson's disease.* Neurobiol Dis, 2019. **130**: p. 104524.

77. Lewis, D.A., D.S. Melchitzky, and J.W. Haycock, *Four isoforms of tyrosine hydroxylase are expressed in human brain.* Neuroscience, 1993. **54**(2): p. 477-492.

78. Urano, F., et al., *Molecular mechanism for pterin-mediated inactivation of tyrosine hydroxylase: formation of insoluble aggregates of tyrosine hydroxylase.* J Biochem, 2006. **139**(4): p. 625-35.

79. Baumann, A., et al., *Tyrosine Hydroxylase Binding to Phospholipid Membranes Prompts Its Amyloid Aggregation and Compromises Bilayer Integrity.* Scientific Reports, 2016. **6**(1): p. 39488.

80. Vigny, A., M.-F. Flamand, and J.-P. Henry, *Bovine adrenal medulla tyrosine hydroxylase: Separation of the native and aggregate forms.* FEBS Letters, 1978. **86**(2): p. 235-238.

81. Nakashima, A., et al., *Deletion of N-terminus of human tyrosine hydroxylase type 1 enhances stability of the enzyme in AtT-20 cells.* Journal of Neuroscience Research, 2005. **81**(1): p. 110-120.

82. Anikster, Y., et al., *Biallelic Mutations in DNAJC12 Cause Hyperphenylalaninemia, Dystonia, and Intellectual Disability.* The American Journal of Human Genetics, 2017. **100**(2): p. 257-266.

83. Gallego, D., et al., *Pathogenic variants of DNAJC12 and evaluation of the encoded cochaperone as a genetic modifier of hyperphenylalaninemia.* Human Mutation, 2020. **41**(7): p. 1329-1338.

84. Døskeland, A.P. and T. Flatmark, *Ubiquitination of soluble and membrane-bound tyrosine hydroxylase and degradation of the soluble form.* European Journal of Biochemistry, 2002. **269**(5): p. 1561-1569.

85. Carbajosa, N.A.L., et al., *Tyrosine Hydroxylase Is Short-Term Regulated by the Ubiquitin-Proteasome System in PC12 Cells and Hypothalamic and Brainstem Neurons from Spontaneously Hypertensive Rats: Possible Implications in Hypertension.* PLOS ONE, 2015. **10**(2): p. e0116597.

86. Kawahata, I. and K. Fukunaga, *Degradation of Tyrosine Hydroxylase by the Ubiquitin-Proteasome System in the Pathogenesis of Parkinson's Disease and Dopa-Responsive Dystonia.* International Journal of Molecular Sciences, 2020. **21**(11): p. 3779.

87. Kawahata, I., et al., *Dopamine or biopterin deficiency potentiates phosphorylation at 40 Ser and ubiquitination of tyrosine hydroxylase to be degraded by the ubiquitin proteasome system.* Biochemical and Biophysical Research Communications, 2015. **465**(1): p. 53-58.

88. Michaud-Soret, I., et al., *Resonance Raman Studies of Catecholate and Phenolate Complexes of Recombinant Human Tyrosine Hydroxylase.* Biochemistry, 1995. **34**(16): p. 5504-5510.

89. Flydal, M.I., et al., *Levalbuterol lowers the feedback inhibition by dopamine and delays misfolding and aggregation in tyrosine hydroxylase.* Biochimie, 2020.

90. Hole, M., et al., *Discovery of compounds that protect tyrosine hydroxylase activity through different mechanisms.* Biochim Biophys Acta, 2015. **1854**(9): p. 1078-89.

91. Calvo, A.C., et al., *Effect of pharmacological chaperones on brain tyrosine hydroxylase and tryptophan hydroxylase 2.* Journal of Neurochemistry, 2010. **114**(3): p. 853-863.

92. Thöny, B., et al., *Tetrahydrobiopterin shows chaperone activity for tyrosine hydroxylase.* Journal of Neurochemistry, 2008. **106**(2): p. 672-681.

93. Willemsen, M.A., et al., *Tyrosine hydroxylase deficiency: a treatable disorder of brain catecholamine biosynthesis.* Brain, 2010. **133**(Pt 6): p. 1810-22.

94. Korner, G., et al., *Brain catecholamine depletion and motor impairment in a Th knock-in mouse with type B tyrosine hydroxylase deficiency.* Brain, 2015. **138**(Pt 10): p. 2948-63.

95. Haavik, J. and K. Toska, *Tyrosine hydroxylase and Parkinson's disease.* Mol Neurobiol, 1998. **16**(3): p. 285-309.

96. Thibaut, F., et al., *Association of DNA polymorphism in the first intron of the tyrosine hydroxylase gene with disturbances of the catecholaminergic system in schizophrenia.* Schizophrenia Research, 1997. **23**(3): p. 259-264.

97. Leboyer, M., et al., *Tyrosine hydroxylase polymorphisms associated with manic-depressive illness.* The Lancet, 1990. **335**(8699): p. 1219.

98. Fu, A.L., et al., *A novel therapeutic approach to depression via supplement with tyrosine hydroxylase.* Biochemical and Biophysical Research Communications, 2006. **351**(1): p. 140-145.

99. Fossbakk, A., et al., *Functional studies of tyrosine hydroxylase missense variants reveal distinct patterns of molecular defects in Dopa-responsive dystonia.* Hum Mutat, 2014. **35**(7): p. 880-90.

100. Chen, Y., et al., *Clinical and Genetic Heterogeneity in a Cohort of Chinese Children With Dopa-Responsive Dystonia.* Frontiers in Pediatrics, 2020. **8**.

101. Jeon, B.S., *Dopa-responsive dystonia: a syndrome of selective nigrostriatal dopaminergic deficiency.* Journal of Korean Medical Science, 1997. **12**(4): p. 269.

102. Segawa, M., et al., *Hereditary progressive dystonia with marked diurnal fluctuation.* Adv Neurol, 1976. **14**: p. 215-33.

103. Ichinose, H., et al., *Hereditary progressive dystonia with marked diurnal fluctuation caused by mutations in the GTP cyclohydrolase I gene.* Nature Genetics, 1994. **8**(3): p. 236-242.

104. Ghebremedhin, E., et al., *Diminished tyrosine hydroxylase immunoreactivity in the cardiac conduction system and myocardium in Parkinson's disease: an anatomical study.* Acta Neuropathol, 2009. **118**(6): p. 777-84.

105. Isaacson, S. and J. Skettini, *Neurogenic orthostatic hypotension in Parkinson's disease: evaluation, management, and emerging role of droxidopa.* Vascular Health and Risk Management, 2014: p. 169.

106. Beach, T.G., et al., *Reduced striatal tyrosine hydroxylase in incidental Lewy body disease.* Acta Neuropathol, 2008. **115**(4): p. 445-51.

107. Ferrer, I., et al., *Neuropathology of sporadic Parkinson disease before the appearance of parkinsonism: preclinical Parkinson disease.* J Neural Transm (Vienna), 2011. **118**(5): p. 821-39.

108. Nakashima, S. and F. Ikuta, *Tyrosine hydroxylase protein in Lewy bodies of parkinsonian and senile brains.* Journal of the Neurological Sciences, 1984. **66**(1): p. 91-96.

109. Kawahata, I., et al., *Accumulation of phosphorylated tyrosine hydroxylase into insoluble protein aggregates by inhibition of an ubiquitin-proteasome system in PC12D cells.* J Neural Transm (Vienna), 2009. **116**(12): p. 1571-8.

110. Salvatore, M.F., E.S. Calipari, and S.R. Jones, *Regulation of Tyrosine Hydroxylase Expression and Phosphorylation in Dopamine Transporter-Deficient Mice.* ACS Chemical Neuroscience, 2016. **7**(7): p. 941-951.

111. Kim, S.J., et al., *Non-cell autonomous modulation of tyrosine hydroxylase by HMGB1 released from astrocytes in an acute MPTP-induced Parkinsonian mouse model.* Laboratory Investigation, 2019. **99**(9): p. 1389-1399.

112. Klune, J.R., et al., *HMGB1: Endogenous Danger Signaling.* Molecular Medicine, 2008. **14**(7-8): p. 476-484.

113. Ong, L.K., et al., *Peripheral inflammation induces long-term changes in tyrosine hydroxylase activation in the substantia nigra.* Neurochemistry International, 2021. **146**: p. 105022.

114. Obeso, J.A., et al., *Past, present, and future of Parkinson's disease: A special essay on the 200th Anniversary of the Shaking Palsy.* Movement Disorders, 2017. **32**(9): p. 1264-1310.

115. Schapira, A.H. and P. Jenner, *Etiology and pathogenesis of Parkinson's disease.* Movement Disorders, 2011. **26**(6): p. 1049-1055.

116. Fahn, S., *Description of Parkinson's disease as a clinical syndrome.* ANNALS-NEW YORK ACADEMY OF SCIENCES, 2003. **991**: p. 1-14.

117. Hughes, A.J., et al., *The accuracy of diagnosis of parkinsonian syndromes in a specialist movement disorder service.* Brain, 2002. **125**(4): p. 861-870.

118. Morales-Briceño, H., et al., *Clinical and neuroimaging phenotypes of genetic parkinsonism from infancy to adolescence.* Brain, 2020. **143**(3): p. 751-770.

119. Shimura, H., et al., *Familial Parkinson disease gene product, parkin, is a ubiquitin-protein ligase.* Nature Genetics, 2000. **25**(3): p. 302-305.

120. Spillantini, M.G., et al., *α-Synuclein in Lewy bodies.* Nature, 1997. **388**(6645): p. 839-840.

121. Kalia, L.V. and S.K. Kalia, *alpha-Synuclein and Lewy pathology in Parkinson's disease.* Curr Opin Neurol, 2015. **28**(4): p. 375-81.

122. Leclair-Visonneau, L., et al., *The gut in Parkinson's disease: Bottom-up, top-down, or neither?* Neurogastroenterology & Motility, 2020. **32**(1).

123. Goedert, M., et al., *100 years of Lewy pathology.* Nat Rev Neurol, 2013. **9**(1): p. 13-24.

124. Farrer, M.J., *Genetics of Parkinson disease: paradigm shifts and future prospects.* Nature Reviews Genetics, 2006. **7**(4): p. 306-318.

125. Ascherio, A. and M.A. Schwarzschild, *The epidemiology of Parkinson's disease: risk factors and prevention.* The Lancet Neurology, 2016. **15**(12): p. 1257-1272.

126. Klein, C., *Implications of Genetics on the Diagnosis and Care of Patients With Parkinson Disease.* Archives of Neurology, 2006. **63**(3): p. 328.

127. Blauwendraat, C., M.A. Nalls, and A.B. Singleton, *The genetic architecture of Parkinson's disease.* The Lancet Neurology, 2020. **19**(2): p. 170-178.

128. Vernier, P., *The Degeneration of Dopamine Neurons in Parkinson's Disease: Insights from Embryology and Evolution of the Mesostriatocortical System.* Annals of the New York Academy of Sciences, 2004. **1035**(1): p. 231-249.

129. Chung, Y.C., S.R. Kim, and B.K. Jin, *Paroxetine Prevents Loss of Nigrostriatal Dopaminergic Neurons by Inhibiting Brain Inflammation and Oxidative Stress in an Experimental Model of Parkinson's Disease.* The Journal of Immunology, 2010. **185**(2): p. 1230-1237.

130. Wei, Z., et al., *Oxidative Stress in Parkinson's Disease: A Systematic Review and Meta-Analysis.* Frontiers in Molecular Neuroscience, 2018. **11**.

131. Henchcliffe, C. and M.F. Beal, *Mitochondrial biology and oxidative stress in Parkinson disease pathogenesis.* Nat Clin Pract Neurol, 2008. **4**(11): p. 600-9.

132. Bubak, A.N., et al., *A Potential Compensatory Role for Endogenous Striatal Tyrosine Hydroxylase-Positive Neurons in a Nonhuman Primate Model of Parkinson's Disease.* Cell Transplantation, 2015. **24**(4): p. 673-680.

133. Engelender, S. and O. Isacson, *The Threshold Theory for Parkinson's Disease.* Trends in Neurosciences, 2017. **40**(1): p. 4-14.

134. Hoehn, M.M. and M.D. Yahr, *Parkinsonism: onset, progression, and mortality.* Neurology, 1967. **17**(5): p. 427-427.

135. Postuma, R.B. and D. Berg, *Advances in markers of prodromal Parkinson disease.* Nature Reviews Neurology, 2016. **12**(11): p. 622-634.

136. Maiti, P., J. Manna, and G.L. Dunbar, *Current understanding of the molecular mechanisms in Parkinson's disease: Targets for potential treatments.* Translational Neurodegeneration, 2017. **6**(1).

137. Selikhova, M., et al., *A clinico-pathological study of subtypes in Parkinson's disease.* Brain, 2009. **132**(11): p. 2947-2957.

138. Cotzias, G.C., P.S. Papavasiliou, and R. Gellene, *Modification of Parkinsonism — Chronic Treatment with L-Dopa.* New England Journal of Medicine, 1969. **280**(7): p. 337-345.

139. Yahr, M.D., et al., *Treatment of Parkinsonism With Levodopa.* Archives of Neurology, 1969. **21**(4): p. 343-354.

140. Armstrong, M.J. and M.S. Okun, *Diagnosis and Treatment of Parkinson Disease.* JAMA, 2020. **323**(6): p. 548.

141. Olanow, C.W., *Levodopa/dopamine replacement strategies in Parkinson's disease-Future directions.* Movement Disorders, 2008. **23**(S3): p. S613-S622.

142. Wang, L., J. Li, and J. Chen, *Levodopa-Carbidopa Intestinal Gel in Parkinson's Disease: A Systematic Review and Meta-Analysis.* Frontiers in Neurology, 2018. **9**(620).

143. Bronstein, J.M., et al., *Deep Brain Stimulation for Parkinson Disease.* Archives of Neurology, 2011. **68**(2).

144. Bergman, H., T. Wichmann, and M.R. DeLong, *Reversal of experimental parkinsonism by lesions of the subthalamic nucleus.* Science, 1990. **249**(4975): p. 1436-1438.

145. Boutet, A., et al., *Predicting optimal deep brain stimulation parameters for Parkinson's disease using functional MRI and machine learning.* Nature Communications, 2021. **12**(1).

146. Deuschl, G., et al., *A Randomized Trial of Deep-Brain Stimulation for Parkinson's Disease.* New England Journal of Medicine, 2006. **355**(9): p. 896-908.

147. Schenkman, M., et al., *Effect of High-Intensity Treadmill Exercise on Motor Symptoms in Patients With De Novo Parkinson Disease.* JAMA Neurology, 2018. **75**(2): p. 219.

148. Keun, J.T.B., et al., *Dietary Approaches to Improve Efficacy and Control Side Effects of Levodopa Therapy in Parkinson's Disease: A Systematic Review.* Advances in Nutrition, 2021.

149. Elkouzi, A., et al., *Emerging therapies in Parkinson disease — repurposed drugs and new approaches.* Nature Reviews Neurology, 2019. **15**(4): p. 204-223.

150. Ueda, J., et al., *Perampanel Inhibits α-Synuclein Transmission in Parkinson's Disease Models.* Movement Disorders, 2021. **36**(7): p. 1554-1564.

151. Feng, Y., J. Ma, and L. Yuan, *β-Methylphenylalanine exerts neuroprotective effects in a Parkinson's disease model by protecting against tyrosine hydroxylase depletion.* Journal of Cellular and Molecular Medicine, 2020. **24**(17): p. 9871-9880.

152. Vijiaratnam, N., et al., *Progress towards therapies for disease modification in Parkinson's disease.* The Lancet Neurology, 2021. **20**(7): p. 559-572.

153. Tomishima, M. and A. Kirkeby, *Bringing Advanced Therapies for Parkinson's Disease to the Clinic: The Scientist's Perspective.* Journal of Parkinson's Disease, 2021. **11**: p. S135-S140.

154. Merola, A., et al., *Gene therapy for Parkinson's disease: contemporary practice and emerging concepts.* Expert Review of Neurotherapeutics, 2020. **20**(6): p. 577-590.

155. Chu, Y., et al., *Long-term post-mortem studies following neurturin gene therapy in patients with advanced Parkinson's disease.* Brain, 2020. **143**(3): p. 960-975.

156. Parmar, M., S. Grealish, and C. Henchcliffe, *The future of stem cell therapies for Parkinson disease.* Nature Reviews Neuroscience, 2020. **21**(2): p. 103-115.

157. Li, W., et al., *Extensive graft-derived dopaminergic innervation is maintained 24 years after transplantation in the degenerating parkinsonian brain.* Proceedings of the National Academy of Sciences, 2016. **113**(23): p. 6544-6549.

158. Khan, M.S., et al., *Targeting Parkinson's - tyrosine hydroxylase and oxidative stress as points of interventions.* CNS Neurol Disord Drug Targets, 2012. **11**(4): p. 369-80.

159. Zhang, Y., et al., *Normalization of striatal tyrosine hydroxylase and reversal of motor impairment in experimental parkinsonism with intravenous nonviral gene therapy and a brain-specific promoter.* Hum Gene Ther, 2004. **15**(4): p. 339-50.

160. Rosenblad, C., et al., *Vector-mediated l-3,4-dihydroxyphenylalanine delivery reverses motor impairments in a primate model of Parkinson's disease.* Brain, 2019. **142**(8): p. 2402-2416.

161. Palfi, S., et al., *Long-term safety and tolerability of ProSavin, a lentiviral vector-based gene therapy for Parkinson's disease: a dose escalation, open-label, phase 1/2 trial.* The Lancet, 2014. **383**(9923): p. 1138-1146.

162. Ryu, M.Y., et al., *Brain Transplantation of Neural Stem Cells Cotransduced with Tyrosine Hydroxylase and GTP Cyclohydrolase 1 in Parkinsonian Rats.* Cell Transplantation, 2005. **14**(4): p. 193-202.

163. Wang, Z.H., et al., *Therapeutic effects of astrocytes expressing both tyrosine hydroxylase and brain-derived neurotrophic factor on a rat model of Parkinson's disease.* Neuroscience, 2002. **113**(3): p. 629-640.

164. Parascandola, J., *The Public Health Service and the control of biologics.* Public Health Rep, 1995. **110**(6): p. 774-5.

165. Ways, J.P., et al., *Good manufacturing practice (GMP) compliance in the biologics sector: plasma fractionation.* Biotechnol Appl Biochem, 1999. **30**(3): p. 257-65.

166. Anselmo, A.C., Y. Gokarn, and S. Mitragotri, *Non-invasive delivery strategies for biologics.* Nature Reviews Drug Discovery, 2019. **18**(1): p. 19-40.

167. Hirsh, J., et al., *Guide to Anticoagulant Therapy: Heparin.* Circulation, 2001. **103**(24): p. 2994-3018.

168. Royston, D., *The serine antiprotease aprotinin (Trasylol): a novel approach to reducing postoperative bleeding.* Blood Coagulation & Fibrinolysis, 1990. **1**(1).

169. Banting, F.G., et al., *Pancreatic Extracts in the Treatment of Diabetes Mellitus.* Canadian Medical Association journal, 1922. **12**(3): p. 141-146.

170. Johnson, I.S., *The trials and tribulations of producing the first genetically engineered drug.* Nature Reviews Drug Discovery, 2003. **2**(9): p. 747-751.

171. Ahmad, K., *Insulin sources and types: a review of insulin in terms of its mode on diabetes mellitus.* Journal of Traditional Chinese Medicine, 2014. **34**(2): p. 234-237.

172. Müller, T.D., et al., *The New Biology and Pharmacology of Glucagon.* Physiol Rev, 2017. **97**(2): p. 721-766.

173. Arieff, A.J., et al., *Glucagon in insulin coma therapy: its use in a small psychiatric unit of a general hospital.* Q Bull Northwest Univ Med Sch, 1960. **34**(1): p. 7-10.

174. Leader, B., Q.J. Baca, and D.E. Golan, *Protein therapeutics: a summary and pharmacological classification.* Nature Reviews Drug Discovery, 2008. **7**(1): p. 21-39.

175. Chirino, A.J. and A. Mire-Sluis, *Characterizing biological products and assessing comparability following manufacturing changes.* Nature Biotechnology, 2004. **22**(11): p. 1383-1391.

176. Van De Vooren, K., A. Curto, and L. Garattini, *Biosimilar Versus Generic Drugs: Same But Different?* Applied Health Economics and Health Policy, 2015. **13**(2): p. 125-127.

177. Polistena, B., et al., *The impact of biologic therapy in chronic plaque psoriasis from a societal perspective: an analysis based on Italian actual clinical practice.* Journal of the European Academy of Dermatology and Venereology, 2015. **29**(12): p. 2411-2416.

178. Huscher, D., et al., *Evolution of cost structures in rheumatoid arthritis over the past decade.* Annals of the Rheumatic Diseases, 2015. **74**(4): p. 738-745.

179. Lu, R.-M., et al., *Development of therapeutic antibodies for the treatment of diseases.* Journal of Biomedical Science, 2020. **27**(1).

180. Scheinberg, M. and J.J. Gomez-Reino, *The NICE position on indications for biologics and biosimilars.* Nature Reviews Rheumatology, 2016. **12**(5): p. 255-256.

181. Bennett, C.L., et al., *Regulatory and clinical considerations for biosimilar oncology drugs.* The Lancet Oncology, 2014. **15**(13): p. e594-e605.

182. Bray, G., et al., *A multicenter study of recombinant factor VIII (recombinate): safety, efficacy, and inhibitor risk in previously untreated patients with hemophilia A. The Recombinate Study Group.* Blood, 1994. **83**(9): p. 2428-2435.

183. Roth, D.A., et al., *Human recombinant factor IX: safety and efficacy studies in hemophilia B patients previously treated with plasma-derived factor IX concentrates.* Blood, 2001. **98**(13): p. 3600-3606.

184. Klinge, L., et al., *Safety and efficacy of recombinant acid alpha-glucosidase (rhGAA) in patients with classical infantile Pompe disease: results of a phase II clinical trial.* Neuromuscular Disorders, 2005. **15**(1): p. 24-31.

185. Muenzer, J., et al., *A phase II/III clinical study of enzyme replacement therapy with idursulfase in mucopolysaccharidosis II (Hunter syndrome).* Genetics in Medicine, 2006. **8**(8): p. 465-473.

186. Gorzelany, J.A. and M.P. De Souza, *Protein Replacement Therapies for Rare Diseases: A Breeze for Regulatory Approval?* Science Translational Medicine, 2013. **5**(178): p. 178fs10-178fs10.

187. Liang, S. and C. Zhang, *Prediction of immunogenicity for humanized and full human therapeutic antibodies.* PLOS ONE, 2020. **15**(8): p. e0238150.

188. Duncan, R., *Polymer conjugates as anticancer nanomedicines.* Nature Reviews Cancer, 2006. **6**(9): p. 688-701.

189. Graham, M., *Pegaspargase: a review of clinical studies.* Advanced Drug Delivery Reviews, 2003. **55**(10): p. 1293-1302.

190. De Duve, C., et al., *Tissue fractionation studies. 6. Intracellular distribution patterns of enzymes in rat-liver tissue*.* Biochemical Journal, 1955. **60**(4): p. 604-617.

191. de Duve, C., *Lysosomes revisited.* European Journal of Biochemistry, 1983. **137**(3): p. 391-397.

192. Ries, M., *Enzyme replacement therapy and beyond-in memoriam Roscoe O. Brady, M.D. (1923-2016).* J Inherit Metab Dis, 2017. **40**(3): p. 343-356.

193. Barton, N.W., et al., *Replacement therapy for inherited enzyme deficiency--macrophage-targeted glucocerebrosidase for Gaucher's disease.* N Engl J Med, 1991. **324**(21): p. 1464-70.

194. Avenali, M., F. Blandini, and S. Cerri, *Glucocerebrosidase Defects as a Major Risk Factor for Parkinson's Disease.* Frontiers in Aging Neuroscience, 2020. **12**.

195. Mechler, K., et al., *Pressure for drug development in lysosomal storage disorders – a quantitative analysis thirty years beyond the US orphan drug act.* Orphanet Journal of Rare Diseases, 2015. **10**(1).

196. Grabowski, G.A., et al., *Enzyme therapy in type 1 Gaucher disease: comparative efficacy of mannose-terminated glucocerebrosidase from natural and recombinant sources.* Annals of internal medicine, 1995. **122**(1): p. 33-39.

197. Eng, C.M., et al., *Safety and Efficacy of Recombinant Human α-Galactosidase A Replacement Therapy in Fabry's Disease.* New England Journal of Medicine, 2001. **345**(1): p. 9-16.

198. Hershfield, M.S., S. Chaffee, and R.U. Sorensen, *Enzyme Replacement Therapy with Polyethylene Glycol-Adenosine Deaminase in Adenosine Deaminase Deficiency: Overview and Case Reports of Three Patients, Including Two Now Receiving Gene Therapy.* Pediatric Research, 1993. **33**: p. S42-S48.

199. Rosado, J.L., et al., *Enzyme Replacement Therapy for Primary Adult Lactase Deficiency.* Gastroenterology, 1984. **87**(5): p. 1072-1082.

200. Gámez, A., et al., *Toward PKU Enzyme Replacement Therapy: PEGylation with Activity Retention for Three Forms of Recombinant Phenylalanine Hydroxylase.* Molecular Therapy, 2004. **9**(1): p. 124-129.

201. Levy, H.L., C.N. Sarkissian, and C.R. Scriver, *Phenylalanine ammonia lyase (PAL): From discovery to enzyme substitution therapy for phenylketonuria.* Molecular Genetics and Metabolism, 2018. **124**(4): p. 223-229.

202. Sarkissian, C.N., et al., *Preclinical evaluation of multiple species of PEGylated recombinant phenylalanine ammonia lyase for the treatment of phenylketonuria.* Proceedings of the National Academy of Sciences, 2008. **105**(52): p. 20894-20899.

203. Bell, S.M., et al., *Formulation and PEGylation optimization of the therapeutic PEGylated phenylalanine ammonia lyase for the treatment of phenylketonuria.* PLOS ONE, 2017. **12**(3): p. e0173269.

204. Mitragotri, S., P.A. Burke, and R. Langer, *Overcoming the challenges in administering biopharmaceuticals: formulation and delivery strategies.* Nature Reviews Drug Discovery, 2014. **13**(9): p. 655-672.

205. Krol, S., *Challenges in drug delivery to the brain: Nature is against us.* Journal of Controlled Release, 2012. **164**(2): p. 145-155.

206. Pardridge, W.M., *Blood–brain barrier delivery.* Drug Discovery Today, 2007. **12**(1-2): p. 54-61.

207. Feynman, R.P., *There's plenty of room at the bottom.* Resonance, 2011. **16**(9): p. 890-905.

208. Freundlich, M.M., *Origin of the Electron Microscope.* Science, 1963. **142**(3589): p. 185-188.

209. Binnig, G. and H. Rohrer, *Scanning tunneling microscopy—from birth to adolescence.* Reviews of Modern Physics, 1987. **59**(3): p. 615-625.

210. Binnig, G., et al., *Surface Studies by Scanning Tunneling Microscopy.* Physical Review Letters, 1982. **49**(1): p. 57-61.

211. Wu, M. and G.C. Lander, *Present and Emerging Methodologies in Cryo-EM Single-Particle Analysis.* Biophysical Journal, 2020. **119**(7): p. 1281-1289.

212. Nakane, T., et al., *Single-particle cryo-EM at atomic resolution.* Nature, 2020. **587**(7832): p. 152-156.

213. Eigler, D.M. and E.K. Schweizer, *Positioning single atoms with a scanning tunnelling microscope.* Nature, 1990. **344**(6266): p. 524-526.

214. Severin, M., et al., *Manipulation and overstretching of genes on solid substrates.* Nano Letters, 2004. **4**(4): p. 577-579.

215. Leterrier, C., P. Dubey, and S. Roy, *The nano-architecture of the axonal cytoskeleton.* Nat Rev Neurosci, 2017. **18**(12): p. 713-726.

216. Davidovich, C., et al., *The Proto-Ribosome: An Ancient Nano-machine for Peptide Bond Formation.* Israel Journal of Chemistry, 2010. **50**(1): p. 29-35.

217. Austefjord, M.W., H.H. Gerdes, and X. Wang, *Tunneling nanotubes: Diversity in morphology and structure.* Commun Integr Biol, 2014. **7**(1): p. e27934.

218. Acaron Ledesma, H., et al., *An atlas of nano-enabled neural interfaces.* Nat Nanotechnol, 2019. **14**(7): p. 645-657.

219. Wenderott, J.K., et al., *Elucidating nanoscale mechanical properties of diabetic human adipose tissue using atomic force microscopy.* Sci Rep, 2020. **10**(1): p. 20423.

220. Ma, S., et al., *Nanoscale mechanisms in age-related hip-fractures.* Sci Rep, 2020. **10**(1): p. 14208.

221. Gao, H., et al., *Materials become insensitive to flaws at nanoscale: Lessons from nature.* Proceedings of the National Academy of Sciences, 2003. **100**(10): p. 5597-5600.

222. Wallace, J.M., *Applications of atomic force microscopy for the assessment of nanoscale morphological and mechanical properties of bone.* Bone, 2012. **50**(1): p. 420-427.

223. Soria, F.N., et al., *Synucleinopathy alters nanoscale organization and diffusion in the brain extracellular space through hyaluronan remodeling.* Nat Commun, 2020. **11**(1): p. 3440.

224. Talebian, S., et al., *Facts and Figures on Materials Science and Nanotechnology Progress and Investment.* ACS Nano, 2021. **15**(10): p. 15940-15952.

225. Potočnik, J., *COMMISSION RECOMMENDATION on the definition of nanomaterial*, in *Official Journal of the European Union*. 2011, Publications Office of the European Union. p. 38-40.

226. Pouliquen, D., et al., *Iron-Oxide Nanoparticles for Use as an MRI Contrast Agent - Pharmacokinetics and Metabolism.* Magnetic Resonance Imaging, 1991. **9**(3): p. 275-283.

227. Hainfeld, J.F., et al., *Gold nanoparticles: a new X-ray contrast agent.* Br J Radiol, 2006. **79**(939): p. 248-53.

228. Cole, L.E., et al., *Gold nanoparticles as contrast agents in x-ray imaging and computed tomography.* Nanomedicine, 2015. **10**(2): p. 321-341.

229. Barenholz, Y., *Doxil® — The first FDA-approved nano-drug: Lessons learned.* Journal of Controlled Release, 2012. **160**(2): p. 117-134.

230. Mitchell, M.J., et al., *Engineering precision nanoparticles for drug delivery.* Nature Reviews Drug Discovery, 2021. **20**(2): p. 101-124.

231. D'Souza, G.G. and V. Weissig, *Subcellular targeting: a new frontier for drug-loaded pharmaceutical nanocarriers and the concept of the magic bullet.* Expert Opin Drug Deliv, 2009. **6**(11): p. 1135-48.

232. Anselmo, A.C. and S. Mitragotri, *Nanoparticles in the clinic.* Bioengineering & Translational Medicine, 2016. **1**(1): p. 10-29.

233. Anselmo, A.C. and S. Mitragotri, *Nanoparticles in the clinic: An update.* Bioengineering & Translational Medicine, 2019. **4**(3).

234. Baeza, A., D. Ruiz-Molina, and M. Vallet-Regí, *Recent advances in porous nanoparticles for drug delivery in antitumoral applications: inorganic nanoparticles and nanoscale metal-organic frameworks.* Expert Opinion on Drug Delivery, 2017. **14**(6): p. 783-796.

235. Pugazhendhi, A., et al., *Inorganic nanoparticles: A potential cancer therapy for human welfare.* International Journal of Pharmaceutics, 2018. **539**(1-2): p. 104-111.

236. Thi, T.T.H., et al., *Lipid-Based Nanoparticles in the Clinic and Clinical Trials: From Cancer Nanomedicine to COVID-19 Vaccines.* Vaccines, 2021. **9**(4): p. 359.

237. Working, P.K., et al., *Pharmacokinetics, Biodistribution and Therapeutic Efficacy of Doxorubicin Encapsulated in Stealth® Liposomes (Doxil®).* Journal of Liposome Research, 1994. **4**(1): p. 667-687.

238. Anselmo, A.C. and S. Mitragotri, *Nanoparticles in the clinic: An update post COVID -19 vaccines.* Bioengineering & Translational Medicine, 2021. **6**(3).

239. Kristen, A.V., et al., *Patisiran, an RNAi therapeutic for the treatment of hereditary transthyretin-mediated amyloidosis.* Neurodegenerative Disease Management, 2019. **9**(1): p. 5-23.

240. Anselmo, A.C., et al., *Clinical and commercial translation of advanced polymeric nanoparticle systems: opportunities and material challenges.* Translational Materials Research, 2017. **4**(1): p. 014001.

241. Curcio, M., et al., *Natural Polysaccharide Carriers in Brain Delivery: Challenge and Perspective.* Pharmaceutics, 2020. **12**(12): p. 1183.

242. Elsharkasy, O.M., et al., *Extracellular vesicles as drug delivery systems: Why and how?* Advanced Drug Delivery Reviews, 2020. **159**: p. 332-343.

243. Tomao, S., *Albumin-bound formulation of paclitaxel (Abraxane® ABI-007) in the treatment of breast cancer.* International Journal of Nanomedicine, 2009: p. 99.

244. Gradishar, W.J., et al., *Phase III Trial of Nanoparticle Albumin-Bound Paclitaxel Compared With Polyethylated Castor Oil–Based Paclitaxel in Women With Breast Cancer.* Journal of Clinical Oncology, 2005. **23**(31): p. 7794-7803.

245. Soo Choi, H., et al., *Renal clearance of quantum dots.* Nature Biotechnology, 2007. **25**(10): p. 1165-1170.

246. Luo, Y.-L., et al., *Effective Renal Clearance and Photothermal Therapy of a Cyclodextrin-Modified Quaterrylene Derivative.* ACS Applied Bio Materials, 2020. **3**(5): p. 3390-3400.

247. Du, B., et al., *Glomerular barrier behaves as an atomically precise bandpass filter in a sub-nanometre regime.* Nature Nanotechnology, 2017. **12**(11): p. 1096-1102.

248. Kolhar, P., et al., *Using shape effects to target antibody-coated nanoparticles to lung and brain endothelium.* Proceedings of the National Academy of Sciences, 2013. **110**(26): p. 10753-10758.

249. Codoni, D., et al., *Disc-shaped polyoxyethylene glycol glycerides gel nanoparticles as novel protein delivery vehicles.* Int J Pharm, 2015. **496**(2): p. 1015-25.

250. Anselmo, A.C., et al., *Elasticity of Nanoparticles Influences Their Blood Circulation, Phagocytosis, Endocytosis, and Targeting.* ACS Nano, 2015. **9**(3): p. 3169-3177.

251. Nguyen-Thi, N.-T., et al., *The Engineering of Porous Silica and Hollow Silica Nanoparticles to Enhance Drug-loading Capacity.* Processes, 2019. **7**(11): p. 805.

252. Alshehri, S., et al., *Progress of Cancer Nanotechnology as Diagnostics, Therapeutics, and Theranostics Nanomedicine: Preclinical Promise and Translational Challenges.* Pharmaceutics, 2020. **13**(1): p. 24.

253. Luo, D., et al., *Recent Development of Gold Nanoparticles as Contrast Agents for Cancer Diagnosis.* Cancers, 2021. **13**(8): p. 1825.

254. Xiao, K., et al., *The effect of surface charge on in vivo biodistribution of PEG-oligocholic acid based micellar nanoparticles.* Biomaterials, 2011. **32**(13): p. 3435-3446.

255. Anglin, E., et al., *Porous silicon in drug delivery devices and materials.* Advanced Drug Delivery Reviews, 2008. **60**(11): p. 1266-1277.

256. Jung, Y., Y. Huh, and D. Kim, *Recent advances in surface engineering of porous silicon nanomaterials for biomedical applications.* Microporous and Mesoporous Materials, 2021. **310**: p. 110673.

257. Zhao, Z., et al., *Effect of physicochemical and surface properties on in vivo fate of drug nanocarriers.* Advanced Drug Delivery Reviews, 2019. **143**: p. 3-21.

258. Blanco, E., H. Shen, and M. Ferrari, *Principles of nanoparticle design for overcoming biological barriers to drug delivery.* Nat Biotechnol, 2015. **33**(9): p. 941-51.

259. Esmaeili, F., et al., *PLGA nanoparticles of different surface properties: Preparation and evaluation of their body distribution.* International Journal of Pharmaceutics, 2008. **349**(1): p. 249-255.

260. Silva, S., A. Almeida, and N. Vale, *Combination of Cell-Penetrating Peptides with Nanoparticles for Therapeutic Application: A Review.* Biomolecules, 2019. **9**(1): p. 22.

261. Johnsen, K.B., et al., *Targeting transferrin receptors at the blood-brain barrier improves the uptake of immunoliposomes and subsequent cargo transport into the brain parenchyma.* Scientific Reports, 2017. **7**(1).

262. Zeb, A., et al., *Potential and Applications of Nanocarriers for Efficient Delivery of Biopharmaceuticals.* Pharmaceutics, 2020. **12**(12): p. 1184.

263. Sábio, R.M., et al., *Exploiting mesoporous silica nanoparticles as versatile drug carriers for several routes of administration.* Microporous and Mesoporous Materials, 2021. **312**: p. 110774.

264. Lim, G.B., *Drug delivery using inhaled nanoparticles.* Nature Reviews Cardiology, 2018. **15**(3): p. 133-133.

265. Abd-Allah, H., R.T.A. Abdel-Aziz, and M. Nasr, *Chitosan nanoparticles making their way to clinical practice: A feasibility study on their topical use for acne treatment.* International Journal of Biological Macromolecules, 2020. **156**: p. 262-270.

266. Abbott, N.J., L. Rönnbäck, and E. Hansson, *Astrocyte–endothelial interactions at the blood–brain barrier.* Nature Reviews Neuroscience, 2006. **7**(1): p. 41-53.

267. Gasca-Salas, C., et al., *Blood-brain barrier opening with focused ultrasound in Parkinson's disease dementia.* Nature Communications, 2021. **12**(1).

268. Smith, S.A., et al., *The Endosomal Escape of Nanoparticles: Toward More Efficient Cellular Delivery.* Bioconjugate Chemistry, 2019. **30**(2): p. 263-272.

269. Kuczenski, R.T. and A.J. Mandell, *Allosteric activation of hypothalamic tyrosine hydroxylase by ions and sulphated mucopolysaccharides.* Journal of Neurochemistry, 1972. **19**(1): p. 131-137.

270. Katz, I.R., T. Yamauchi, and S. Kaufman, *Activation of tyrosine hydroxylase by polyanions and salts An electrostatic effect.* Biochimica et Biophysica Acta (BBA) - Enzymology, 1976. **429**(1): p. 84-95.

271. Joh, T.H. and D.J. Reis, *Different forms of tyrosine hydroxylase in central dopaminergic and noradrenergic neurons and sympathetic ganglia.* Brain Research, 1975. **85**(1): p. 146-151.

272. Nagatsu, T., et al., *Effects of melanin on tyrosine hydroxylase and phenylalanine hydroxylase.* Biochimica et Biophysica Acta (BBA) - Enzymology, 1978. **523**(1): p. 47-52.

273. Raese, J., R.L. Patrick, and J.D. Barchas, *Phospholipid-induced activation of tyrosine hydroxylase from rat brain striatal synaptosomes.* Biochemical Pharmacology, 1976. **25**(20): p. 2245-2250.

274. Lloyd, T. and S. Kaufman, *The stimulation of partially purified bovine caudate tyrosine hydroxylase by phosphatidyl-L-serine.* Biochemical and Biophysical Research Communications, 1974. **59**(4): p. 1262-1269.

275. Vulliet, P.R. and N. Weiner, *A schematic model for the allosteric activation of tyrosine hydroxylase*. 1981, Palgrave Macmillan UK. p. 15-24.

276. Haavik, J., et al., *Soluble tyrosine hydroxylase (tyrosine 3-monooxygenase) from bovine adrenal medulla: Large-scale purification and physicochemical properties.* Biochimica et Biophysica Acta (BBA) - Protein Structure and Molecular Enzymology, 1988. **953**: p. 142-156.

277. Abeer, M.M., et al., *Silica nanoparticles: A promising platform for enhanced oral delivery of macromolecules.* Journal of Controlled Release, 2020. **326**: p. 544-555.

278. Park, J.-H., et al., *Biodegradable luminescent porous silicon nanoparticles for in vivo applications.* Nature Materials, 2009. **8**(4): p. 331-336.

279. Paillard, A., et al., *Positively-Charged, Porous, Polysaccharide Nanoparticles Loaded with Anionic Molecules Behave as 'Stealth' Cationic Nanocarriers.* Pharmaceutical Research, 2010. **27**(1): p. 126-133.

280. Mayne, A.H., et al., *Biologically Interfaced Porous Silicon Devices.* physica status solidi (a), 2000. **182**(1): p. 505-513.

281. Létant, S.E., et al., *Integration of porous silicon chips in an electronic artificial nose.* Sensors and Actuators B: Chemical, 2000. **69**(1-2): p. 193-198.

282. Orosco, M.M., C. Pacholski, and M.J. Sailor, *Real-time monitoring of enzyme activity in a mesoporous silicon double layer.* Nature Nanotechnology, 2009. **4**(4): p. 255-258.

283. Uhlir Jr, A., *Electrolytic shaping of germanium and silicon.* Bell System Technical Journal, 1956. **35**(2): p. 333-347.

284. Sailor, M.J. and E.C. Wu, *Photoluminescence-Based Sensing With Porous Silicon Films, Microparticles, and Nanoparticles.* Advanced Functional Materials, 2009. **19**(20): p. 3195-3208.

285. Sailor, M.J., *Porous Silicon in Practice: Preparation, Characterization and Applications*. 2012: Wiley-VCH. 249.

286. Qin, Z., et al., *Size Control of Porous Silicon Nanoparticles by Electrochemical Perforation Etching.* Particle & Particle Systems Characterization, 2014. **31**(2): p. 252-256.

287. Santos, H.A., et al., *Porous silicon nanoparticles for nanomedicine: preparation and biomedical applications.* Nanomedicine (Lond), 2014. **9**(4): p. 535-54.

288. Kang, J., et al., *Self-Sealing Porous Silicon-Calcium Silicate Core–Shell Nanoparticles for Targeted siRNA Delivery to the Injured Brain.* Advanced Materials, 2016. **28**(36): p. 7962-7969.

289. Lee, S., J. Kang, and D. Kim, *A Mini Review: Recent Advances in Surface Modification of Porous Silicon.* Materials, 2018. **11**(12): p. 2557.

290. Jurkić, L.M., et al., *Biological and therapeutic effects of ortho-silicic acid and some ortho-silicic acid-releasing compounds: New perspectives for therapy.* Nutrition & Metabolism, 2013. **10**(1): p. 2.

291. Jugdaohsingh, R., et al., *Dietary silicon intake and absorption.* The American Journal of Clinical Nutrition, 2002. **75**(5): p. 887-893.

292. Carlisle, E.M., *Silicon as a trace nutrient.* Science of The Total Environment, 1988. **73**(1-2): p. 95-106.

293. Carlisle, E.M., *Silicon: an essential element for the chick.* Science, 1972. **178**(4061): p. 619-621.

294. Jugdaohsingh, R., et al., *Dietary Silicon Intake Is Positively Associated With Bone Mineral Density in Men and Premenopausal Women of the Framingham Offspring Cohort.* Journal of Bone and Mineral Research, 2003. **19**(2): p. 297-307.

295. Henstock, J.R., L.T. Canham, and S.I. Anderson, *Silicon: the evolution of its use in biomaterials.* Acta Biomater, 2015. **11**: p. 17-26.

296. Reffitt, D.M., et al., *Silicic acid: its gastrointestinal uptake and urinary excretion in man and effects on aluminium excretion.* Journal of Inorganic Biochemistry, 1999. **76**(2): p. 141-147.

297. Jarvis, K.L., T.J. Barnes, and C.A. Prestidge, *Thermal Oxidation for Controlling Protein Interactions with Porous Silicon.* Langmuir, 2010. **26**(17): p. 14316-14322.

298. Prestidge, C.A., et al., *Peptide and protein loading into porous silicon wafers.* physica status solidi (a), 2008. **205**(2): p. 311-315.

299. Karlsson, L.M., et al., *Penetration and loading of human serum albumin in porous silicon layers with different pore sizes and thicknesses.* Journal of Colloid and Interface Science, 2003. **266**(1): p. 40-47.

300. Chen, M.Y. and M.J. Sailor, *Charge-Gated Transport of Proteins in Nanostructured Optical Films of Mesoporous Silica.* Analytical Chemistry, 2011. **83**(18): p. 7186-7193.

301. Liu, H.-J. and P. Xu, *Smart Mesoporous Silica Nanoparticles for Protein Delivery.* Nanomaterials, 2019. **9**(4): p. 511.

302. Wu, C.-C., et al., *Protection and Delivery of Anthelmintic Protein Cry5B to Nematodes Using Mesoporous Silicon Particles.* ACS Nano, 2015. **9**(6): p. 6158-6167.

303. Kao, K.-C., T.-S. Lin, and C.-Y. Mou, *Enhanced Activity and Stability of Lysozyme by Immobilization in the Matching Nanochannels of Mesoporous Silica Nanoparticles.* The Journal of Physical Chemistry C, 2014. **118**(13): p. 6734-6743.

304. Xu, C., C. Lei, and C. Yu, *Mesoporous Silica Nanoparticles for Protein Protection and Delivery.* Frontiers in Chemistry, 2019. **7**.

305. Andrew, J.S., et al., *Sustained Release of a Monoclonal Antibody from Electrochemically Prepared Mesoporous Silicon Oxide.* Adv Funct Mater, 2010. **20**(23): p. 4168-4174.

306. Canham, L.T., *Silicon quantum wire array fabrication by electrochemical and chemical dissolution of wafers.* Applied physics letters, 1990. **57**(10): p. 1046-1048.

307. Heinrich, J.L., C.L. Curtis, and et al., *Luminescent Colloidal Silicon Suspensions from Porous Silicon.* Science, 1992. **255**(5040): p. 66.

308. Joo, J., et al., *Photoluminescent Porous Si/SiO2Core/Shell Nanoparticles Prepared by Borate Oxidation.* Advanced Functional Materials, 2014. **24**(36): p. 5688-5694.

309. Gu, L., et al., *In vivo time-gated fluorescence imaging with biodegradable luminescent porous silicon nanoparticles.* Nature Communications, 2013. **4**(1).

310. Hofman, D.L., V.J. Van Buul, and F.J.P.H. Brouns, *Nutrition, Health, and Regulatory Aspects of Digestible Maltodextrins.* Critical Reviews in Food Science and Nutrition, 2016. **56**(12): p. 2091-2100.

311. Major, M., et al., *Characterisation and phase behaviour of phospholipid bilayers adsorbed on spherical polysaccharidic nanoparticles.* Biochimica et Biophysica Acta (BBA) - Biomembranes, 1997. **1327**(1): p. 32-40.

312. Loiseau, P.M., et al., *Design and antileishmanial activity of amphotericin B-loaded stable ionic amphiphile biovector formulations.* Antimicrob Agents Chemother, 2002. **46**(5): p. 1597-601.

313. Qiu, C., et al., *Preparation of active polysaccharide-loaded maltodextrin nanoparticles and their stability as a function of ionic strength and pH.* LWT - Food Science and Technology, 2017. **76**: p. 164-171.

314. Jung, E., et al., *Stimulus-activatable echogenic maltodextrin nanoparticles as nanotheranostic agents for peripheral arterial disease.* Biomaterials, 2019. **192**: p. 282-291.

315. Desai, N.M., J. Gilbert Stanley, and P.S. Murthy, *Green coffee nanoparticles: optimisation, in vitro bioactivity and bio-release property.* Journal of Microencapsulation, 2020. **37**(1): p. 52-64.

316. De Miguel, I., et al., *Synthesis and characterization of supramolecular biovector (SMBV) specifically designed for the entrapment of ionic molecules.* Biochimica et Biophysica Acta (BBA) - Biomembranes, 1995. **1237**(1): p. 49-58.

317. Jung, E., et al., *Molecularly Engineered Theranostic Nanoparticles for Thrombosed Vessels: H2O2-Activatable Contrast-Enhanced Photoacoustic Imaging and Antithrombotic Therapy.* ACS Nano, 2018. **12**(1): p. 392-401.

318. Pagels, R.F. and R.K. Prud'Homme, *Polymeric nanoparticles and microparticles for the delivery of peptides, biologics, and soluble therapeutics.* Journal of Controlled Release, 2015. **219**: p. 519-535.

319. Fasquelle, F., et al., *Importance of the Phospholipid Core for Mucin Hydrogel Penetration and Mucosal Cell Uptake of Maltodextrin Nanoparticles.* ACS Applied Bio Materials, 2020. **3**(9): p. 5741-5749.

320. Prieur, E., et al., *Combination of human cytomegalovirus recombinant immediate-early protein (IE1) with 80 nm cationic biovectors: protection from proteolysis and potentiation of presentation to CD4+ T-cell clones in vitro.* Vaccine, 1996. **14**(6): p. 511-520.

321. Carpentier, R., et al., *Porous Maltodextrin-Based Nanoparticles: A Safe Delivery System for Nasal Vaccines.* Journal of Nanomaterials, 2018. **2018**: p. 9067195.

322. Dombu, C.Y., et al., *Characterization of endocytosis and exocytosis of cationic nanoparticles in airway epithelium cells.* Nanotechnology, 2010. **21**(35): p. 355102.

323. Jallouli, Y., et al., *Influence of surface charge and inner composition of porous nanoparticles to cross blood-brain barrier in vitro.* Int J Pharm, 2007. **344**(1-2): p. 103-9.

324. Lê, M.Q., et al., *Protein delivery by porous cationic maltodextrin-based nanoparticles into nasal mucosal cells: Comparison with cationic or anionic nanoparticles.* International Journal of Pharmaceutics: X, 2019. **1**: p. 100001.

325. Dimier-Poisson, I., et al., *Porous nanoparticles as delivery system of complex antigens for an effective vaccine against acute and chronic Toxoplasma gondii infection.* Biomaterials, 2015. **50**: p. 164-75.

326. Castignolles, N., et al., *Stabilization and enhancement of interleukin-2 in vitro bioactivity by new carriers: supramolecular biovectors.* Vaccine, 1994. **12**(15): p. 1413-1418.

327. Nakashima, A., et al., *Expression of human tyrosine hydroxylase type I in Escherichia coli as a protease-cleavable fusion protein.* Journal of Neural Transmission, 1999. **106**(9-10): p. 819-824.

328. Higgins, C.A., et al., *Expression and purification of recombinant human tyrosine hydroxylase as a fusion protein in Escherichia coli.* Protein Expr Purif, 2012. **84**(2): p. 219-23.

329. Calamini, B. and R.I. Morimoto, *Protein homeostasis as a therapeutic target for diseases of protein conformation.* Curr Top Med Chem, 2012. **12**(22): p. 2623-40.

330. Lundahl, M.L.E., et al., *Aggregation of protein therapeutics enhances their immunogenicity: causes and mitigation strategies.* RSC Chemical Biology, 2021. **2**(4): p. 1004-1020.

331. Esposito, D. and D.K. Chatterjee, *Enhancement of soluble protein expression through the use of fusion tags.* Current Opinion in Biotechnology, 2006. **17**(4): p. 353-358.

332. Raran-Kurussi, S. and D.S. Waugh, *The ability to enhance the solubility of its fusion partners is an intrinsic property of maltose-binding protein but their folding is either spontaneous or chaperone-mediated.* PLoS One, 2012. **7**(11): p. e49589.

333. Nilsson, B., et al., *A synthetic IgG-binding domain based on staphylococcal protein A.* Protein Eng, 1987. **1**(2): p. 107-13.

334. Mertens, H.D. and D.I. Svergun, *Structural characterization of proteins and complexes using small-angle X-ray solution scattering.* J Struct Biol, 2010. **172**(1): p. 128-41.

335. Zheng, W. and M. Tekpinar, *Accurate flexible fitting of high-resolution protein structures to small-angle x-ray scattering data using a coarse-grained model with implicit hydration shell.* Biophys J, 2011. **101**(12): p. 2981-91.

336. Szigetvari, P.D., et al., *The quaternary structure of human tyrosine hydroxylase: effects of dystonia-associated missense variants on oligomeric state and enzyme activity.* J Neurochem, 2019. **148**(2): p. 291-306.

337. De Vocht, C., et al., *Assessment of stability, toxicity and immunogenicity of new polymeric nanoreactors for use in enzyme replacement therapy of MNGIE.* J Control Release, 2009. **137**(3): p. 246-54.

338. Liu, F., et al., *Modulating the Activity of Protein Conjugated to Gold Nanoparticles by Site-Directed Orientation and Surface Density of Bound Protein.* ACS Applied Materials & Interfaces, 2015. **7**(6): p. 3717-3724.

339. Long, J., et al., *Preparation of Streptavidin-Coated Magnetic Nanoparticles for Specific Immobilization of Enzymes with High Activity and Enhanced Stability.* Industrial & Engineering Chemistry Research, 2021. **60**(4): p. 1542-1552.

340. Chapman, R. and M.H. Stenzel, *All Wrapped up: Stabilization of Enzymes within Single Enzyme Nanoparticles.* Journal of the American Chemical Society, 2019. **141**(7): p. 2754-2769.

341. Haavik, J. and T. Flatmark, *Rapid and sensitive assay of tyrosine 3-monooxygenase activity by high-performance liquid chromatography using the native fluorescence of DOPA.* J Chromatogr, 1980. **198**(4): p. 511-5.

342. Reinhard, J.F., G.K. Smith, and C.A. Nichol, *A rapid and sensitive assay for tyrosine-3-monooxygenase based upon the release of 3H2O and adsorption of [3H]-tyrosine by charcoal.* Life Sciences, 1986. **39**(23): p. 2185-2189.

343. Vermeer, L.M., et al., *Real-time monitoring of tyrosine hydroxylase activity using a plate reader assay.* Anal Biochem, 2013. **432**(1): p. 11-5.

344. Martinez, A., et al., *Conformational properties and stability of tyrosine hydroxylase studied by infrared spectroscopy. Effect of iron/catecholamine binding and phosphorylation.* J Biol Chem, 1996. **271**(33): p. 19737-42.

345. Bucher, M.L., et al., *Acquired dysregulation of dopamine homeostasis reproduces features of Parkinson's disease.* npj Parkinson's Disease, 2020. **6**(1).

346. Mueller, L.A., U. Hinz, and J.-P. Zrÿd, *Characterization of a tyrosinase from Amanita muscaria involved in betalain biosynthesis.* Phytochemistry, 1996. **42**(6): p. 1511-1515.

347. Mayer, A.M., *Polyphenol oxidases in plants and fungi: Going places? A review.* Phytochemistry, 2006. **67**(21): p. 2318-2331.

348. Jaenicke, E. and H. Decker, *Tyrosinases from crustaceans form hexamers.* Biochemical Journal, 2003. **371**(2): p. 515-523.

349. Nakagawa, A., et al., *Selection of the optimal tyrosine hydroxylation enzyme for (S)-reticuline production in Escherichia coli.* Applied Microbiology and Biotechnology, 2021. **105**(13): p. 5433-5447.

350. Sunnadeniya, R., et al., *Tyrosine Hydroxylation in Betalain Pigment Biosynthesis Is Performed by Cytochrome P450 Enzymes in Beets (Beta vulgaris).* PLOS ONE, 2016. **11**(2): p. e0149417.

351. Prieto, M.A. and J.L. Garcia, *Molecular characterization of 4-hydroxyphenylacetate 3-hydroxylase of Escherichia coli. A two-protein component enzyme.* J Biol Chem, 1994. **269**(36): p. 22823-9.

352. Wei, T., B.-Y. Cheng, and J.-Z. Liu, *Genome engineering Escherichia coli for L-DOPA overproduction from glucose.* Scientific Reports, 2016. **6**(1): p. 30080.

353. Muñoz, A.J., et al., *Metabolic engineering of Escherichia coli for improving l-3,4-dihydroxyphenylalanine (l-DOPA) synthesis from glucose.* Journal of Industrial Microbiology & Biotechnology, 2011. **38**(11): p. 1845-1852.

354. Das, A., et al., *Metabolic engineering of Escherichia coli W3110 strain by incorporating genome-level modifications and synthetic plasmid modules to enhance L-Dopa production from glycerol.* Preparative Biochemistry & Biotechnology, 2018. **48**(8): p. 671-682.

355. Yao, J., et al., *Developing a highly efficient hydroxytyrosol whole-cell catalyst by de-bottlenecking rate-limiting steps.* Nature Communications, 2020. **11**(1).

356. Gupta, S., et al., *Association of immune response with efficacy and safety outcomes in adults with phenylketonuria administered pegvaliase in phase 3 clinical trials.* EBioMedicine, 2018. **37**: p. 366-373.

357. Satoh, Y., et al., *Engineering of l-tyrosine oxidation in Escherichia coli and microbial production of hydroxytyrosol.* Metabolic Engineering, 2012. **14**(6): p. 603-610.

358. van den Berg, S., et al., *Improved solubility of TEV protease by directed evolution.* J Biotechnol, 2006. **121**(3): p. 291-8.

359. Markham, A., *Pegvaliase: First Global Approval.* BioDrugs, 2018. **32**(4): p. 391-395.

360. Fu, A., et al., *Intravenous treatment of experimental Parkinson's disease in the mouse with an IgG-GDNF fusion protein that penetrates the blood-brain barrier.* Brain Res, 2010. **1352**: p. 208-13.

361. Kim, M.J., et al., *Tat-Frataxin protects dopaminergic neuronal cells against MPTP-induced toxicity in a mouse model of Parkinson's disease.* Biochimie, 2012. **94**(11): p. 2448-56.

362. Tunesi, M., et al., *Hydrogel-based delivery of Tat-fused protein Hsp70 protects dopaminergic cells in vitro and in a mouse model of Parkinson's disease.* NPG Asia Materials, 2019. **11**(1).

363. Bezard, E., J.M. Brotchie, and C.E. Gross, *Pathophysiology of levodopa-induced dyskinesia: Potential for new therapies.* Nature Reviews Neuroscience, 2001. **2**(8): p. 577-588.

364. Lachmann, R.H., *Enzyme replacement therapy for lysosomal storage diseases.* Current Opinion in Pediatrics, 2011. **23**(6).

365. Huang, L., et al., *β-asarone and levodopa co-administration increase striatal dopamine level in 6-hydroxydopamine induced rats by modulating P-glycoprotein and tight junction proteins at the blood-brain barrier and promoting levodopa into the brain.* Clinical and Experimental Pharmacology and Physiology, 2016. **43**(6): p. 634-643.

366. Felice, B.R., et al., *Safety Evaluation of Chronic Intrathecal Administration of Idursulfase-IT in Cynomolgus Monkeys.* Toxicologic Pathology, 2011. **39**(5): p. 879-892.

367. Morabito, G., et al., *AAV-PHP.B-Mediated Global-Scale Expression in the Mouse Nervous System Enables GBA1 Gene Therapy for Wide Protection from Synucleinopathy.* Molecular Therapy, 2017. **25**(12): p. 2727-2742.

368. Eberling, J.L., et al., *Results from a phase I safety trial of hAADC gene therapy for Parkinson disease.* Neurology, 2008. **70**(21): p. 1980-1983.

369. Pardridge, W.M., *Tyrosine hydroxylase replacement in experimental Parkinson's disease with transvascular gene therapy.* NeuroRX, 2005. **2**(1): p. 129-138.

370. Richardson, R.M., et al., *Novel Platform for MRI-Guided Convection-Enhanced Delivery of Therapeutics: Preclinical Validation in Nonhuman Primate Brain.* Stereotactic and Functional Neurosurgery, 2011. **89**(3): p. 141-151.

371. Fiandaca, M.S., et al., *Advancing gene therapies, methods, and technologies for Parkinson's Disease and other neurological disorders.* Neurologia i Neurochirurgia Polska, 2020. **54**(3): p. 220-231.

372. Schnepp, B.C., et al., *Characterization of Adeno-Associated Virus Genomes Isolated from Human Tissues.* Journal of Virology, 2005. **79**(23): p. 14793-14803.

373. Aubi, O., et al., *The Pah-R261Q mouse reveals oxidative stress associated with amyloid-like hepatic aggregation of mutant phenylalanine hydroxylase.* Nature Communications, 2021. **12**(1).

374. Villiger, L., et al., *Treatment of a metabolic liver disease by in vivo genome base editing in adult mice.* Nature Medicine, 2018. **24**(10): p. 1519-1525.

375. Barker, R.A., *Designing stem-cell-based dopamine cell replacement trials for Parkinson's disease.* Nature Medicine, 2019. **25**(7): p. 1045-1053.

376. Takahashi, K., et al., *Induction of Pluripotent Stem Cells from Adult Human Fibroblasts by Defined Factors.* Cell, 2007. **131**(5): p. 861-872.

377. Schweitzer, J.S., et al., *Personalized iPSC-Derived Dopamine Progenitor Cells for Parkinson's Disease.* New England Journal of Medicine, 2020. **382**(20): p. 1926-1932.

378. Wang, G., et al., *Highly sensitive sensors based on the immobilization of tyrosinase in chitosan.* Bioelectrochemistry, 2002. **57**(1): p. 33-38.

379. Beal, M.F., *Experimental models of Parkinson's disease.* Nature Reviews Neuroscience, 2001. **2**(5): p. 325-332.

380. Zhuang, J., et al., *Multimodal Enzyme Delivery and Therapy Enabled by Cell Membrane-Coated Metal–Organic Framework Nanoparticles.* Nano Letters, 2020. **20**(5): p. 4051-4058.

381. Grosso, A.D., et al., *Brain-targeted enzyme-loaded nanoparticles: A breach through the blood-brain barrier for enzyme replacement therapy in Krabbe disease.* Science Advances, 2019. **5**(11): p. eaax7462.

382. Rigon, L., et al., *Targeting Brain Disease in MPSII: Preclinical Evaluation of IDS-Loaded PLGA Nanoparticles.* International Journal of Molecular Sciences, 2019. **20**(8): p. 2014.

383. Kim, D.H., et al., *Single enzyme nanoparticle, an effective tool for enzyme replacement therapy.* Arch Pharm Res, 2020. **43**(1): p. 1-21.

384. Chao, O.Y., et al., *Intranasally applied l-DOPA alleviates parkinsonian symptoms in rats with unilateral nigro-striatal 6-OHDA lesions.* Brain Research Bulletin, 2012. **87**(2-3): p. 340-345.

385. De Souza Silva, M.A., et al., *Intranasal dopamine application increases dopaminergic activity in the neostriatum and nucleus accumbens and enhances motor activity in the open field.* Synapse, 2008. **62**(3): p. 176-184.

386. García-Pardo, J., et al., *Bioinspired Theranostic Coordination Polymer Nanoparticles for Intranasal Dopamine Replacement in Parkinson's Disease.* ACS Nano, 2021. **15**(5): p. 8592-8609.

387. Quan Le, M., et al., *Prevention of influenza virus infection and transmission by intranasal administration of a porous maltodextrin nanoparticle-formulated vaccine.* International Journal of Pharmaceutics, 2020. **582**: p. 119348.

388. Ducournau, C., et al., *Effective Nanoparticle-Based Nasal Vaccine Against Latent and Congenital Toxoplasmosis in Sheep.* Frontiers in Immunology, 2020. **11**.

389. Lombardo, S.M., et al., *Key for crossing the BBB with nanoparticles: the rational design.* Beilstein Journal of Nanotechnology, 2020. **11**: p. 866-883.

390. Di Gioia, S., et al., *Intranasal delivery of dopamine to the striatum using glycol chitosan/sulfobutylether-β-cyclodextrin based nanoparticles.* European Journal of Pharmaceutics and Biopharmaceutics, 2015. **94**: p. 180-193.

391. Jackson-Lewis, V. and S. Przedborski, *Protocol for the MPTP mouse model of Parkinson's disease.* Nature Protocols, 2007. **2**(1): p. 141-151.

392. Hegazy, M.A., et al., *Cerium oxide nanoparticles could ameliorate behavioral and neurochemical impairments in 6-hydroxydopamine induced Parkinson's disease in rats.* Neurochemistry International, 2017. **108**: p. 361-371.

393. Hernando, S., et al., *Intranasal Administration of TAT-Conjugated Lipid Nanocarriers Loading GDNF for Parkinson's Disease.* Molecular Neurobiology, 2018. **55**(1): p. 145-155.

394. Blanco, S., et al., *Hyaluronate Nanoparticles as a Delivery System to Carry Neuroglobin to the Brain after Stroke.* Pharmaceutics, 2020. **12**(1): p. 40.

395. Wen, Z., et al., *Odorranalectin-conjugated nanoparticles: Preparation, brain delivery and pharmacodynamic study on Parkinson's disease following intranasal administration.* Journal of Controlled Release, 2011. **151**(2): p. 131-138.

396. Tong, P.-H., et al., *Metal-organic frameworks (MOFs) as host materials for the enhanced delivery of biomacromolecular therapeutics.* Chemical Communications, 2021.

I

Paper I

Stable Preparations of Tyrosine Hydroxylase Provide the Solution Structure of the Full-Length Enzyme

Maria T. Bezem, Anne Baumann, Lars Skjærven, Romain Meyer, Petri Kursula, Aurora Martinez and Marte I. Flydal

Scientific Reports, **6**(1), 1-14, 2016.

Tyrosine hydroxylase (TH) catalyzes the rate-limiting step in the biosynthesis of catecholamine neurotransmitters. TH is a highly complex enzyme at mechanistic, structural, and regulatory levels, and the preparation of kinetically and conformationally stable enzyme for structural characterization has been challenging. Here, we report on improved protocols for purification of recombinant human TH isoform 1 (TH1), which provide large amounts of pure, stable, active TH1 with an intact N-terminus. TH1 purified through fusion with a His-tagged maltose-binding protein on amylose resin was representative of the iron-bound functional enzyme, showing high activity and stabilization by the natural feedback inhibitor dopamine. TH1 purified through fusion with a His-tagged ZZ domain on TALON is remarkably stable, as it was partially inhibited by resin-derived cobalt. This more stable enzyme preparation provided high-quality small-angle X-ray scattering (SAXS) data and reliable structural models of fulllength tetrameric TH1. The SAXS-derived model reveals an elongated conformation (Dmax = 20 nm) for TH1, different arrangement of the catalytic domains compared with the crystal structure of truncated forms, and an N-terminal region with an unstructured tail that hosts the phosphorylation sites and a separated Ala-rich helical motif that may have a role in regulation of TH by interacting with binding partners.

SCIENTIFIC REPORTS

OPEN

Stable preparations of tyrosine hydroxylase provide the solution structure of the full-length enzyme

Received: 11 April 2016
Accepted: 30 June 2016
Published: 27 July 2016

Maria T. Bezem[1,*], Anne Baumann[1,2,3,*], Lars Skjærven[1], Romain Meyer[4], Petri Kursula[1], Aurora Martinez[1,2] & Marte I. Flydal[1,5]

Tyrosine hydroxylase (TH) catalyzes the rate-limiting step in the biosynthesis of catecholamine neurotransmitters. TH is a highly complex enzyme at mechanistic, structural, and regulatory levels, and the preparation of kinetically and conformationally stable enzyme for structural characterization has been challenging. Here, we report on improved protocols for purification of recombinant human TH isoform 1 (TH1), which provide large amounts of pure, stable, active TH1 with an intact N-terminus. TH1 purified through fusion with a His-tagged maltose-binding protein on amylose resin was representative of the iron-bound functional enzyme, showing high activity and stabilization by the natural feedback inhibitor dopamine. TH1 purified through fusion with a His-tagged ZZ domain on TALON is remarkably stable, as it was partially inhibited by resin-derived cobalt. This more stable enzyme preparation provided high-quality small-angle X-ray scattering (SAXS) data and reliable structural models of full-length tetrameric TH1. The SAXS-derived model reveals an elongated conformation (D_{max} = 20 nm) for TH1, different arrangement of the catalytic domains compared with the crystal structure of truncated forms, and an N-terminal region with an unstructured tail that hosts the phosphorylation sites and a separated Ala-rich helical motif that may have a role in regulation of TH by interacting with binding partners.

Tyrosine hydroxylase (TH, 1.14.16.2) catalyzes the conversion of L-tyrosine (L-Tyr) to L-3,4-dihydroxyphenylalanine (L-DOPA), which is the rate-limiting step in the synthesis of the catecholamine neurotransmitters and hormones dopamine (DA), noradrenaline, and adrenaline[1]. TH requires an enzyme-bound non-heme ferrous iron (Fe^{2+}), 6*R*-tetrahydrobiopterin (BH_4) as cofactor, and molecular oxygen (O_2) as additional substrate for catalysis[1]. Mutations in TH lead to the disease tyrosine hydroxylase deficiency, and TH is also a marker for the dopaminergic neurons that degenerate in Parkinson's disease[2]. Thus, TH is of considerable scientific interest and a focus of intense research.

TH belongs to the BH_4-dependent aromatic amino acid hydroxylases (AAAH), a family of enzymes that catalyze physiologically and medically important reactions. Phenylalanine hydroxylase (PAH) and tryptophan hydroxylase 1 and 2 (TPH1 and TPH2) are the rate-limiting enzymes in the degradation of excess L-phenylalanine and the production of serotonin, respectively[3]. The three enzymes are homotetramers, with each subunit consisting of a regulatory ACT domain with an unstructured N-terminal tail of different length, a catalytic domain including the iron coordinated to a 2-His-1-carboxylate facial triad motif[4], and an oligomerization domain[3,5]. For PAH, structures of the full-length tetramer from rat were recently solved[6,7] but for TH, only truncated forms are available. These have provided the crystal structure of the catalytic and oligomerization domains (PDB IDs 1TOH and 2XSN)[4] and the NMR structure of the regulatory ACT domain (PDB ID 2MDA)[8] and enabled construction of structural models for full-length TH[3,5,8], which await experimental validation.

A complete understanding of the complex structure, catalytic mechanism, and regulatory properties of TH and other AAAHs requires protein preparations of high homogeneity. The first studies on isolated TH used

[1]Department of Biomedicine, University of Bergen, Bergen, Norway. [2]K.G. Jebsen Centre for Neuropsychiatric Disorders, University of Bergen, Bergen, Norway. [3]Kronstad District Psychiatric Centre, Haukeland University Hospital Bergen, Norway. [4]Centre for Geobiology and Department of Earth Science, University of Bergen, Bergen, Norway and GFZ German Research Centre for Geosciences, Section 3.3, Earth Surface Geochemistry, Telegrafenberg, Potsdam, Germany. [5]Department of Neurology, Haukeland University Hospital, Bergen, Norway. *These authors contributed equally to this work. Correspondence and requests for materials should be addressed to A.M. (email: aurora.martinez@uib.no) or M.I.F. (email: marte.flydal@uib.no)

native enzyme isolated from neuroendocrine tissues, purified as a partially inhibited catecholamine–enzyme complex[9,10], and later strategies have provided recombinant human TH in large quantities as a pure, uninhibited enzyme with high enzymatic activity[11,12]. However, structural investigations of full-length TH have so far been unsuccessful. TH manifests inherent kinetic and conformational instability, which is partly counteracted by the binding of regulatory catecholamines[13,14].

Recombinant proteins often aggregate either during expression and purification, or upon storage and handling at high concentrations. A common strategy to reduce aggregation is to fuse the target protein to a more stable protein, which is removed by specific proteases in the last step of the purification. In this respect, not only the yield and purity, but also properties such as solubility, conformation, and toxicity of the protein of interest may be dependent on the chosen fusion partner[15]. Nakashima *et al.* expressed TH with maltose-binding protein (MBP) as an N-terminal fusion partner already in 1991[16]. However, they discovered that Factor Xa, the protease required to separate fusion partners in the pMAL system, also cuts within the N-terminus of TH. Higgins *et al.* circumvented this problem by using a tobacco etch virus (TEV) protease-cleavable MBP-TH variant[17]. However, compared to other published data on recombinant TH[11,18], they obtained an enzyme with low activity.

Since Nagatsu *et al.* first isolated TH, it has been known that the addition of Fe^{2+} stimulates TH activity[1]. Native TH has been reported to contain significant amounts of iron (0.66 mol/mol TH subunit) and zinc (0.13 mol/mol TH subunit) when isolated from bovine adrenal medulla[10], or up to 1 mol iron/mol TH subunit when isolated from rat pheochromocytoma (PC12) cells[19]. The use of buffers containing 1 mM ethylenediaminetetra-acetic acid (EDTA) provided recombinant TH largely as an apoenzyme, with a metal content reported to be as low as 0.04 mol iron and 0.02 mol zinc per mol of TH[11]. The requirement of TH for Fe^{2+} for catalytic activity, associated to the formation of the reactive Fe(IV) = O hydroxylating intermediate[20], appears absolute, and TH activity is inhibited by other divalent metals, such as Zn^{2+}, Co^{2+} and Ni^{2+}[11]. The absolute requirement for iron also applies to the important regulatory function of DA. DA, produced by DOPA decarboxylase from L-DOPA, and the other downstream catecholamines noradrenaline and adrenaline act as feedback inhibitors of TH by coordinating directly to the iron and inhibiting catalysis. Recently, the importance of the concomitant stabilizing effect of DA has also been shown to be crucial for the correct localization of TH in the brain[18].

In the current study, we aimed to produce stable, homogeneous preparations of recombinant human TH isoform 1 (TH1) for structural investigations. Of the four human TH isoforms, originated by alternative splicing (TH1-TH4), TH1, which is very abundant in brain and aligns well with rodent TH, is the one customarily used in *in vitro* investigations[21]. We present strategies that resulted in two preparations of TH1, expressed from pET-1a vectors, with improved stability and homogeneity. These are thus more suitable for both functional and structural studies compared to TH1 expressed without a fusion partner[22]. Interestingly, the most stable preparation was a partly inhibited enzyme that contains cobalt in the active site. These purification strategies resulted in TH1 samples that provided high-quality small-angle X-ray scattering (SAXS) data and allowed the construction of structural models for the full-length enzyme.

Results

Cloning, expression, and purification of TH1 with different partners. We tested and compared recombinant human TH1 expressed without fusion partner and purified on Heparin Sepharose (TH1(Ctrl); Fig. 1a)[11] with TH1 expressed as fusion proteins. The original TH1(Ctrl) preparations, with a flexible, unprotected N-terminal tail during expression, often show heterogeneity in the N-terminus and variable stability between different purifications. We therefore designed constructs for expressing TH1 fused *via* a TEV protease site to either His_6-ZZ – with ZZ being a synthetic IgG-binding domain – or to His_6-MBP. These were purified on TALON metal affinity resin *via* their His_6-tags and, in the case of His_6-MBP-TH1, also on amylose resin. The yield from TALON was higher for His_6-ZZ-TH1 than for His_6-MBP-TH1 so we preferred the former for purifications on TALON and the latter for purification on amylose resin (Fig. 1). Cleaved fusion proteins were centrifuged to remove insoluble aggregates and subjected to gel filtration to separate tetrameric TH1 from soluble aggregates and cleavage products (fusion partner and TEV protease). We observed a markedly higher proportion of soluble aggregates for TH1(MBP) than for TH1(ZZ) (Fig. 1b). Edman analysis confirmed that both TH1 proteins have an identical and complete N-terminus (Fig. 1a). Although not as good as for TH1(Ctrl), the yield of TH1(MBP) and TH1(ZZ) was still sufficiently high (4–6 mg/L culture, when using autoinduction medium).

TH activity and time-dependent inactivation of TH1. In order to determine if the activity of TH1 is affected by the used purification strategies, we measured the specific activity of the preparations using a standard reaction mixture both with and without 10 μM Fe^{2+}. Addition of Fe^{2+} is customarily used in TH activity assays to ensure that maximal activity is reached[11]. As expected, the activity was higher upon addition of iron, notably for TH1(Ctrl) and TH1(MBP). Under the standard activity assay conditions, with Fe^{2+} added, TH1(MBP) showed the largest activity, followed by TH1(Ctrl) and TH1(ZZ) (Fig. 2a). However, when time-dependent loss of activity was measured upon incubation of the enzyme at 37 °C, both TH1(Ctrl) and TH1(MBP) lost >50% of their initial activity after 5 h and ≥80% after 24 h. Surprisingly, TH1(ZZ) maintained >50% of its activity up to 24 h (Fig. 2b).

Thermal stability of TH1. The conformation and thermal stability of TH1(ZZ) and TH1(MBP) were investigated by circular dichroism (CD) spectroscopy. The far-UV spectra (Fig. 3a, inset) showed local minima at 208 and 222 nm, characteristic of a well-folded helical structure. The estimated α-helical content ranged between 35% and 41% and correlated well with reported values for TH1(Ctrl) (Table 1)[23]. Thermal unfolding experiments provided the midpoint melting temperature (T_m) after normalization and fitting of the profiles to a two-state model (Fig. 3a, Table 1). The results revealed that both TH1(ZZ) and TH1(MBP) were more stable than the control TH1, but surprisingly, the T_m of TH1(ZZ) was almost 3 °C higher than that of TH1(MBP) (Table 1).

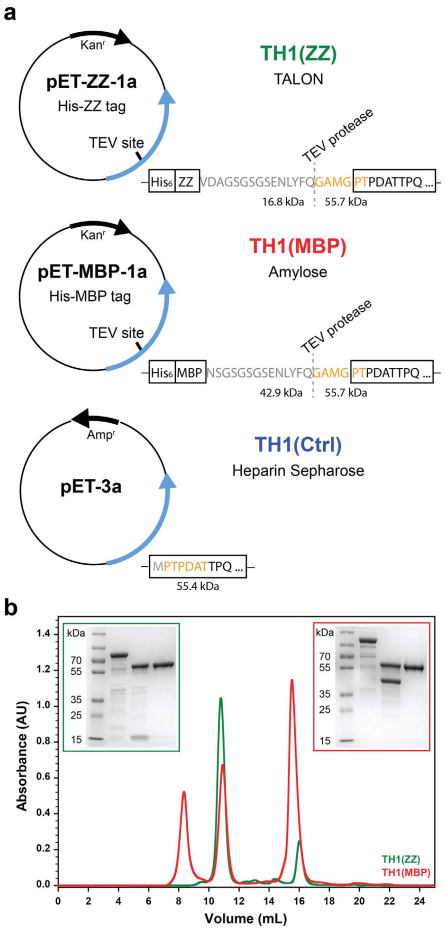

Figure 1. The three TH1 preparations. (**a**) Simplified illustration of vector constructs used in this study, leading to the following TH1 forms: TH1(ZZ) purified on TALON resin as His_6-ZZ-TH1 and cleaved by TEV protease (green), TH1(MBP) purified on amylose resin as His_6-MBP-TH1 and cleaved by TEV protease (red) and TH1(Ctrl) purified on Heparin Sepharose (blue). Open reading frames for ampicillin (Amp) or kanamycin (Kan) resistance genes and TH1 fusion proteins are shown as arrows, and cleavage sites for proteases are indicated. Amino acids of the N-termini revealed by Edman analysis are highlighted in orange. (**b**) Analytical gel filtration chromatogram of TH1(ZZ) (green) and TH1(MBP) (red) on a Superdex 200 Increase 10/300 column. The elution profile illustrates the separation of aggregates, tetrameric TH1 and the other cleavage products (fusion partner and TEV protease). Insets: SDS-PAGE of 2 μg purified protein. Lane 1: prestained protein ladder; lane 2: fusion protein; lane 3: cut fusion protein; lane 4: purified TH1.

Aggregation propensity of TH1(ZZ) and TH1(MBP). As a further characterization of the improved recombinant TH1 forms, we applied dynamic light scattering (DLS) to investigate how the hydrodynamic diameter of TH1(ZZ) and TH1(MBP) changed as a function of temperature. The intensity size distribution in DLS showed two populations at 5 °C for both TH1 preparations (Fig. 3b, inset), a large population of TH1 with a diameter of ~15 nm, and a smaller one of ~105 nm. The former value corresponds well to the expected diameter of TH in tetrameric structural models[3], whereas the population with a larger diameter points to soluble oligomeric aggregates. On the other hand, the volume size distribution obtained from the DLS scans at 5 °C revealed single populations with an apparent hydrodynamic diameter of 11.9 ± 1.2 nm and 13.2 ± 1.4 nm for TH1(ZZ) and TH1(MBP), respectively (Fig. 3b). This result indicates that the highly scattering aggregates detected in the size distribution profiles are only present in tiny amounts. DLS thermal scans showed a lower aggregation propensity for TH1(ZZ) than for TH1(MBP) (Fig. 3c), supporting the results from gel filtration chromatography of

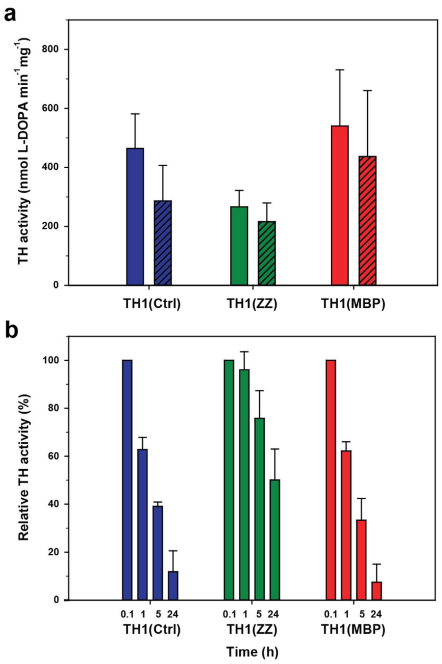

Figure 2. The activity of the TH1 preparations. (**a**) Specific TH1 activity of TH1(Ctrl) (blue), TH1(ZZ) (green) and TH1(MBP) (red), with (closed bars) and without (hatched bars) addition of 10 μM Fe^{2+} in the assay. The data represent the mean ± combined SD of at least four independent measurements each performed in triplicates. (**b**) Remaining TH1 activity (% of initial activity) as a function of pre-incubation time. The activity of TH1(Ctrl) (blue), TH1(ZZ) (green), and TH1(MBP) (red) was measured with 50 μM L-Tyr and 200 μM BH_4 after 5 min, 1 h, 5 h and 24 h pre-incubation at 37 °C, pH 7.0. The data represent the mean ± combined SD of two independent measurements where each data set was performed in triplicates and normalized to the initial activity (5 min pre-incubation).

cleaved fusion proteins (Fig. 1b) and the higher thermal stability for TH1(ZZ) measured by thermal scanning CD (Fig. 3a).

Metal content in TH1 preparations. As a part of the characterization of the physicochemical properties of TH1(ZZ) and TH1(MBP), we investigated their metal content. Both TH1 forms are expressed from similar pET-1a vectors, with the only difference being the fusion partner and the type of affinity resin used during purification, *i.e.* TALON for the purification of TH1(ZZ) and amylose resin for the purification of TH1(MBP). TH1 shows an absolute requirement for iron for catalysis, while other metals have been reported to bind and inhibit TH1, leading to an inability to catalyze L-DOPA formation from L-Tyr[11,24]. As measured by inductively coupled plasma mass spectrometry (ICP-MS), TH1(ZZ) contained almost no iron (0.06 ± 0.07 mol/mol TH1 subunit) compared to TH1(MBP) (0.25 ± 0.18 mol/mol TH1 subunit). The specific activity of TH1(ZZ) was lowest, regardless of added Fe^{2+} (Fig. 2a), and resembles the activity of TH1(Ctrl) without added Fe^{2+}, which is largely purified as an apoenzyme. We thus hypothesized that the active site might be occupied by another metal than iron, most probably cobalt, the metal that coordinates to the His tag on the TALON resin. We performed further metal quantifications and did, indeed, observe high amounts of cobalt in TH1(ZZ) (0.70 ± 0.25 mol/mol TH1 subunit), while no cobalt was detected in TH1(MBP).

The origin of the higher stability of TH1(ZZ). In order to investigate whether the unique high stability of TH1(ZZ) (high T_m and low aggregation propensity) is intrinsically associated to the cobalt in the active site, or to its fusion with the ZZ partner during expression and initial purification, we purified His_6-ZZ-TH1 on Heparin Sepharose, following the purification protocol for TH1(Ctrl). This TH1, obtained after cleavage with TEV protease, had thus not been in contact with the cobalt-containing TALON resin during purification and was – as TH1(MBP) – found to be devoid of cobalt. CD-monitored thermal denaturation provided a T_m-value of 50.1 ± 0.6 °C for $TH1(ZZ)_{Heparin\ Sepharose}$ (Fig. 4a), 3 °C higher than the T_m for TH1(Ctrl) but ~5 °C lower than for $TH1(ZZ)_{TALON}$ (Table 1). This shows that the substantial increase in stability of TH1(ZZ) is conferred not by the protein construct itself, but by the purification on TALON metal affinity resin, which most likely releases cobalt to the enzyme preparation.

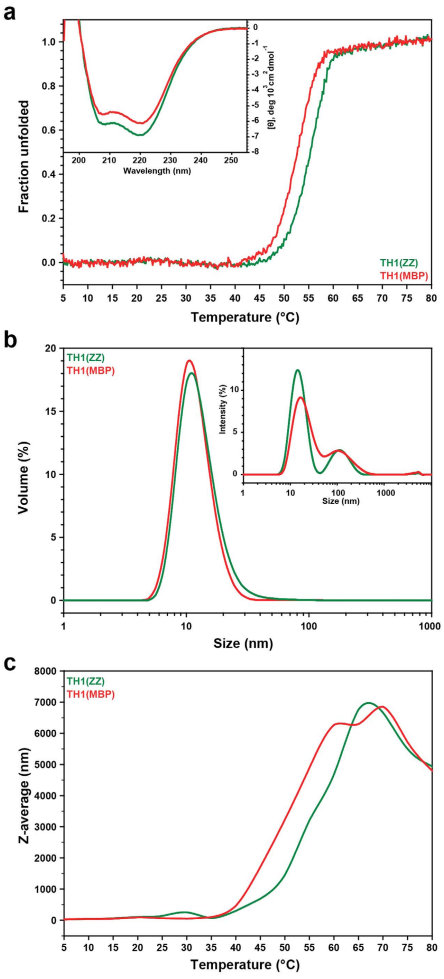

Figure 3. Stability of the TH1 forms. (**a**) CD-monitored (at 222 nm) thermal denaturation of TH1(ZZ) (green) and TH1(MBP) (red). TH1 (4 μM subunit) was in 10 mM Na-HEPES pH 7.0, 100 mM NaCl. The fraction unfolded TH1 data are the mean of six replicates. Inset: Far-UV CD spectra of 4 μM TH1(ZZ) (green) and TH1(MBP) (red) at 5 °C in 10 mM Na-HEPES pH 7.0, 100 mM NaCl. The data represent the mean of six replicates. T_m values and estimated α-helical content are summarized in Table 1. (**b**) DLS size distribution of TH1. Volume size distribution of TH1(ZZ) and TH1(MBP) at 5 °C in 10 mM Na-HEPES pH 7.0, 100 mM NaCl. Inset: Intensity size distribution at 5 °C. The DLS data represent the mean of three replicates. (**c**) DLS thermal stability of TH1(ZZ) and TH1(MBP). DLS thermal scans of TH1(ZZ) (green) and TH1(MBP) (red), both with 18 μM subunit in 10 mM Na-HEPES pH 7.0, 100 mM NaCl.

	Circular dichroism	
	α-helix content (%)	T_m (°C)
TH1(Ctrl)	42 ± 2[23]	47[23]
$TH1(ZZ)_{TALON}$	39.8 ± 9.1	55.1 ± 0.6
TH1(MBP)	34.9 ± 4.8	52.5 ± 0.3
$TH1(ZZ)_{Heparin\ Sepharose}$	40.7 ± 13.8	50.5 ± 0.3

Table 1. Alpha-helical content and thermal stability of the different TH1 constructs. In all cases, n = 6.

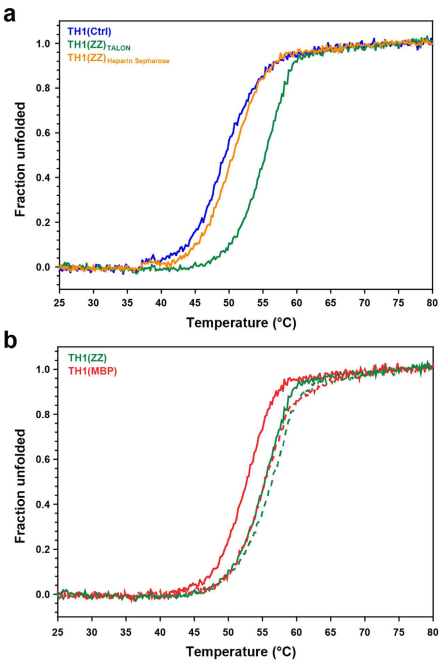

Figure 4. Effect of purification on metal affinity resin on TH1 stability. CD-monitored (at 222 nm) thermal denaturation of TH1 (4 μM subunit) in 10 mM Na-HEPES pH 7.0, 100 mM NaCl. (**a**) TH1 purified as a His_6-ZZ fusion, either on TALON ($TH1(ZZ)_{TALON}$, green) or on Heparin Sepharose ($TH1(ZZ)_{Heparin\ Sepharose}$, orange). The denaturation profile for control TH1 purified without fusion partner is also shown (TH1(Ctrl), blue). The data represent the mean of six replicates. (**b**) TH1(ZZ) purified on TALON and TH1(MBP), both in the absence (solid line) and presence (dotted line) of twice the stoichiometric amounts of DA (8 μM). The data represent the mean of four replicates.

Dopamine binding. An important regulatory mechanism for TH is the binding of DA to the iron in the active site that both inhibits and stabilizes TH[9,13,14]. Although TH1(ZZ) has desirable properties with regards to stability, TH1 used for functional studies must be properly regulated. Therefore, we tested whether our improved TH1 proteins can bind and be stabilized by DA using CD-monitored thermal denaturation. The T_m for TH1(MBP), as also recently shown by Korner *et al.* using differential scanning fluorimetry[18], increased by approximately 3 °C upon the addition of 8 μM DA, *i.e.* a saturating concentration based on the IC_{50} of 1.9 μM for DA[25]. The T_m of DA-bound TH1(MBP) is similar to that of purified Co-bound TH1(ZZ), which was only slightly stabilized by DA (≤1 °C) under similar conditions (Fig. 4b).

The SAXS solution structure of full-length TH1. Based on the good conformational properties of TH1(MBP) and TH1(ZZ), we expected that these enzyme forms would be amenable to structural characterization and proceeded to perform synchrotron SAXS measurements. Due to its higher stability, we argued that TH1(ZZ) was the most promising candidate for further structural studies. Indeed, several preparations of this sample were tested that presented little aggregation or radiation damage. While both TH1(MBP) and TH1(ZZ) provided similar scattering curves, notably TH1(MBP) presented some aggregation (see Supplementary Fig. S1). SAXS data collection and parameters obtained for TH1(ZZ) are shown in Table 2. These data were used for modelling of the full-length solution structure of TH1. The MW based on forward scattering confirmed the presence of a tetramer, with an experimental radius of gyration $R_g = 4.74 \pm 0.33$ nm and a maximum interatomic distance $D_{max} = 20$ nm, indicating an elongated shape. This conformation is supported by both the distance distribution function (Fig. 5a) and *ab initio* modelling. The chain-like *ab initio* shape, built using the expected P222 symmetry, shows approximate dimensions of 17 × 9 × 9 nm, with a dense equatorial core, corresponding to the catalytic and oligomerization domains, and two smaller densities on each side of the core, extending out into the solvent (see Supplementary Fig. S2).

To obtain a more detailed structure of the complex we employed a multiscale modelling protocol using (1) components determined previously from crystallography and NMR, (2) homology modelling, and (3) protein structure folding through molecular simulations. These components were combined through SAXS-based simulated annealing protocols (see Methods). The 70-amino-acid N-terminal sequence was divided into three segments: (1) residues 1–35, (2) residues 36–44, and (3) residues 45–70. Residues 1–35 were modelled *ab initio*

SAXS analyses	
Data-collection parameters	
Instrument	P12 beam line (PETRA-III, DESY)
Wavelength (nm)	0.124
s range (nm^{-1})	0.02–4.8
Exposure time (s)	0.045
Concentration range (mg/mL)	0.5–2.0
Temperature (°C)	20
Structural parameters	
I(0) (relative) [from $p(r)$]*	63,360.0
R_g (nm) [from $p(r)$]	4.93
I(0) (relative) [from Guinier]*	62,494.4 ± 124.65
R_g (nm) [from Guinier]	4.74 ± 0.33
D_{max} (nm)	20.0
Porod volume estimate (nm^3)	519.79
Dry volume of a monomer calculated from sequence (nm^3)	67.56
Molecular mass determination	
Molecular mass M_r (kDa) [from I(0) using $p(r)$]	287.8
Molecular mass M_r (kDa) [from I(0) using Guinier]	283.8
Calculated monomeric M_r from sequence	55.8
Software employed	
Primary data reduction	PRIMUS
Data processing	PRIMUS
Ab initio analysis	GASBOR
Validation and averaging	PRIMUS
Rigid-body modelling	BUNCH
Computation of model intensities	CRYSOL
Three-dimensional graphics representation	PyMOL

Table 2. SAXS data-collection and scattering-derived parameters. *After normalization to a concentration of 1 mg/mL.

during the simulated annealing protocol of the full complex using BUNCH[26]. Residues 36–44 contain a motif that aligns well with the corresponding residues in PAH (see Supplementary Fig. S3). Since these residues are resolved in the PAH crystal structure[27], we used homology modelling to obtain coordinates for this segment in TH. Residues 45–70 contain an Ala-rich segment, which we suspected could obtain a folded structure due to the ability of poly-Ala peptides to form α-helices. This Ala-rich N-terminal segment (Ala45-Ala70) was issued to extensive replica exchange molecular dynamics (REMD) simulations to explore a likely three-dimensional structure (see Methods). Cluster analysis based on pairwise structural deviations grouped the 10,000 conformations into five distinct clusters. 9,572 of the 10,000 conformations were grouped into one major cluster (cluster 1) dominated by members with high α-helix propensity and a compact structure with a mean R_g of 0.88 nm (SD = 0.06 nm). A majority of the cluster members showed an α-helix at residues Lys47-Ala56 (see Supplementary Fig. S4). In contrast, the remaining 428 conformations (clusters 2–5) showed a more elongated configuration with a mean R_g of 1.44 nm (SD = 0.21 nm), also showing several members with an α-helix in the same region as for cluster 1. The cluster representative from cluster 1 contains an α-helix from Lys47 to Ala58 and a random coil from Val60 to Ala70. This configuration is in agreement with secondary structure predictions using PSIPRED[28], which suggest Arg46-Ala59 to be an α-helix. This fragment of the N-terminal segment was connected to the ACT domains for SAXS-based rigid body modelling.

SAXS-based rigid body modelling was performed with BUNCH using P222 symmetry with the subunit chain built up from residues 1–35 (unstructured); residues 36–44 covering over the active site of the catalytic domains modelled through homology with equivalent residues from PAH[6]; residues 45–70 folded through REMD simulations described above; ACT domains obtained from the NMR structure[8]; the catalytic and oligomerization domains derived from crystallography[4]. The ACT, catalytic domains, and tetramerization domains were connected with flexible linkers allowing these domains to move relative to each other during simulated annealing. The simulations yielded a model with an overall very good fit to the raw SAXS data with χ^2 of 1.55 (Fig. 5b). The model shows a tetramer, in which the catalytic domains orient in a similar way as in the crystal structure (PDB ID 2XSN), but with a tilt between the two dimers, making an out-of-plane tetramer (see Supplementary Fig. S5 for comparison with in-plane configuration in the crystal structure). The ACT domains are oriented above the tetramerization helix bundle, with the N-terminus of each ACT domain pointing towards the corresponding catalytic domain active site.

The importance of the disordered N-terminal tails of the model on the fit to the SAXS data is apparent; removing residues Met1-Ile35 provides a worse fit to the SAXS curves with a χ^2 of 2.0. This supports the notion that the flexible N-terminal tails extend into bulk solvent from the protein core. Furthermore, modelling of TH based on

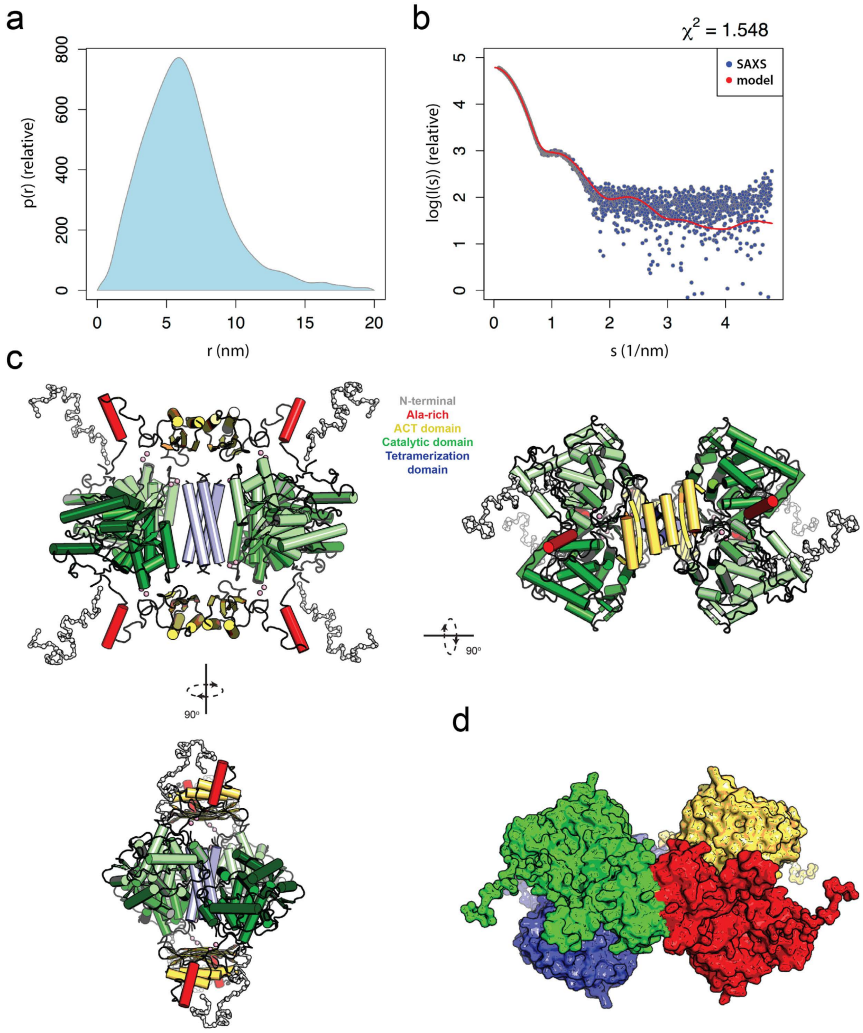

Figure 5. Small-angle X-ray scattering of TH1(ZZ). (**a**) Distance distribution function. (**b**) Raw X-ray scattering data (blue dots) and the fit of the model (red line). (**c**) Model of TH obtained by hybrid modelling shown in three orientations. Coloring depicts the various structural elements and domains of TH1: N-terminal tails (Met1-Asp44); Ala-rich region of N-terminal region (Ala45-Ala70); ACT domain (Val71-Arg156); catalytic domains (Ser157-Asp470); and tetramerization helices (Ser471-Gly497); numbering corresponds to human TH1. (**d**) Model in surface representation with colors representing the four subunits in the complex.

the tetrameric organization of the catalytic and tetramerization domains (as seen in the crystal structures, PDB ID 2XSN and 1TOH) combined with the NMR structures of the dimerized ACT domains (PDB ID 2MDA) without rigid body movements of the catalytic domains and without the N-terminal residues (1–35) gives a suboptimal fit with a χ^2 of 10.5 (Fig. 6a). Including the N-terminal residues improves the agreement with the SAXS data (χ^2 of 5.8; Fig. 6b), but the fit is much worse than for the model with the catalytic domains adjusted (out-of-plane as shown in Fig. 5). Fitting was also inadequate when the dimerized ACT domains were substituted by separated ACT domains, as encountered in the recently solved crystal structure of inactivated PAH (PDB ID 5DEN)[6] (Fig. 6c). Also in this case a large increase in χ^2 is observed (to 7.83), supporting our SAXS-derived model.

SAXS measurements were also carried out with TH1(MBP) in order to analyze the structural effects of DA binding. The results in the absence and presence of DA indicate that DA binding does not induce large conformational changes in TH1 (see Supplementary Fig. S1), in agreement with H/D exchange studies showing that DA binding mainly affects the N-terminus and some residues close to the active site[29].

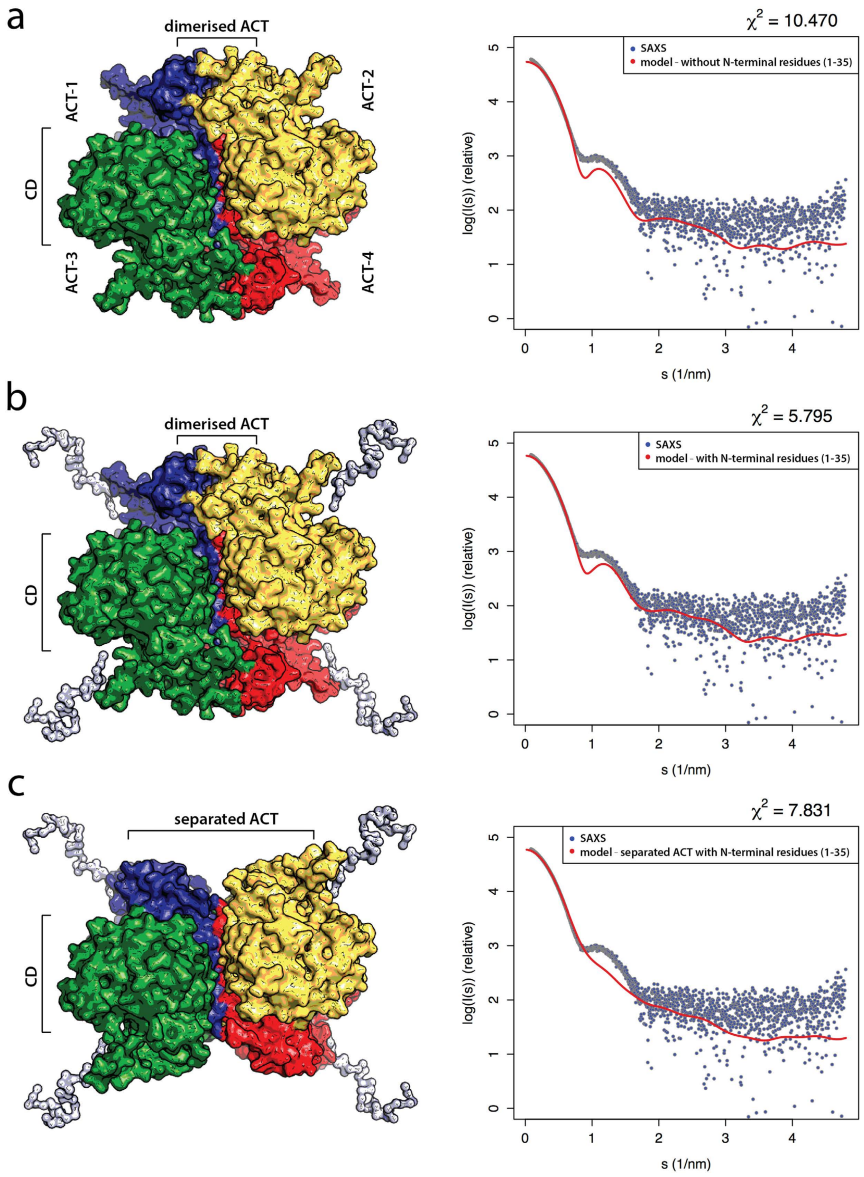

Figure 6. Evaluation of models. The models were evaluated using the tetrameric organization of catalytic domains (CD) as seen in the crystal structures (shown for human TH, PDB ID 2XSN) combined with dimerized ACT domains without (**a**) and with (**b**) N-terminal residues (1–35). These models without adjusting the positions of the CD provide χ^2 values of 10.5 and 5.8, respectively. The model with ACT domains separated (**c**) shows a clear difference in the SAXS profile.

Discussion

Improved TH1 purifications. The preparations of TH1 characterized in this work show differences in TH1 activity and thermal stability depending on the choice of fusion partner and/or type of affinity chromatography resin. Compared to the control TH1, which has no fusion partner and is purified on Heparin Sepharose, our new preparations have higher thermal stability and are less prone to aggregation, most likely due to a more homogeneous N-terminal region. The N-terminal tail of TH1 is very flexible, and residues 1-43 were shown to have a

disordered conformation by solution NMR[8], CD, and molecular dynamics simulations[30], rendering it vulnerable to proteolytic degradation. To overcome this problem, we designed several fusion proteins of TH1, all containing the fusion partner at the N-terminal end of TH1. In addition to facilitating purification, the fusion partner MBP can enhance solubility and promote folding by acting as a general molecular chaperone. The latter is thought to be due to MBP binding the protein of interest *via* its exposed hydrophobic residues and by MBP recruiting chaperones, like GroEL, present in the *E. coli* host cell[31]. Differently to the case with fusion proteins of MBP with a Factor Xa cleavage site[16], we obtained full-length TH1(MBP) preparations with an intact N-terminus and a high activity from the His_6-MBP-TH1 fusion protein cleaved by TEV protease. This protease is also used with TH1 from pET-ZZ-1a that produces TH1 with His_6-ZZ, a smaller fusion tag of 17 kDa (Fig. 1a). The ZZ fusion may pose less of a metabolic burden on the host cell than the larger fusion partner MBP, and the ZZ domain has also been used to solubilize proteins that tend to aggregate during expression[32], probably explaining the higher yield of TH1 obtained from His_6-ZZ-TH1 than from His_6-MBP-TH1 purified on TALON.

Cobalt-bound TH1(ZZ) is remarkably stable. Although it is generally not recommended to purify metal-containing proteins on metal affinity resins, we have previously successfully purified several bacterial forms of PAH as His_6-tagged fusion proteins on TALON columns[33,34]. One of these was, indeed, purified almost solely as an apoenzyme, but it displayed very high activity upon reconstitution with iron[33]. This was, however, not the case for TH1. The increase in enzymatic activity of TH1(ZZ) purified on TALON upon addition of iron in the assay was not significant and much lower than that observed for both TH1(Ctrl) and TH1(MBP) (Fig. 2a). However, the activity and conformation of TH1(ZZ) show increased thermostability. As measured by ICP-MS, TH1(ZZ) contains cobalt in substantial amounts, and we assumed that the cobalt – originating from the purification resin – is the inhibiting and stabilizing element[24]. The enzyme purified from the same His_6-ZZ-TH1 construct, but on Heparin Sepharose instead of TALON, did not exhibit this increase in stability (Fig. 4a). Indeed, it has also been shown for other metalloenzymes that their cobalt-bound state is more stable than the iron-bound form[35,36]. Although we acknowledge the fact that a cobalt-containing TH1(ZZ) is not suited for specific functional and regulatory studies, its improved stability makes it a promising candidate protein for structural studies of full-length TH1 — a long awaited milestone in the study of this enzyme. For functional studies, we may prefer to use TH1(MBP), an enzyme that presents high specific activity, a homogeneous N-terminus, and stabilization by the natural end-product inhibitor DA.

The SAXS-derived structure of full-length TH1. We obtained the first experimental three-dimensional structure of full-length tetrameric TH1 by SAXS using TH1(ZZ) preparations. The SAXS structure resembles that of structural models of TH1 prepared recently based on combinations of crystal and NMR structures of the different domains[3,8]. Nevertheless, whereas the crystal structure of tetrameric catalytic and oligomerization domains presents all four catalytic domains in-plane[4], the SAXS data fit best to a model in which the catalytic domains are out-of-plane (see Supplementary Fig. S5). Structural differences between solution and crystalline states have been reported for several proteins[6,7,37]. For instance, the recent solution structure of PAH[7] revealed a V-shaped asymmetry in the tetramer that adds to the asymmetry in the dispositions of the domains that is already encountered in the crystal structures of tetrameric PAH[6,38] and that has been interpreted to be related to the flexible nature of an allosteric tetramer that shows positive cooperativity for its substrate[7]. Despite devoid of the positive cooperativity for its substrate, characteristic of PAH[3,5], allosteric effects of the natural BH_4 cofactor on TH activity have been described, including both positive cooperativity that is counteracted by DA neurotoxin[39], as well as negative cooperativity[40], which might also been related to allosteric and/or regulatory conformational changes in TH.

Even though TH and PAH have a very similar geometry and size with respect to the core ACT, catalytic and regulatory domains, the dimensions of TH1 and PAH are rather different. TH1 adopts a more elongated shape ($R_g = 4.74 \pm 0.33$ nm, $D_{max} = 20$ nm) than full-length PAH ($R_g = 4.05$ nm, $D_{max} = 11.7$ nm)[6], which is only 10% smaller in MW than TH1, revealing the large impact of the unstructured N-terminal region on the shape of TH1 (Fig. 5). Our SAXS-based structure contributes to the structural and functional understanding of TH and complements previous models by including the modelled N-terminal region (residues 1–70; see Supplementary Fig. S3). Previous conformational studies using the isolated 1-43 residues from the N-terminal tail have shown that it presents intrinsic disorder, but that it has a tendency to adopt α-helical secondary structure, *e.g.* upon interaction with membranes[30]. This mobile and unstructured tail is the part of TH1 that contains the phosphorylation sites Thr8, Ser19, Ser31, and Ser40 that regulate activity and interactions with partners[21,41]. Interestingly, the modelled structure maintains Ser40 close to the entrance of the active site, at a suitable distance to interact with DA and other catecholamines, and to contribute to the high-affinity binding of these feedback inhibitors, an interaction that is released upon Ser40 phosphorylation by cAMP dependent protein kinase[42]. Furthermore, the SAXS model reveals an arrangement of the N-terminal tail pointing out from the globular domains, which is in agreement with the site of binding of the 14-3-3γ protein in the phosphoSer19-TH:14-3-3γ complex, as observed by EM[43]. Actually, the Ala-rich motif also appears as a well-located docking interface for partner protein interactions that may modulate the localization, function and stability of TH. Recently, affinity capture-MS data on the human interactome has revealed a large number of protein-protein interactions of TH, as expected for a tightly regulated enzyme[44] and the present structural model of the N-terminal region of TH certainly shows features compatible with a multi-partner protein. Finally, the SAXS data and derived model validate a dimeric disposition of the ACT domains (Fig. 6c). A recent study has also shown that the ACT domains of TPH1 form a structural homodimer, indicating that a dimeric arrangement of adjacent domains may also be a feature in the full-length TPH[45]. This is similar to the arrangement found for PAH only when it is activated by its substrate L-Phe. In the inactivated PAH the ACT domains do not interact with one another and transition to dimeric state is associated to activation by L-Phe[6,7]. Neither TH nor the TPHs are activated by their substrates and thus such a monomer-dimer exchange

may not take place in these hydroxylases. Importantly, a dimerized configuration of the regulatory domains seems to provide increased stability[45].

In conclusion, we present the preparation of highly pure, stable forms of full-length TH1. TH1(MBP) shows a high activity level, is activated by Fe^{2+}, and is stabilized by regulatory DA, but it is less stable than TH1(ZZ). On the other hand, TH1(ZZ) is stabilized by cobalt, which largely inhibits its activity but protects the enzyme from denaturation and aggregation. This preparation allowed the characterization of the structural organization of full-length TH by SAXS, which has until now been hindered, most likely by the low stability and large heterogeneity in earlier TH preparations. The SAXS-derived structure presents full-length TH with dimeric ACT domains and an elongated conformation due to a large influence of the unstructured N-terminal region compared with PAH. This long N-terminal region (residues 1–70) is important for regulation of TH by phosphorylation and for interaction with partners.

Methods

Cloning strategies. The pET-TH expression vector, generated by Le Bourdellès *et al.*[22] by cloning the *TH1* cDNA into pET-3a, was used as a basis for constructing other expression vectors. Insertion of *TH1* into both pET-ZZ-1a and pET-MBP-1a was performed by PCR using the primers 5′- GCTTCCATGGGACCCACCCCCGA-3′ and 5′-GCTTGGTACCCAGTGCAGGACCA-3′ and the restriction enzymes NcoI and Acc65I, resulting in an extra glycine residue in position 2 and the residues glycine and alanine in front of the starting methionine after removal of the fusion partner. Correct sequences were verified by sequencing.

Expression and purification of recombinant TH1 proteins. TH1 protein variants were overexpressed in *E. coli* BL21-CodonPlus(DE3)RIL. Briefly, cells were grown at 28 °C and 200 rpm in LB medium with 1 mM isopropyl β-D-thiogalactoside added for induction at an OD_{600nm} of 0.6 for 6 h, or in autoinduction medium for 24 h, supplemented with 0.2–1 mM Fe^{2+} (as ferrous ammonium sulfate) and the appropriate antibiotic (Fig. 1a). Fusion proteins were purified at 4 °C using the appropriate affinity chromatography resin (Fig. 1a). The equilibration and wash buffers used were 20 mM Na-HEPES pH 7.0, 200 mM NaCl for amylose resin, 20 mM Na-phosphate pH 7.0, 300 mM NaCl, 15 mM imidazole for TALON® Superflow™ Metal Affinity Resin, and 20 mM Tris-HCl pH 7.5, 1 mM EDTA, 1 mM dithiothreitol (DTT), 5% sucrose (w/v) with Heparin Sepharose. Bacterial cells were disrupted by sonication (3 × 45 s pulses at 20% power) or French press in buffers with 1 mM phenylmethanesulfonyl fluoride, 10 mM benzamidine and cOmplete™ EDTA-free Protease Inhibitor Cocktail. The clarified extract was applied to the resin at 1–2 mL/min. After washing, bound proteins were eluted using wash buffers with either 15 mM maltose (amylose resin), 135–250 mM imidazole (TALON Superflow resin), or 0.5 M NaCl (Heparin Sepharose). Imidazole was removed from eluted fractions by buffer exchange.

The fusion protein, incubated with TEV protease[46] at 4 °C for 1–3 h, was loaded into a HiLoad™ Superdex™ 200 prep grade column (1.6 cm × 60 cm) to purify soluble tetrameric TH1 or into a Superdex 200 Increase GL column (1.0 cm × 30 cm) for analytical purposes. Protein concentration was measured at 280 nm, using the theoretical molar extinction coefficient of 40,715 M^{-1} cm^{-1}.

N-terminal sequencing. N-terminal sequencing was performed by the Proteome Factory AG (Berlin, Germany), using Edman analysis. Samples were prepared according to standard protocols for semidry blotting on a polyvinylidene difluoride membrane. TH1(Ctrl), TH1(ZZ), and TH1(MBP) samples (Fig. 1a) were sequenced with 5 steps to determine a 5-amino-acid sequence.

TH activity assay. TH activity was measured as described[11] with minor modifications. Briefly, TH1 (0.1 mg/mL, 1.8 μM subunit) was pre-incubated with 1% BSA (w/v) in 20 mM Na-HEPES pH 7.0, 200 mM NaCl on ice. 5 μL aliquots were incubated for 1 min in a standard reaction mixture containing 50 μM L-Tyr, 0.1 mg/mL catalase, and 10 μM Fe^{2+} in 40 mM Na-HEPES pH 7.0, or in this mix without Fe^{2+}. The reaction was started by adding 200 μM BH_4 in 2 mM DTT, stopped after 5 min with 2% acetic acid in ethanol (v/v), frozen at -20 °C for at least 30 min, and centrifuged for 15 min at 4 °C and 18,000 × g. The amount of L-DOPA was measured in the supernatants by high-performance liquid chromatography analysis with fluorescence detection, as described[47]. For the time-dependent TH activity assay, the pre-incubation was at 37 °C and included 1 μM Fe^{2+}, and aliquots were taken out after 5 min, 1 h, 5 h, and 24 h and measured in the standard reaction mix.

Circular dichroism spectroscopy. CD measurements were performed on a Jasco J-810 spectropolarimeter equipped with a CDF-426S Peltier element for temperature control. Far-UV CD spectra between 180–260 nm were acquired at 5 °C by using 0.2 nm data pitch, 2 nm band width, 20 nm/min scan speed, and accumulation of 4 spectra. CD spectra of TH1 (4 μM subunit) in a 1 mm quartz cell were acquired in 10 mM Na-HEPES pH 7.0, 100 mM NaCl. Baseline buffer spectra were subtracted. Thermal denaturation of TH1 (4 μM subunit) was recorded from 5 to 80 °C at 222 nm with a scan rate of 2 °C/min and 0.2 °C data pitch. DA binding to TH1(ZZ) and TH1(MBP) was tested by adding twice the stoichiometric amount of DA. All thermal scans were normalized, fitted to a two-state unfolding model[48], and further converted to fraction of unfolded protein as described[49]. CDNN[50] was used to estimate secondary structure content.

Dynamic light scattering. DLS was performed on a Malvern Zetasizer Nano ZS instrument, using a HeNe laser at 633 nm and a fixed scattering angle of 173° (back scatter). Temperature scans were recorded from 5 to 80 °C, with a temperature interval of 5 °C. TH1 preparations were diluted to 1 mg/mL (18 μM subunit) in 10 mM Na-HEPES pH 7.0, 100 mM NaCl. Data analysis was performed on intensity and volume size distribution curves and the Z-average size using the Malvern DTS software.

Metal measurements. Iron and cobalt content of the TH1 preparations was measured by ICP-MS with a microwave digestion method. Briefly, TH1 (3 mg/mL, 54 μM subunit) was mixed with ultrapure nitric acid (HNO_3, 60%) and hydrogen peroxide (H_2O_2, 30%) in a 5:5:2 v/v/v ratio. Using the Milestone 1200 MEGA (Sorisole, Italy), complete TH1 digestion was achieved by a six-stage program and a maximum microwave power of 600 W. 20 mM Na-HEPES pH 7.0, 200 mM NaCl and Seronorm™ Trace Elements Serum L-1 (SERO) prepared in the same way were used as blank and quality control of the digestion method, respectively. The digested samples (n = 3 for each TH1 form) were transferred to metal-free tubes and quantitatively further diluted by a factor of 32.6 with Milli-Q water. Sample introduction into the ICP-MS was performed by the SC-FAST (Elemental Scientific) fully automated sample introduction system, in combination with an online internal standard addition of 1 μg/L indium solution to monitor and correct for instrumental fluctuations. Calibration standard solutions were prepared from certified single-element standard solutions (Spectrapure Standards AS). Analysis was done with the Thermo Finnigan Element 2 high-resolution magnetic sector field ICP-MS. The ICP-MS measuring accuracy and calibration curves were monitored by the standard reference material SPS-SW2 (Spectrapure Standards AS).

SAXS measurements. SAXS measurements were carried out on the EMBL P12 synchrotron BioSAXS beamline[51] at PETRA III/DESY, Hamburg, Germany on TH1(ZZ) and TH1(MBP) in 20 mM Na-HEPES pH 7.0, 200 mM NaCl (0.5–2.0 mg/mL, 9–36 μM subunit). DA in stoichiometric amounts compared to an enzyme subunit was added, when indicated. Data were collected at 20 °C using an X-ray wavelength of 0.124 nm and an exposure time of 45 ms/frame. 20 consecutive frames were collected for each sample; the sample was flowing through the capillary during the measurement. Frames were controlled for radiation damage and averaged. The data were recorded using a PILATUS 2M detector (Dectris, Baden, Switzerland) at a sample-detector distance of 3.0 m, covering a momentum transfer range, s ($4\pi\sin\theta/\lambda$) of 0.02–4.8 nm^{-1}, where 2θ is the scattering angle and λ the wavelength and s is in units of nm^{-1}.

Data processing and analysis were carried out using the ATSAS package[52]. Solvent scattering was identically measured from the corresponding buffer before and after each sample, and the average background scattering was subtracted with PRIMUS[53]. R_g was determined using Guinier analysis. The maximum particle dimension D_{max} and the distance distribution function $p(r)$ were calculated using GNOM[54]. Molecular weights were estimated based on forward scattering I(0) from the sample, compared to standard samples of either glucose isomerase or BSA.

Structural modelling. To obtain unbiased shape information for full-length TH1, chain-like models were built *ab initio* using GASBOR[55]. P222 symmetry, as seen in crystal structures of tetrameric species of truncated TH and homologues, was used during modelling.

BUNCH was used for SAXS-based rigid body modelling of TH1, using existing crystal and NMR structures as rigid body subunits interconnected by flexible loops. We divided the TH1 subunit chain into 3 rigid bodies interconnected by flexible loops: (1) the tetramerization helix (coordinates from PDB ID 1TOH[4]); (2) catalytic domain (coordinates from PDB ID 1TOH); (3) ACT domain (atomic coordinates obtained from PDB ID 2MDA[8]). To maintain known interfaces (from the crystal and NMR structures) between domains in the simulated annealing protocol we employed distance restraints between (1) two adjacent ACT domains, (2) two adjacent catalytic domains, and (3) the tetramerization bundle. CRYSOL[56] was subsequently used to calculate the final fit to the experimental SAXS data. P222 symmetry and default values for the simulated annealing protocols in BUNCH were used, with 100 temperature steps and a maximum of 24,850 iterations at each temperature.

The Ala-rich N-terminal segment Ala45-Ala70 upstream from the ACT domain in TH was issued to extensive replica exchange molecular dynamics simulations[57] to obtain a representative three-dimensional structure of this fragment. A linear all-atom model of the fragment was generated using AmberTools, employing the Amber99SB force field[58] and implicit solvent model using generalized born[59]. The replica exchange simulations were run over 20 temperatures spanning from 270 to 509 K. Each replica was heated to its respective starting temperature during 200 ps. The replica exchange simulations consisted of 10,000 exchanges, each of 4 ps (2×10^7 steps for each replica). The simulations were carried out using multisander in the Amber package. The resulting conformations at 300 K were extracted and clustered using cpptraj[60]. The representative structures from the most frequently populated cluster were extracted and included adjacent to the ACT domains in the model prior to the SAXS-based rigid body simulation. Independent of the replica exchange simulation, PSIPRED was used to predict the secondary structure elements in this fragment. The N-terminal residues Gly36-Asp44 of TH1 align well with the equivalent residues of PAH (see Supplementary Fig. S3), with high sequence identity, including the motif [SXIED]. Based on this alignment, the residues Gly36-Ala45 were modelled in TH1 corresponding to the PAH structure (PDB ID 5DEN)[6].

References

1. Nagatsu, T., Levitt, M. & Udenfriend, S. Tyrosine Hydroxylase. The Initial Step In Norepinephrine Biosynthesis. *J. Biol. Chem.* **239,** 2910–2917 (1964).
2. Dauer, W. & Przedborski, S. Parkinson's disease: mechanisms and models. *Neuron* **39,** 889–909, doi: 10.1016/S0896-6273(03)00568-3 (2003).
3. Skjærven, L., Teigen, K. & Martinez, A. Structure-Function Relationships in the Aromatic Amino Acid Hydroxylases Enzyme Family: Evolutionary Insights. *eLS.* doi: 10.1002/9780470015902.a0025581 (2014).
4. Goodwill, K. E. *et al.* Crystal structure of tyrosine hydroxylase at 2.3 A and its implications for inherited neurodegenerative diseases. *Nat. Struct. Biol.* **4,** 578–585, doi: 10.1038/nsb0797-578 (1997).
5. Fitzpatrick, P. F. Structural insights into the regulation of aromatic amino acid hydroxylation. *Curr. Opin. Struct. Biol.* **35,** 1–6, doi: 10.1016/j.sbi.2015.07.004 (2015).

6. Arturo, E. C. *et al.* First structure of full-length mammalian phenylalanine hydroxylase reveals the architecture of an autoinhibited tetramer. *Proc Natl Acad Sci USA* **113,** 2394–2399, doi: 10.1073/pnas.1516967113 (2016).
7. Meisburger, S. P. *et al.* Domain Movements upon Activation of Phenylalanine Hydroxylase Characterized by Crystallography and Chromatography-Coupled Small-Angle X-ray Scattering. *Journal of the American Chemical Society* **138,** 6506–6516, doi: 10.1021/jacs.6b01563 (2016).
8. Zhang, S., Huang, T., Ilangovan, U., Hinck, A. P. & Fitzpatrick, P. F. The solution structure of the regulatory domain of tyrosine hydroxylase. *Journal of molecular biology* **426,** 1483–1497, doi: 10.1016/j.jmb.2013.12.015 (2014).
9. Andersson, K. K., Cox, D. D., Que, L. Jr., Flatmark, T. & Haavik, J. Resonance Raman studies on the blue-green-colored bovine adrenal tyrosine 3-monooxygenase (tyrosine hydroxylase). Evidence that the feedback inhibitors adrenaline and noradrenaline are coordinated to iron. *The Journal of biological chemistry* **263,** 18621–18626 (1988).
10. Haavik, J., Andersson, K. K., Petersson, L. & Flatmark, T. Soluble tyrosine hydroxylase (tyrosine 3-monooxygenase) from bovine adrenal medulla: large-scale purification and physicochemical properties. *Biochimica et biophysica acta* **953,** 142–156, doi: 10.1016/0167-4838(88)90019-2 (1988).
11. Haavik, J., Le Bourdelles, B., Martinez, A., Flatmark, T. & Mallet, J. Recombinant human tyrosine hydroxylase isozymes. Reconstitution with iron and inhibitory effect of other metal ions. *Eur. J. Biochem.* **199,** 371–378 (1991).
12. Nasrin, S., Ichinose, H., Hidaka, H. & Nagatsu, T. Recombinant human tyrosine hydroxylase types 1–4 show regulatory kinetic properties for the natural (6R)-tetrahydrobiopterin cofactor. *Journal of biochemistry* **116,** 393–398 (1994).
13. Martinez, A., Haavik, J., Flatmark, T., Arrondo, J. L. & Muga, A. Conformational properties and stability of tyrosine hydroxylase studied by infrared spectroscopy. Effect of iron/catecholamine binding and phosphorylation. *J. Biol. Chem.* **271,** 19737–19742, doi: 10.1074/jbc.271.33.19737 (1996).
14. Okuno, S. & Fujisawa, H. Conversion of tyrosine hydroxylase to stable and inactive form by the end products. *J Neurochem* **57,** 53–60, doi: 10.1111/j.1471-4159.1991.tb02098.x (1991).
15. Bogomolovas, J., Simon, B., Sattler, M. & Stier, G. Screening of fusion partners for high yield expression and purification of bioactive viscotoxins. *Protein expression and purification* **64,** 16–23, doi: 10.1016/j.pep.2008.10.003 (2009).
16. Nakashima, A., Mori, K., Nagatsu, T. & Ota, A. Expression of human tyrosine hydroxylase type I in Escherichia coli as a protease-cleavable fusion protein. Short communication. *J Neural Transm* **106,** 819–824, doi: 10.1007/s007020050202 (1999).
17. Higgins, C. A., Vermeer, L. M., Doorn, J. A. & Roman, D. L. Expression and purification of recombinant human tyrosine hydroxylase as a fusion protein in Escherichia coli. *Protein expression and purification* **84,** 219–223, doi: 10.1016/j.pep.2012.05.007 (2012).
18. Korner, G. *et al.* Brain catecholamine depletion and motor impairment in a Th knock-in mouse with type B tyrosine hydroxylase deficiency. *Brain* **138,** 2948–2963, doi: 10.1093/brain/awv224 (2015).
19. Dix, T. A., Kuhn, D. M. & Benkovic, S. J. Mechanism of oxygen activation by tyrosine hydroxylase. *Biochemistry* **26,** 3354–3361, doi: 10.1021/bi00386a016 (1987).
20. Eser, B. E. *et al.* Direct spectroscopic evidence for a high-spin Fe(IV) intermediate in tyrosine hydroxylase. *Journal of the American Chemical Society* **129,** 11334–11335, doi: 10.1021/ja074446s (2007).
21. Daubner, S. C., Le, T. & Wang, S. Tyrosine hydroxylase and regulation of dopamine synthesis. *Archives of biochemistry and biophysics* **508,** 1–12, doi: 10.1016/j.abb.2010.12.017 (2011).
22. Le Bourdelles, B. *et al.* Phosphorylation of human recombinant tyrosine hydroxylase isoforms 1 and 2: an additional phosphorylated residue in isoform 2, generated through alternative splicing. *The Journal of biological chemistry* **266,** 17124–17130 (1991).
23. Thorolfsson, M., Doskeland, A. P., Muga, A. & Martinez, A. The binding of tyrosine hydroxylase to negatively charged lipid bilayers involves the N-terminal region of the enzyme. *FEBS letters* **519,** 221–226, doi: 10.1016/S0014-5793(02)02745-X (2002).
24. Ogawa, S. & Ichinose, H. Effect of metals and phenylalanine on the activity of human tryptophan hydroxylase-2: comparison with that on tyrosine hydroxylase activity. *Neuroscience letters* **401,** 261–265, doi: 10.1016/j.neulet.2006.03.031 (2006).
25. Almas, B., Le Bourdelles, B., Flatmark, T., Mallet, J. & Haavik, J. Regulation of recombinant human tyrosine hydroxylase isozymes by catecholamine binding and phosphorylation. Structure/activity studies and mechanistic implications. *Eur. J. Biochem.* **209,** 249–255, doi: 10.1111/j.1432-1033.1992.tb17283.x (1992).
26. Petoukhov, M. V. & Svergun, D. I. Global rigid body modeling of macromolecular complexes against small-angle scattering data. *Biophysical journal* **89,** 1237–1250, doi: 10.1529/biophysj.105.064154 (2005).
27. Kobe, B. *et al.* Structural basis of autoregulation of phenylalanine hydroxylase. *Nat Struct Biol* **6,** 442–448, doi: 10.1038/8247 (1999).
28. Buchan, D. W., Minneci, F., Nugent, T. C., Bryson, K. & Jones, D. T. Scalable web services for the PSIPRED Protein Analysis Workbench. *Nucleic acids research* **41,** W349–357, doi: 10.1093/nar/gkt381 (2013).
29. Wang, S., Sura, G. R., Dangott, L. J. & Fitzpatrick, P. F. Identification by hydrogen/deuterium exchange of structural changes in tyrosine hydroxylase associated with regulation. *Biochemistry* **48,** 4972–4979, doi: 10.1021/bi9004254 (2009).
30. Skjevik, A. A. *et al.* The N-terminal sequence of tyrosine hydroxylase is a conformationally versatile motif that binds 14-3-3 proteins and membranes. *J. Mol. Biol.* **426,** 150–168, doi: 10.1016/j.jmb.2013.09.012 (2014).
31. Costa, S., Almeida, A., Castro, A. & Domingues, L. Fusion tags for protein solubility, purification and immunogenicity in Escherichia coli: the novel Fh8 system. *Front. Microbiol.* **5,** 63, doi: 10.3389/fmicb.2014.00063 (2014).
32. Inouye, S. & Sahara, Y. Soluble protein expression in E. coli cells using IgG-binding domain of protein A as a solubilizing partner in the cold induced system. *Biochem. Biophys. Res. Commun.* **376,** 448–453, doi: 10.1016/j.bbrc.2008.08.149 (2008).
33. Flydal, M. I. *et al.* Phenylalanine hydroxylase from Legionella pneumophila is a thermostable enzyme with a major functional role in pyomelanin synthesis. *PLoS One* **7,** e46209, doi: 10.1371/journal.pone.0046209 (2012).
34. Leiros, H. K. *et al.* Structure of phenylalanine hydroxylase from Colwellia psychrerythraea 34H, a monomeric cold active enzyme with local flexibility around the active site and high overall stability. *J. Neurochem.* **282,** 21973–21986, doi: 10.1074/jbc.M610174200 (2007).
35. Kovacs, J. A. Synthetic analogues of cysteinate-ligated non-heme iron and non-corrinoid cobalt enzymes. *Chemical reviews* **104,** 825–848, doi: 10.1021/cr020619e (2004).
36. Strand, K. R., Karlsen, S. & Andersson, K. K. Cobalt substitution of mouse R2 ribonucleotide reductase as a model for the reactive diferrous state: spectroscopic and structural evidence for a ferromagnetically coupled dinuclear cobalt cluster. *The Journal of biological chemistry* **277,** 34229–34238, doi: 10.1074/jbc.M203358200 (2002).
37. Ferreira-da-Silva, F. *et al.* The crystal and solution structures of glyceraldehyde-3-phosphate dehydrogenase reveal different quaternary structures. *The Journal of biological chemistry* **281,** 33433–33440, doi: 10.1074/jbc.M605267200 (2006).
38. Fusetti, F., Erlandsen, H., Flatmark, T. & Stevens, R. C. Structure of tetrameric human phenylalanine hydroxylase and its implications for phenylketonuria. *The Journal of biological chemistry* **273,** 16962–16967 (1998).
39. Maruyama, W. & Naoi, M. Inhibition of tyrosine hydroxylase by a dopamine neurotoxin, 1-methyl-4-phenylpyridinium ion: depletion of allostery to the biopterin cofactor. *Life sciences* **55,** 207–212 (1994).
40. Flatmark, T. *et al.* Tyrosine hydroxylase binds tetrahydrobiopterin cofactor with negative cooperativity, as shown by kinetic analyses and surface plasmon resonance detection. *Eur J Biochem* **262,** 840–849 (1999).
41. Dunkley, P. R., Bobrovskaya, L., Graham, M. E., von Nagy-Felsobuki, E. I. & Dickson, P. W. Tyrosine hydroxylase phosphorylation: regulation and consequences. *J Neurochem* **91,** 1025–1043, doi: 10.1111/j.1471-4159.2004.02797.x (2004).
42. Wang, S., Lasagna, M., Daubner, S. C., Reinhart, G. D. & Fitzpatrick, P. F. Fluorescence spectroscopy as a probe of the effect of phosphorylation at serine 40 of tyrosine hydroxylase on the conformation of its regulatory domain. *Biochemistry* **50,** 2364–2370, doi: 10.1021/bi101844p (2011).

43. Kleppe, R. *et al.* Phosphorylation dependence and stoichiometry of the complex formed by tyrosine hydroxylase and 14-3-3gamma. *Molecular & cellular proteomics: MCP* **13,** 2017–2030, doi: 10.1074/mcp.M113.035709 (2014).
44. Huttlin, E. L. *et al.* The BioPlex Network: A Systematic Exploration of the Human Interactome. *Cell* **162,** 425–440, doi: 10.1016/j.cell.2015.06.043 (2015).
45. Patel, D., Kopec, J., Fitzpatrick, F., McCorvie, T. J. & Yue, W. W. Structural basis for ligand-dependent dimerization of phenylalanine hydroxylase regulatory domain. *Scientific reports* **6,** 23748, doi: 10.1038/srep23748 (2016).
46. van den Berg, S., Lofdahl, P. A., Hard, T. & Berglund, H. Improved solubility of TEV protease by directed evolution. *Journal of biotechnology* **121,** 291–298, doi: 10.1016/j.jbiotec.2005.08.006 (2006).
47. Haavik, J. & Flatmark, T. Rapid and sensitive assay of tyrosine 3-monooxygenase activity by high-performance liquid chromatography using the native fluorescence of DOPA. *Journal of chromatography* **198,** 511–515, doi: 10.1016/S0021-9673(00)80522-1 (1980).
48. Swint, L. & Robertson, A. D. Thermodynamics of unfolding for turkey ovomucoid third domain: thermal and chemical denaturation. *Protein science: a publication of the Protein Society* **2,** 2037–2049, doi: 10.1002/pro.5560021205 (1993).
49. Agashe, V. R. & Udgaonkar, J. B. Thermodynamics of denaturation of barstar: evidence for cold denaturation and evaluation of the interaction with guanidine hydrochloride. *Biochemistry* **34,** 3286–3299, doi: 10.1021/bi00010a019 (1995).
50. Bohm, G., Muhr, R. & Jaenicke, R. Quantitative analysis of protein far UV circular dichroism spectra by neural networks. *Protein Eng* **5,** 191–195, doi: 10.1093/protein/5.3.191 (1992).
51. Blanchet, C. E. *et al.* Versatile sample environments and automation for biological solution X-ray scattering experiments at the P12 beamline (PETRA III, DESY). *J. Appl. Cryst.* **48,** 431–443, doi: 10.1107/S160057671500254X (2015).
52. Petoukhov, M. V. *et al.* New developments in the program package for small-angle scattering data analysis. *J. Appl. Cryst.* **45,** 342–350, doi: 10.1107/S0021889812007662 (2012).
53. Konarev, P. V., Volkov, V. V., Sokolova, A. V., Koch, M. H. J. & Svergun, D. I. PRIMUS: a Windows PC-based system for small-angle scattering data analysis. *J. Appl. Cryst.* **36,** 1277–1282, doi: 10.1107/s0021889803012779 (2003).
54. Svergun, D. Determination of the regularization parameter in indirect-transform methods using perceptual criteria. *J. Appl. Cryst.* **25,** 495–503, doi: 10.1107/S0021889892001663 (1992).
55. Svergun, D. I., Petoukhov, M. V. & Koch, M. H. Determination of domain structure of proteins from X-ray solution scattering. *Biophysical journal* **80,** 2946–2953, doi: 10.1016/S0006-3495(01)76260-1 (2001).
56. Svergun, D., Barberato, C. & Koch, M. H. J. CRYSOL - a Program to Evaluate X-ray Solution Scattering of Biological Macromolecules from Atomic Coordinates. *J. Appl. Cryst.* **28,** 768–773, doi: 10.1107/S0021889895007047 (1995).
57. Sugita, Y. & Okamoto, Y. Replica-exchange molecular dynamics method for protein folding. *Chem. Phys. Lett.* **314,** 141–151, doi: 10.1016/S0009-2614(99)01123-9 (1999).
58. Hornak, V. *et al.* Comparison of multiple Amber force fields and development of improved protein backbone parameters. *Proteins* **65,** 712–725, doi: 10.1002/prot.21123 (2006).
59. Onufriev, A., Bashford, D. & Case, D. A. Exploring protein native states and large-scale conformational changes with a modified generalized born model. *Proteins* **55,** 383–394, doi: 10.1002/prot.20033 (2004).
60. Roe, D. R. & Cheatham, T. E. 3rd. PTRAJ and CPPTRAJ: Software for Processing and Analysis of Molecular Dynamics Trajectory Data. *Journal of chemical theory and computation* **9,** 3084–3095, doi: 10.1021/ct400341p (2013).

Acknowledgements

The pET-ZZ-1a and pET-MBP-1a were gifts from Gunter Stier (EMBL, Heidelberg, Germany) and the pTH24 vector encoding TEV protease from Jeffrey McKinney. We thank Ali Javier Sepulveda and Khanh Kim Dao for technical assistance and Dr. Paul Johan Høl for expert assistance with sample preparation for metal measurements. We also wish to acknowledge the beamtime and excellent support at the EMBL/DESY P12 beamline. This work was supported by the Research Council of Norway (to AM, project number 214012 and to PK and AM through Synknøyt program), the K. G. Jebsen Foundation and the Western Norway Regional Health Authority (to MIF, project number 911959).

Author Contributions

M.T.B., A.B., A.M. and M.I.F. designed research. M.T.B. and M.I.F. made the plasmid constructs. M.T.B., A.B. and M.I.F. purified TH. A.B. prepared samples for Edman analysis and ICP-MS and performed CD and iron-measurements. M.T.B. performed activity assays and DLS. A.B. and R.M. performed ICP-MS. P.K. designed SAXS experiments, A.B., M.I.F. and P.K. performed SAXS. A.B., L.S. P.K. and A.M. analysed SAXS data. L.S. did the structure modelling and MD-simulations. M.T.B., A.B., L.S., A.M. and M.I.F. wrote the paper. All authors reviewed and approved the manuscript.

Additional Information

Supplementary information accompanies this paper at http://www.nature.com/srep

Competing financial interests: The authors declare no competing financial interests.

How to cite this article: Bezem, M. T. *et al.* Stable preparations of tyrosine hydroxylase provide the solution structure of the full-length enzyme. *Sci. Rep.* **6**, 30390; doi: 10.1038/srep30390 (2016).

Supplementary Information

Stable preparations of tyrosine hydroxylase provide the solution structure of the full-length enzyme

Maria T. Bezem+, Anne Baumann+, Lars Skjærven, Romain Meyer, Petri Kursula, Aurora Martinez, Marte I. Flydal

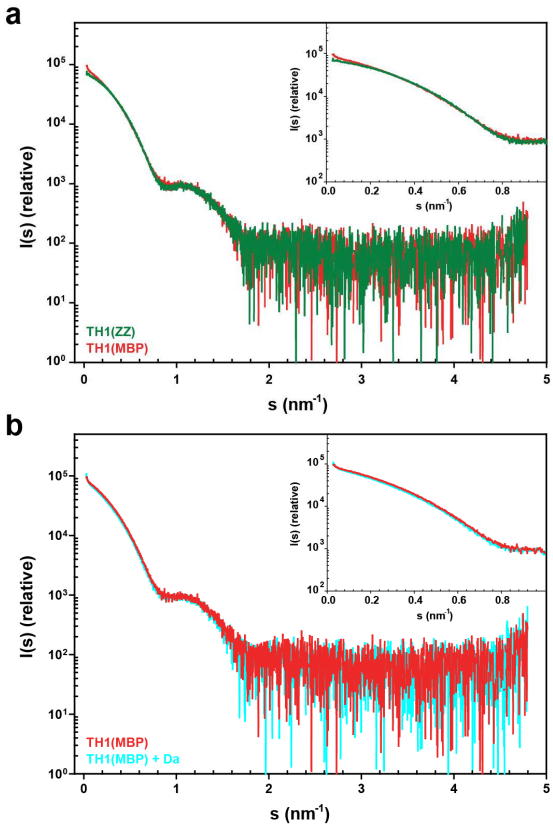

Supplementary Figure S1: Small-angle X-ray scattering. (a) SAXS curves of TH1(ZZ) (green) and TH1(MBP) (red). (b) SAXS curves of TH1(MBP) (red) and TH1(MBP) in the presence (cyan) of stoichiometric amounts of DA.

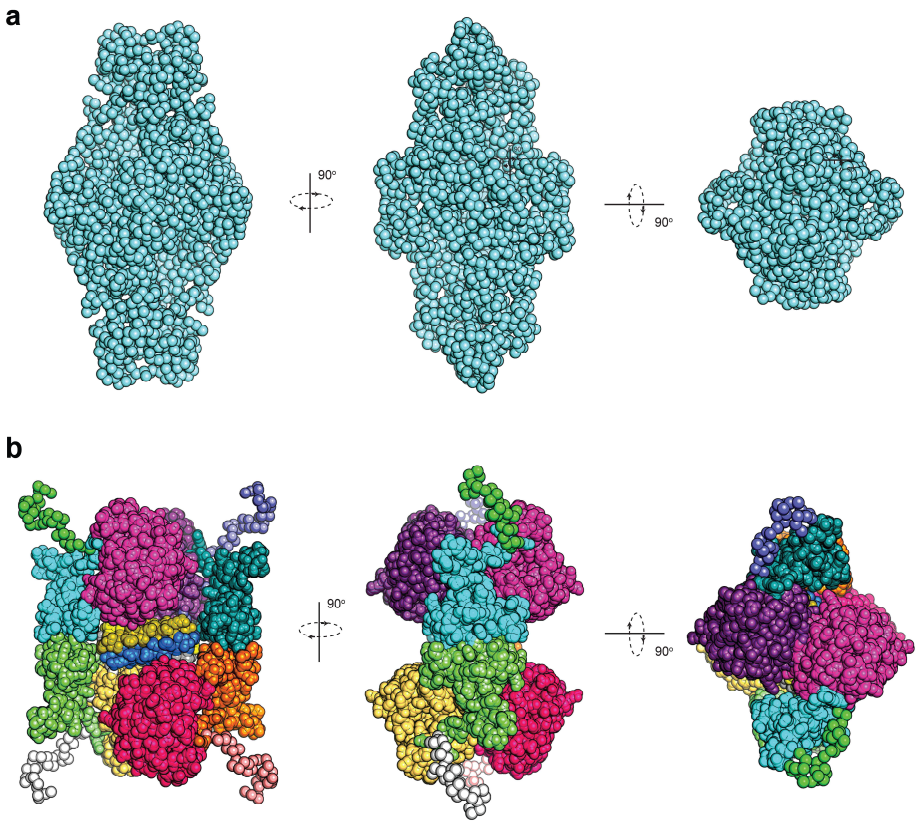

Supplementary Figure S2: Comparison of (a) *ab initio* model, and (b) hybrid model of TH1(ZZ). Dimensions of the *ab initio* model are ~17x9x9 nm and the model yields a fit to the experimental scattering data with a χ^2 value of 0.74. Dimensions of hybrid model are 15x12x10 (with a χ^2 of 1.55). Coloring represent the various structural elements and domains of TH1 used in the rigid body modeling protocol.

a

b

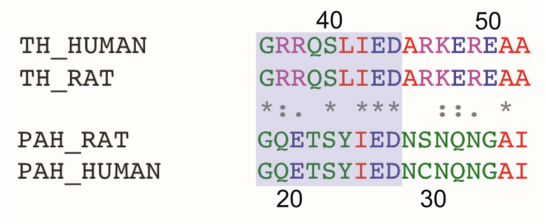

Supplementary Figure S3: The N-terminal region of TH1. (a) The N-terminal region of TH1 includes residues 1-70, for which the structure is unknown. The N-terminal tail is shown in gray and the Ala-rich segment in red (preceding the ACT-domain). (b) Sequence alignment of TH1 and human phenylalanine hydroxylase (PAH) at positions Gly36-Ala52 (for TH1), and Gly19-Ile35 (for PAH) (see main text for details).

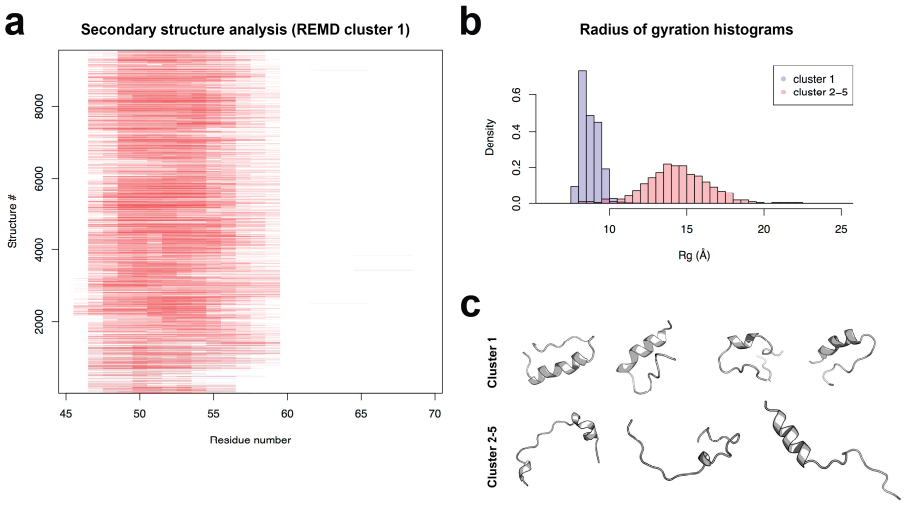

Supplementary Figure S4: Replica exchange molecular dynamics (REMD) simulations summary. (a) Schematic representation of the α-helix propensity for each of the resulting conformers in cluster 1 obtained from REMD simulations. Red colors depict presence of α-helix while white color depicts no secondary structure element. (b) Histogram of the radius of gyration for conformers in cluster 1 (blue bars) and clusters 2-5 (red bars). For comparison probability densities (so that the histogram has a total area of one) are plotted instead of frequencies. (c) Example conformers from cluster 1 (first row) and clusters 2-5 (second row).

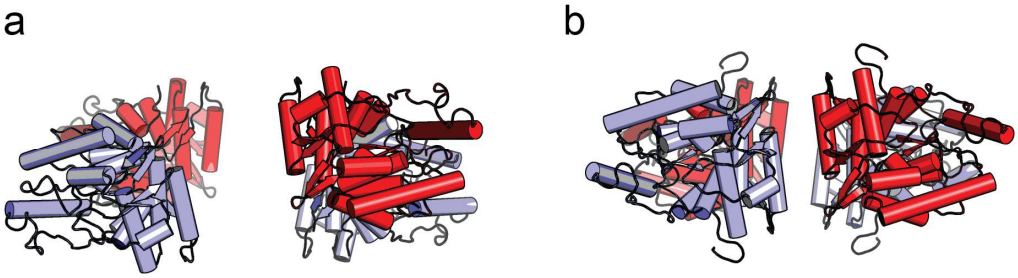

Supplementary Figure S5: Comparison of the configuration of catalytic domains in (a) the SAXS-derived hybrid model of TH1(ZZ) and (b) crystal structure of rat TH (PDB ID 1TOH). Only the catalytic domains are shown for illustration of the out-of-plane (SAXS) and in-plane (crystal) configurations.

III

Paper III

Relevance of Electrostatics for the Interaction of Tyrosine Hydroxylase with Porous Silicon Nanoparticles

Maria T. Bezem, Fredrik G. Johannessen, Trond-André Kråkenes, Michael J. Sailor and Aurora Martinez

Molecular Pharmaceutics, **18**(3), 976-985, 2021.

Tyrosine hydroxylase (TH) is the enzyme catalyzing the rate-limiting step in the synthesis of dopamine in the brain. Developing enzyme replacement therapies using TH could therefore be beneficial to patient groups with dopamine deficiency, and the use of nanocarriers that cross the blood−brain barrier seems advantageous for this purpose. Nanocarriers may also help to maintain the structure and function of TH, which is complex and unstable. Understanding how TH may interact with a nanocarrier is therefore crucial for the investigation of such therapeutic applications. This work describes the interaction of TH with porous silicon nanoparticles (pSiNPs), chosen since they have been shown to deliver other macromolecular therapeutics successfully to the brain. Size distributions obtained by dynamic light scattering show a size increase of pSiNPs upon addition of TH and the changes observed at the surface of pSiNPs by transmission electron microscopy also indicated TH binding at pH 7. As pSiNPs are negatively charged, we also investigated the binding at pH 6, which makes TH less negatively charged than at pH 7. However, as seen by thioflavin-T fluorescence, TH aggregated at this more acidic pH. TH activity was unaffected by the binding to pSiNPs most probably because the active site stays available for catalysis, in agreement with calculations of the surface electrostatic potential pointing to the most positively charged regulatory domains in the tetramer as the interacting regions. These results reveal pSiNPs as a promising delivery device of enzymatically active TH to increase local dopamine synthesis.

molecular pharmaceutics

pubs.acs.org/molecularpharmaceutics

Article

Relevance of Electrostatics for the Interaction of Tyrosine Hydroxylase with Porous Silicon Nanoparticles

Maria T. Bezem,[*,§] Fredrik G. Johannessen,[§] Trond-André Kråkenes, Michael J. Sailor, and Aurora Martinez[*]

Cite This: *Mol. Pharmaceutics* 2021, 18, 976–985

Read Online

ACCESS | Metrics & More | Article Recommendations

ABSTRACT: Tyrosine hydroxylase (TH) is the enzyme catalyzing the rate-limiting step in the synthesis of dopamine in the brain. Developing enzyme replacement therapies using TH could therefore be beneficial to patient groups with dopamine deficiency, and the use of nanocarriers that cross the blood–brain barrier seems advantageous for this purpose. Nanocarriers may also help to maintain the structure and function of TH, which is complex and unstable. Understanding how TH may interact with a nanocarrier is therefore crucial for the investigation of such therapeutic applications. This work describes the interaction of TH with porous silicon nanoparticles (pSiNPs), chosen since they have been shown to deliver other macromolecular therapeutics successfully to the brain. Size distributions obtained by dynamic light scattering show a size increase of pSiNPs upon addition of TH and the changes observed at the surface of pSiNPs by transmission electron microscopy also indicated TH binding at pH 7. As pSiNPs are negatively charged, we also investigated the binding at pH 6, which makes TH less negatively charged than at pH 7. However, as seen by thioflavin-T fluorescence, TH aggregated at this more acidic pH. TH activity was unaffected by the binding to pSiNPs most probably because the active site stays available for catalysis, in agreement with calculations of the surface electrostatic potential pointing to the most positively charged regulatory domains in the tetramer as the interacting regions. These results reveal pSiNPs as a promising delivery device of enzymatically active TH to increase local dopamine synthesis.

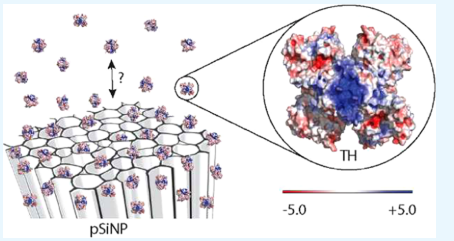

KEYWORDS: *protein aggregation, catalytic activity, enzyme replacement therapy, drug delivery, surface charge distribution*

INTRODUCTION

Tyrosine hydroxylase (TH) is a tetrameric enzyme that belongs to the family of the tetrahydrobiopterin (BH_4)-dependent aromatic amino acid hydroxylases.[1] TH catalyzes the hydroxylation of L-Tyrosine (L-Tyr) to L-3,4-dihydroxyphenylalanine (L-DOPA or levodopa), which is the rate-limiting step in the synthesis of dopamine and other catecholamine neurotransmitters.[2] Dysfunctional TH activity is associated with diseases such as TH deficiency,[3] Parkinson's disease (PD),[4] and neuropsychiatric disorders.[5,6] The traditional treatment of PD, e.g., the oral administration of levodopa, has been linked to undesirable side effects, such as dyskinesia. Other treatments include invasive surgeries like deep brain stimulation, which is often effective but includes a high risk of fatal complications of the surgery.[7] A gentler and more controlled approach to induce production of L-DOPA *in situ* in the brain is enzyme replacement therapy (ERT), for example, the delivery of TH across the blood–brain barrier (BBB) using an appropriate nanoparticle (NP) carrier.[8]

One of the main challenges for the preparation of ERT therapeutics, however, is the need to stabilize the enzyme, which is especially relevant in the case of TH, as this enzyme tends to aggregate and lose activity at 37 °C.[9] Upon interaction with phospholipid monolayers and bilayers, TH aggregates in an amyloid-like manner, causing in turn disruption of cell membranes and compromising cell viability.[10] In previous work,[11] we have shown that nanoparticles (NPs) consisting of maltodextrin with a lipid core could be used to absorb functional TH, contributing to stabilization of the enzyme and enhancing its uptake by SH-SY5Y neuroblastoma cells and brain tissue. Although these NPs cross a model of the BBB,[12] it would also be interesting to investigate interactions of TH in a more readily modifiable and biodegradable NP.

Porous silicon nanoparticles (pSiNPs) are versatile nanocarriers with several advantages; their properties are highly tunable as they are synthesized using electrochemical perforation etching where the pore size, porosity, and particle

Received: September 24, 2020
Revised: December 10, 2020
Accepted: December 28, 2020
Published: January 8, 2021

https://dx.doi.org/10.1021/acs.molpharmaceut.0c00960
Mol. Pharmaceutics 2021, 18, 976–985

size can be controlled by the parameters of the etching procedure.[13] pSiNPs can be modified post synthesis using different surface modifications including oxidation, chemical grafting, etc.[14] These pSiNPs degrade into silicic acid, which is the biological form of silicon and an element naturally present in human tissues that has been implicated in the maintenance of bone mineral density.[15−17] Since the development of porous silicon as a biosensor in 1997,[18] the internalization of proteins into porous silicon films[19−23] or microparticles[24−26] and their various applications have been developed and investigated. Furthermore, *in vivo* biodistribution of pSiNPs, studied after intravenous injection, into mice showed some silicon content in the brain, suggesting that these pSiNPs enter the brain.[27] pSiNPs have successfully delivered siRNA to the injured brain of mice after they had been modified to improve the targeting.[28] Recently, proteins such as lysozyme[29,30] and the antibody FGK4S[31] have been loaded into pSiNPs; thus, these NPs are valuable candidates as nanocarriers of proteins with the potential to be used in drug delivery. Learning more about how proteins, in general, and TH, in particular, can interact with these potential nanocarriers is therefore important.

TH is a homo-tetramer with each subunit consisting of a catalytic, regulatory, and tetramerization domain. The structure of full-length TH is not available yet, probably due to the large number of intrinsically disordered and flexible regions, but the crystal structure of the catalytic and tetramerization domains and the NMR structure of the regulatory domain are known,[32,33] which has provided a small-angle X-ray scattering (SAXS)-based full-length solution structure.[9] The isoelectric point (pI) of purified recombinant TH has been measured to be around 5.5−5.8,[34] rather similar to the theoretically calculated by the web-based software ExPASy ProtParam (pI 5.75). Thus, the net surface charge of TH is expected to be negative at neutral pH and it is therefore easily loaded onto positively charged NPs such as maltodextrin nanoparticles.[11] As pSiNPs are negatively charged, protein loading can best be achieved under or around the isoelectric point of the protein, where the protein is positively charged or neutral.[35] TH has, nevertheless, been shown to bind to negatively charged membranes at both pH 6 and 7 through its N-terminal regulatory domain, a binding that has been associated with the interaction with exposed positively charged residues.[36−38]

In this study, we investigated the interaction between the complex, unstable, and flexible TH protein with the inorganic, rigid pSiNPs, an interaction that is expected to be mainly directed by electrostatics. We investigated the effect of pH on the binding of TH to pSiNPs, as well as the effect of incorporation of TH onto NPs on the conformation, aggregation, and enzymatic activity of TH.

METHODS

Expression and Purification of Recombinant TH. Human TH, isoform TH1, was expressed and purified as described.[9] Briefly, TH was expressed in *Escherichia coli* and purified as a fusion protein with a his-tagged maltose-binding protein (MBP) using TALON Superflow Metal Affinity Resin, then cleaved with tobacco etch virus (TEV) protease, and tetrameric TH was isolated by size exclusion chromatography and stored in liquid nitrogen. Before all experiments, a TH aliquot was thawed, diluted to ca. 2 mg/mL, and centrifuged 15 min at 4 °C and 20 000*g* to remove aggregates formed during storage or freezing/thawing. The concentration of TH in the supernatant was measured using Direct Detect (Bio-Rad).

Preparation of pSiNPs. pSiNPs were prepared using electrochemical etching of silicon wafers and ultrasonic fracture, as described earlier,[13] and the resulting nanoparticles were stored in ethanol. Briefly, highly boron-doped (p++-type) silicon wafers were anodically etched in an electrolyte of 3:1 (v:v) of 48% aqueous HF:ethanol. The etching waveform consisted of alternating pulses of lower current density (50 mA/cm^2 for 1.8 s) and higher current density (400 mA/cm^2 for 0.36 s). This waveform was repeated for 140 cycles, generating a porous silicon film with alternating layers of high and low porosity. The porous silicon film was removed from the wafer by applying a low current density of 3.7 mA/cm^2 for 250 s in an electrolyte consisting of 1:10 (v:v) of 48% aqueous HF:ethanol. The freestanding porous silicon film was placed in ethanol in a sealed vial and fractured by ultrasonication (50T ultrasonic water bath, VWR International) for 12 h, and the resulting nanoparticles were collected by centrifugation (Eppendorf centrifuge model 5424R, 12 000 rpm for 10 min) and then redispersed in ethanol and stored at room temperature (RT) as a stock solution. To obtain the concentration of pSiNPs, 100 μL fractions of the stock solution were evaporated in a fume hood at RT for 24 h. The Eppendorf tubes were weighed before adding the solution, after adding the solution, and after evaporation, and the concentration was calculated from the weight difference.

Dynamic Light Scattering (DLS). The size of pSiNPs was analyzed by DLS, performed on a Zetasizer Nano ZS instrument (Malvern Panalytical), using a HeNe laser at 633 nm and a fixed scattering angle of 173° (back scatter). Measurements were performed in normal resolution mode at automatic run repetition and at room temperature in a 12 μL quartz cuvette, after a 1:10 000 dilution in either ethanol or 5 mM 4-(2-hydroxyethyl)-1-piperazineethanesulfonic acid (HEPES) pH 6.0 or 7.0, 50 mM NaCl with final concentration of 0.63 μg/mL of pSiNPs. The time-dependent stability was evaluated under the same conditions but using ZEN0040 disposable cuvettes, with 200 s intervals between preset measurements of 10 runs of 10 s each. The comparison of the interaction with TH at pH 6 and 7 was performed using 0.2 mg/mL TH and a 1:5000 dilution of pSiNPs (final concentration of 1.26 μg/mL pSiNPs) in 5 mM HEPES and 50 mM NaCl with automatic run repetition. Data analysis was performed on intensity curves and the *Z*-average size using the Malvern DTS software (Malvern Panalytical).

Thioflavin-T (ThT) Fluorescence. TH was incubated with 20 μM ThT in the presence or absence of 1:10 000 pSiNPs in 5 mM HEPES pH 6.0 or 7.0, 50 mM NaCl at RT. ThT fluorescence, with excitation at 440 nm and emission at 482 nm, was recorded in a 96-well plate every 5 min for 18 h at RT on a Synergy H1 Hybrid Reader (BioTek). Samples with only pSiNPs were used as controls and data are presented as averages of three parallel measurements. Blank measurements of buffer with corresponding pH were subtracted from the data sets.

Transmission Electron Microscopy (TEM). Sample preparation for TEM was done as following: 100 μL of a 1:1000 dilution of pSiNPs (6.3 μg/mL) alone or with 0.1 mg/mL TH and a 0.1 mg/mL TH control were incubated in an Eppendorf tube for 1 h at RT. 3 μL were carefully added onto a carbon-coated 300 mesh copper grid and left for 1 min before excess liquid was removed with tissue paper. Samples

https://dx.doi.org/10.1021/acs.molpharmaceut.0c00960
Mol. Pharmaceutics 2021, 18, 976−985

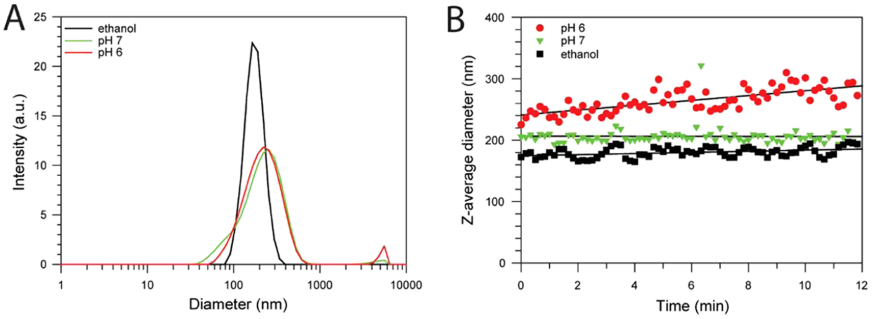

Figure 1. Size distribution and time-dependent stability of pSiNPs studied by dynamic light scattering. Representative size distribution of pSiNPs by intensity (A) at 1:10 000 dilution in ethanol (black) or 5 mM HEPES, 50 mM NaCl at pH 7 (green) or pH 6 (red) at initial dilution, at room temperature. Time-dependent stability (B) of the *Z*-average diameter of pSiNPs at 1:10 000 dilution in ethanol (black) or 5 mM HEPES, 50 mM NaCl, pH 7 (green) or pH 6 (red), with linear regression as solid black lines. Data points are the average of three independent experiments.

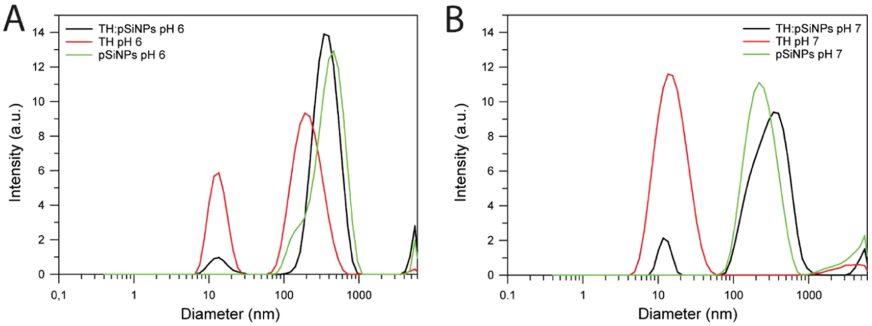

Figure 2. Size distribution of TH and its interaction with pSiNPs studied by dynamic light scattering. Intensity-based size distribution of 0.2 mg/mL TH (red), 1:5000 diluted pSiNPs (green), and both (black) at pH 6 (A) and pH 7 (B), at room temperature. The data are presented as mean of three replicates of representative loading experiments.

were negatively stained twice with 3 μL 2% uranyl acetate for 30 s each time. Images were obtained with a JEM-1230 (Jeol) TEM using 80 keV, and images were taken at 150× magnification giving 8 Å/pixel.

TH Activity. Enzymatic activity of TH was measured as described earlier,[11] with minor modifications. Briefly, TH (0.01 mg/mL) was preincubated at 37 °C with 1% bovine serum albumin (BSA) (w/v) in 5 mM HEPES pH 6.0 or 7.0, 50 mM NaCl in the absence or presence or absence of pSiNPs at 1:10 000 dilution. Aliquots of 5 μL were taken out either immediately after mixing or after 1.5 and 24 h and incubated for 1 min in a standard reaction mixture and then assayed for 5 min. The amount of L-DOPA was measured by high-performance liquid chromatography (HPLC) analysis with fluorescence detection. Controls of only pSiNPs at pH 6.0 and 7.0, and blank measurement of only buffer, showed no activity. Data are presented as an average of three parallel measurements.

Surface Electrostatic Potential Calculations. Structural analysis of TH surface electrostatics was performed at different pH values with the PDB2PQR web service,[39−41] on the SAXS-derived TH model[9] with the AMBER force field and using PROPKA to assign protonation states at different pH values. The resulting.pqr file was loaded into PyMOL (Schrödinger software, version 2.2.2) and visualized using the APBS Electrostatics plugin.

RESULTS AND DISCUSSION

Size Distribution and Stability of pSiNPs Studied by DLS. We characterized the size of pSiNPs using DLS and found that the apparent hydrodynamic diameter of pSiNPs has a peak in the size distribution at 164 nm when diluted 1:10 000 in ethanol and 220 and 255 nm in buffer at pH 6 and 7, respectively (Figure 1A). The pSiNPs were stored in ethanol after synthesis and their size remained stable at RT with a *Z*-average diameter of 180 ± 8 nm (Figure 1B). At pH 7 buffer, the *Z*-average diameter was stable at 206 ± 15 nm, whereas in pH 6 buffer, the size increased steadily from 225 ± 21 to 273 ± 20 nm over a period of 12 h (Figure 1B).

Porous silicon can be readily oxidized by OH^- present in aqueous buffers; thus, the silicon in the outer layer of pSiNP pore walls will form a SiO_2 shell which can be further oxidized into dissolvable silicic acid ($Si(OH)_4$). This process is temperature and pH dependent, with higher rates at higher pH and at higher temperatures.[14,42] pSiNPs were chosen specifically for their ability to break down in aqueous solution, and this process is expected to give an increased diameter due to the first step of the degradation where the expansion of the pore walls accommodates the extra oxygen species during the mild oxidation by OH^- in the buffer. The diameter would eventually decrease due to the second step of the degradation where silicon oxide dissolves into silicic acid. The initial

https://dx.doi.org/10.1021/acs.molpharmaceut.0c00960
Mol. Pharmaceutics 2021, 18, 976−985

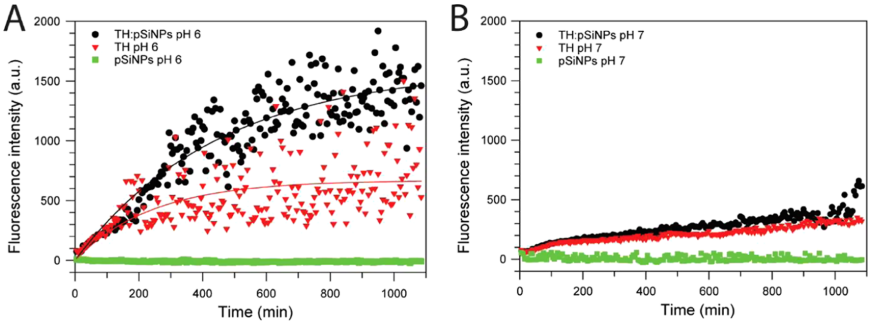

Figure 3. Aggregation propensity studied by thioflavin-T (ThT) fluorescence. Time-dependent ThT fluorescence intensity monitored at 482 nm, with excitation at 440 nm, for TH alone (red data points and line) or in the presence of pSiNPs diluted to 1:10 000 in 5 mM HEPES, 50 mM NaCl (black data points and line) at pH 6 (A) and pH 7 (B), at room temperature. Results for pure pSiNPs (no TH protein) are shown in green. The data are presented as average of three parallel measurements after subtraction of blank measurements.

difference in the diameter of pSiNPs in ethanol or the buffer solutions occurs very rapidly and cannot be captured by DLS as each measurement takes about 2 min. This difference could, however, be due to variations in the hydrodynamic shell of the solvent around pSiNPs. Another possibility is that the ions present in the buffer induce stacking or agglomeration of pSiNPs, since they have a rather flat but irregular shape.[13] This agglomeration effect increased with increasing ion concentrations, indicating that electrostatic interactions between the solvent and pSiNPs are crucial for their stability.

Size Distribution of Human TH and Its Interaction with pSiNPs. We attempted to load TH onto nanoparticles and evaluated if the enzyme could bind on the surface or within pSiNPs. Preliminary experiments showed little difference in *Z*-averages and size distributions between pH 5, 5.5, and 6 (data not shown). Since TH is known to lose its enzymatic activity gradually at pH values smaller than 7 for the human isoform 1 of TH,[43,44] we selected pH 6 as the lowest pH value to study the loading of the enzyme onto NPs. With a pI of 5.5−5.8, TH is expected to have a net negative charge at pH 7 and be almost neutral at pH 6. TH is, however, known to bind to negatively charged membranes through positively charged residues exposed on its regulatory domain. We therefore expected that the interactions between TH and pSiNPs would also happen through the regulatory domain of TH and would be more efficient at pH 6 than at pH 7 due to more favorable interactions with the negative surface charge of pSiNPs.

As measured by DLS, TH shows a size distribution with a peak around 10 nm, corresponding to the size of its tetrameric form,[9] and observed in the intensity-based size distributions at both pH 6 and pH 7 (Figure 2). TH also shows a peak corresponding to the aggregated forms of a larger diameter of 190 nm at pH 6 (Figure 2A).

We previously studied the uptake of TH onto maltodextrin NPs by DLS, following the disappearance of free tetrameric TH from solution and the concomitant increase in size of the NPs as indicated in the size distribution scans.[11] Upon addition of TH (to a final concentration of 0.2 mg/mL) to pSiNPs (with a final concentration of 1.26 μg/mL) and incubation for 1 min at RT, at either pH 6 or 7, we observed a large decrease of free TH (diameter 10−11 nm), both at pH 6 and pH 7 (Figure 2). A small increase of the pSiNP size (shift of the peak from 235 ± 54 to 322 ± 117 nm) was observed at pH 7 (Figure 2B). At pH 6, the size of pSiNPs alone partly overlapped that of aggregated TH, and DLS could thus not differentiate loaded NPs from aggregated TH (Figure 2A).

Aggregation Propensity of TH Measured by Thioflavin-T (ThT) Fluorescence. We investigated the tendency of TH to aggregate and the effect from pSiNPs on the rate of aggregate formation by monitoring the fluorescence from ThT, a dye that binds to cross-β interaction characteristic of amyloid-like aggregation.[45] It has been suggested that all proteins have a tendency to undergo this type of aggregation at certain conditions,[46] as has been previously shown for TH.[10] TH is most stable at neutral pH[43,44] and its aggregation is stimulated by interactions with lipid mono- and bilayers,[10] whereas TH aggregation is prevented by loading into maltodextrin nanoparticles.[11]

TH induces an increase in ThT fluorescence, which is more prominent at pH 6 than pH 7, and this increase is further accelerated by the presence of pSiNPs. The increase is more pronounced at pH 6 than at pH 7 (Figure 3). It seems that pSiNPs act as nucleation points for TH aggregation, which is not an unusual property of nanoparticles, as the nanoparticle surface locally increases protein concentration, promoting oligomer formation by reducing the lag phase in fibril formation.[47] Porous silicon is known to induce nucleation and is a suitable surface for protein crystallization.[48] It is also known that proteins often aggregate at the pI,[49] which can explain the higher rate of TH aggregation observed at pH 6 compared to pH 7 (Figure 3A,B).

Imaging pSiNPs, TH, and TH:pSiNP Complexes by TEM. TEM was used to investigate the interaction of TH with pSiNPs by following structural changes to the surface of pSiNPs that could be attributed to complex formation. The extensive aggregation of TH observed at pH 6, and its amplification in the presence of pSiNPs (Figure 3A) precluded the TEM study at pH 6, and we performed this study at pH 7. The pSiNPs, TH, and the mixture were diluted in 5 mM HEPES, 50 mM NaCl at pH 7.0, and incubated at RT for 1 h with final concentrations of 6.3 μg/mL pSiNPs and 0.1 mg/mL TH, before being deposited on grids, stained, and imaged. Control pSiNP samples without negative staining show irregular shapes possessing a hollow matrix with pores aligned in the same direction and spanning the whole particle diameter (Figure 4A). This is in agreement with earlier reports,[13] and the size of the nanoparticles determined by TEM is in

https://dx.doi.org/10.1021/acs.molpharmaceut.0c00960
Mol. Pharmaceutics 2021, 18, 976−985

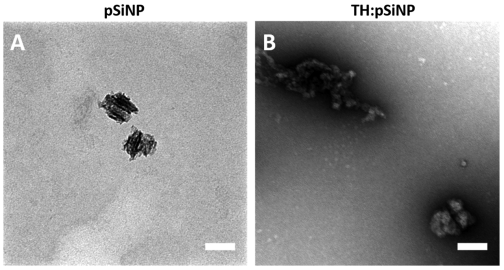

Figure 4. Transmission electron microscope (TEM) images of the interaction of TH with pSiNPs. Representative TEM images of 1:1000 pSiNPs either unstained (A) or with 0.1 mg/mL TH and negatively stained with 4% uranyl acetate (B), illustrating the interaction of TH and NPs. Both samples were prepared in 5 mM HEPES, 50 mM NaCl, pH 7. Scale bars are 100 nm.

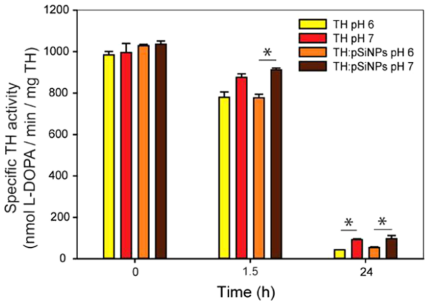

Figure 5. Effect of pSiNPs on TH activity. Specific enzymatic activity of TH *in vitro*, assayed after preincubation with and without pSiNPs at either pH 6 or 7, at 37 °C for the indicated time. Data is presented as the mean of three replicates ± standard deviation (SD). Significance was tested by a Holm−Sidak test in a one-way analysis of variance (ANOVA) and * indicates $p < 0.001$.

correspondence to the DLS results, i.e., around 150−200 nm. The pSiNPs are found as both isolated particles and clusters of particles in the TEM images.

The TH:pSiNPs mix was imaged after negative staining with 4% uranyl acetate (Figure 4B), since staining improves contrast in biological samples such as proteins. The details of the nanostructure of pSiNPs were lost in the staining, as the uranyl acetate solution stains everything but the particles, and thus only the outline of pSiNPs is visible (data not shown). The addition of TH to pSiNPs also seems to increase the incidence of NP aggregates and to smooth out the particle surface (Figure 4B), indicating that the protein resides at the particle surface. The use of TEM and negative staining facilitates the visualization of TH on NPs; however, it did not allow us to evaluate if TH was loaded into the pores of pSiNPs.

Effect of pH and pSiNPs on TH Activity. We also performed activity assays to see if the interaction with pSiNPs would have any effect on the enzymatic function of TH. The activity was assayed in a standard reaction mix at 37 °C with L-tyrosine, and the amount converted to L-DOPA by TH in the presence and absence of pSiNPs was determined by HPLC. TH activity decreased over time and was significantly lower for preincubations at pH 6 than pH 7, as earlier reported,[9,43] but pSiNPs did not seem to affect the TH activity significantly (Figure 5). This result is promising, as many enzymes lose some activity upon binding to nanoparticles, due either to partial coverage or blockage of the active site or to conformational changes.[50,51]

The relatively quick loss of TH activity has been repeatedly observed previously, both during incubation at neutral pH and temperatures in the range of 20−37 °C and under turnover, and has been found to be more pronounced for the purified enzyme than for partially purified preparations.[9,52] The loss of activity is partially associated with the reduction of conformational stability,[53] which may lead to aggregation and a nonreversible loss-of-function.[10] Moreover, it has been shown that oxidative modifications at several residues in TH inactivate the enzyme, where at least the oxidation of thiols in cysteines at controlled conditions may be reversible.[54,55] It appears that an *in vivo* environment can prevent inactivation and even regenerate inactivated TH, which is relevant for the applicability of NPs as TH nanocarriers, as shown by the increased L-DOPA production *in cellulo* after delivery of TH with maltodextrin NPs.[11] Additional TH stabilization is provided by dopamine, which is a feedback inhibitor and stabilizer of TH in brain,[9,53] and by small molecule stabilizers with pharmacological chaperone potential.[56]

Role of Electrostatics on the Binding of TH to pSiNPs. Finally, we investigated the surface electrostatics of TH in a structural model. We applied the structural model of full-length TH derived from small-angle X-ray scattering (SAXS) data as described,[9] based on known structural components, i.e., the crystal structure of the catalytic and tetramerization domains of human TH (PDB ID 2XSN; residues 157−497) and the NMR structure of the regulatory rat ACT-domain (PDB ID 2MDA; residues 71−156). *Ab initio* and homology modeling complemented with molecular dynamics simulations were used to prepare the model of the flexible N-terminal tail up to A70, and all domains and regions were combined through a SAXS-based rigid body modeling.[9] The protonation states of each residue in the model were assigned and the resulting surface electrostatic potential was visualized (Figure 6A), to provide insights on enzyme regions that may likely interact with the oxide surface of pSiNPs, which is negatively charged above pH 2.[57]

Actually, in agreement with the pI of TH, which is just below pH 6, the overall surface electrostatic potential of the enzyme is mainly negative at pH 7, whereas there are about equal amounts of negative (red) and positive (blue) patches on the surface of TH at pH 6 (Figure 6). At both pH values, the ACT-regulatory domain, corresponding to residues 71−156 in TH1, is strongly positively charged at the surface oriented away from the other domains (Figure 6A). The ACT domain thus appears particularly well suited for binding to negatively charged pSiNPs (Figures 6B and 7). A similar binding mode has also been shown for the interaction of TH to negatively charged membranes,[10] allowing the active site to be available for catalysis also in the bound state.

The regulatory ACT-domain of TH presents $\beta\beta\alpha\beta\beta\alpha$ topology,[58] where the antiparallel β-sheet is formed by the four β-strands, and the two α-helices are located, in an antiparallel orientation to each other, on the outer face of this sheet (Figure 6A and inset A, Figure 7).[33] In the dimeric ACT arrangement, the outer area presents many positively charged lysine and arginine residues, some of them are protruding from the outer surface, i.e., R89, K92, R98, K101, R137, and R138, which contribute to the positively charged surface and to the

https://dx.doi.org/10.1021/acs.molpharmaceut.0c00960
Mol. Pharmaceutics 2021, 18, 976−985

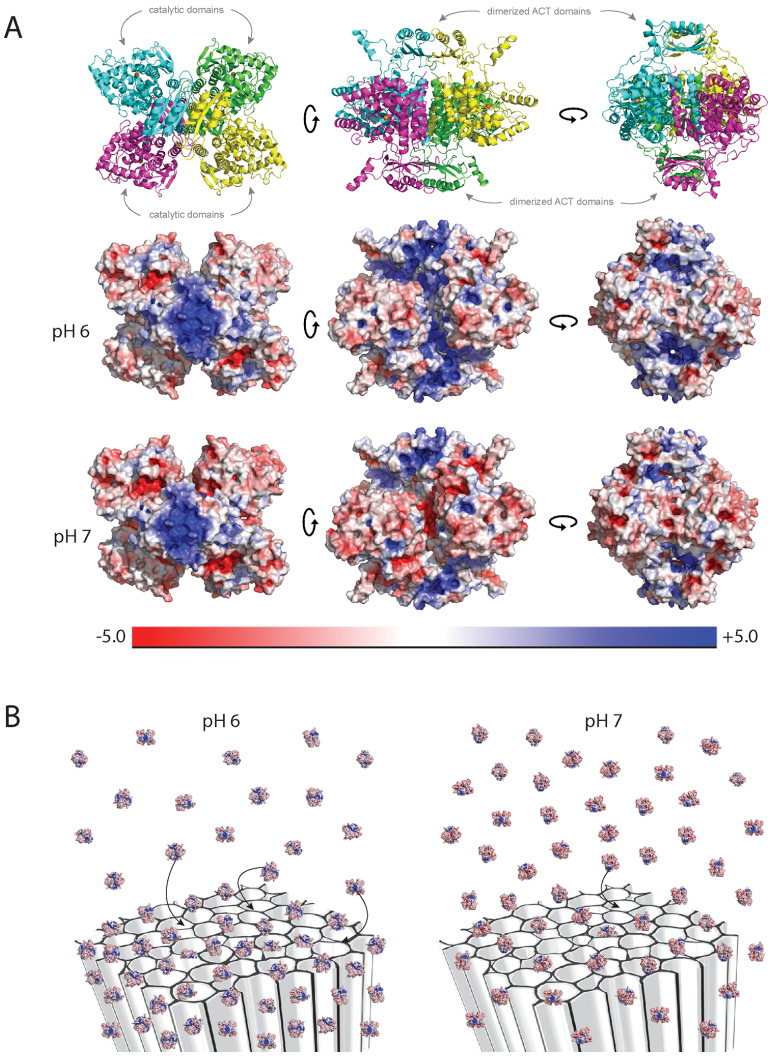

Figure 6. Effect of pH on the surface electrostatic potential of TH and its binding to pSiNPs. The modeled structure of TH and its surface electrostatic potential at pH 6 and 7 (A). At the top row, the structural model of full-length tetrameric TH prepared according to Bezem et al.[9] is shown in ribbon representation (colored by monomer and with iron atom in orange), whereas the two rows below show the surface electrostatic potential at pH 6 and 7, seen from all three orientations. Red and blue indicate negatively and positively charged regions, respectively. Illustration of pH-dependent interactions with pSiNP surfaces (B). At pH 6, which is the closest to the pI of TH, TH binds more extensively to the pSiNP surface than at pH 7. At both pH values, the ACT-regulatory domains of TH (residues 71−156) have a positively charged outer surface (blue patch) that is the most probable region binding to the pSiNP surface, as indicated by the arrows. This orients the mostly negatively charged catalytic domains away from the surface, favoring an interaction where the TH activity is retained even when bound to the nanoparticle surface.

interaction with the negatively charged pSiNP surface (see insets A, B, Figure 7). In this binding mode, the active site in the more negatively charged catalytic domain would be oriented away from the interacting region, as shown in the close-ups (Insets C, D, Figure 7), and would thus be available for catalysis. Some previous studies have shown that pH affects the orientation of the protein bound to silica nanoparticles. For instance, the model protein cytochrome c binds head-on at low pH but side-on at higher pH.[59]

Protein adsorption is not only affected by the protein properties and the pH of the solution but also influenced by factors such as temperature, the ionic strength of the solution, and the adsorbent surface properties including curvature,[60] heterogeneity, hydrophobicity,[61,62] wettability, and charge.[63] Proteins are macro zwitterions, and the distribution of charges determines the direction of their net electric dipole. Charged adsorbent surfaces exert a force on the dipole and can thereby promote a certain orientation, resulting in highly ordered

https://dx.doi.org/10.1021/acs.molpharmaceut.0c00960
Mol. Pharmaceutics 2021, 18, 976−985

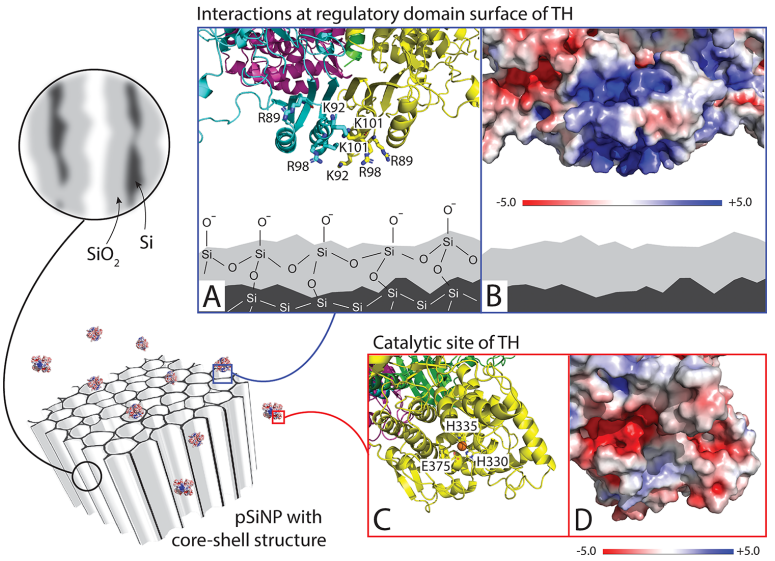

Figure 7. Possible model for the interaction of TH and pSiNPs. pSiNPs have pores of irregular shape that are aligned parallel to each other. The pore walls have a core−shell structure with a layer of silicon oxide (SiO_2) on top of pure silicon (Si), as shown in the close-up (circled in black). The oxide layer is negatively charged, onto which TH can adsorb through the positively charged patch on the outer surface of its dimeric regulatory domains, as shown in the close-ups (insets A, B). The labeled positively charged residues in the outer face of the ACT-domains are the most likely interacting residues with the pSiNP surface, and those most likely involved in the interaction are shown as sticks (inset A), whereas the surface charge distribution is shown as an electrostatic heat map of the close-up (inset B). The TH active site in the catalytic domain is oriented away from the proposed interacting region (insets C, D). The three residues coordinating the catalytic iron (orange) are shown as sticks in inset C.

layers of adsorbed protein on charged surfaces.[64] It has also been shown that it is possible to control the orientation of an adsorbing peptide through varying the electric field, either by pH or an externally applied potential.[65] The surface charge density determines the strength of the electrostatic attraction, and for enzyme haloalkane dehalogenase, the catalytic activity was preserved best upon adsorption on intermediate charged surfaces.[63] These examples show that electrostatic interactions dominate and determine the binding orientation when proteins are adsorbed onto charged surfaces and thus should be tuned for keeping the protein functional.

With respect to the penetration of TH into nanoparticle pores, we might expect that the net negative charge of TH leads to a general repulsion from the negatively charged pSiNPs and that the positively charged regulatory domains only compensate for this as long as the catalytic domains are not brought too close to pSiNPs. In the structure of tetrameric TH, the dimeric regulatory ACT-domains are located at each side and relatively far away from the butterfly-formed tetramer of catalytic domains (Figure 6A), as they are interconnected by flexible loops.[9] This arrangement suggests that TH does not penetrate much into the pores of pSiNPs but interacts primarily at the surface, as depicted in Figure 7.

Potential of pSiNP-Bound TH for Therapeutic Applications. The results presented in this study must be regarded as an initial phase in the process toward the development of therapeutic delivery of TH. Further optimization of the formulation is required for the stabilization of TH, its attachment to pSiNPs, and delivery to the brain, and the approaches to follow would depend on the route of administration.

Existing ERTs are life-long symptom relief treatments administered by intravenous injections on a regular basis, often weekly or biweekly.[66] ERT with intravenous injection of pSiNP-bound TH would require TH stabilization throughout blood circulation and subsequent uptake in the brain through the BBB. Since the pH of blood is slightly basic under normal conditions, the uptake of TH by pSiNPs should be stabilized especially at pH ≥ 7. This can be done by surface modifications of the pSiNP pre- or postloading of TH, to improve loading efficiency, blood circulation time, and cellular uptake. One promising modification seems to be a coating of biopolymers, such as the carbohydrates dextran and heparin, or the extracellular matrix component hyaluronic acid.[67] These polymers easily adsorb onto silicon oxide surfaces through hydrogen bonding, and a dextran coating has been shown to improve the blood half-life of pSiNPs.[27] The effect of such types of modifications must be investigated in future work. Alternatively, functional TH can be provided as an ERT to the brain through direct delivery using hydrogel implants containing TH-loaded pSiNPs. There are several reports on the regeneration of lesions in the CNS through hydrogel implantation into rat[68] or primate[69] brain, and these approaches provide a promising possibility for drug delivery through composite material.[70] Hydrogel implants for PD are a field of extensive study with regards to cell replacement therapies, sustained delivery of dopamine, or delivery of chaperone proteins such as HSP70 (See review by Giordano et al.[71] and references therein). More recently, another protein, Activin B which is a transforming growth factor, has also been delivered to the brain of a PD mouse model using an injectable hydrogel.[72] To our knowledge, there are no reports on TH

https://dx.doi.org/10.1021/acs.molpharmaceut.0c00960
Mol. Pharmaceutics 2021, 18, 976−985

delivery to the brain using a hydrogel implantation and therefore this subject warrants further investigation.

CONCLUSIONS

The properties of the interface between a nanoparticle surface, its payload, and the solvent are important for the interactions occurring in the loading of a therapeutic protein into a nanoparticle carrier. The pH, among other characteristics of the solvent, influences surface charges and can alter this binding. A better understanding of these interactions can improve loading and ensure that the therapeutic protein remains functional. We therefore investigated the relevance of the electrostatic interactions between pSiNPs and TH, an enzyme that potentially could be used to treat dopamine deficiency. TH has a net negative charge but also a well-defined patch of a positively charged surface in its ACT-regulatory domain that is oriented outwards, facilitating the binding to negatively charged surfaces such as that of pSiNPs. The size increase observed by DLS for pSiNPs upon adding TH appears in agreement with this orientation of TH upon binding at the outer surface of pSiNPs. pSiNPs induce more rapid and more extensive aggregation of TH, especially at pH 6, which we attribute to a local increase in TH concentration at the nanoparticle surface such that TH can more effectively form clusters. TH activity is not decreased significantly by the binding to pSiNPs, so its catalytic site is still accessible to substrate, indicating that it is not buried far into the pores of pSiNPs or conformationally disrupted by the interaction. We therefore conclude that TH remains functional upon binding to the pSiNP surface, which most probably happens through the positively charged patch on the surface of its regulatory domain.

AUTHOR INFORMATION

Corresponding Authors

Maria T. Bezem − *Department of Biomedicine, University of Bergen, Bergen 5009, Norway;* orcid.org/0000-0002-2022-1981; Phone: +47 98 80 11 99; Email: Maria.Bezem@uib.no

Aurora Martinez − *Department of Biomedicine, University of Bergen, Bergen 5009, Norway;* orcid.org/0000-0003-1643-6506; Phone: +47 55 58 64 27; Email: Aurora.Martinez@uib.no

Authors

Fredrik G. Johannessen − *Department of Biomedicine, University of Bergen, Bergen 5009, Norway*

Trond-André Kråkenes − *Department of Biomedicine, University of Bergen, Bergen 5009, Norway*

Michael J. Sailor − *Department of Chemistry and Biochemistry, University of California, San Diego, La Jolla, California 92093, United States;* orcid.org/0000-0002-4809-9826

Complete contact information is available at: https://pubs.acs.org/10.1021/acs.molpharmaceut.0c00960

Author Contributions

§M.T.B. and F.G.J. contributed equally to this work.

Author Contributions

Conception of the work: A.M. and M.J.S; collection of data: M.T.B., F.G.J., T-A.K.; analysis of data: M.T.B., F.G.J., T-A.K.; writing of manuscript: M.T.B and A.M. with contributions from all authors. All authors have given approval to the final version of the manuscript. These authors contributed equally.

Notes

The authors declare no competing financial interest.

ACKNOWLEDGMENTS

We thank Endy Spriet from the Molecular Imaging Center at the Department of Biomedicine, University of Bergen for assistance with TEM and for providing carbon-coated copper grids. We are grateful to Marte I. Flydal for purification of TH. This work was supported by grants from the Research Council of Norway (FRIMEDBIO 261826/F20), the U.S. National Science Foundation (CBET-1603177), the K.G. Jebsen Centre for Neuropsychiatric Disorders, and the Western Norway Regional Health Authorities (project 912246) (to A.M.).

REFERENCES

(1) Skjaerven, L.; Teigen, K.; Martinez, A. Structure-Function Relationships in the Aromatic Amino Acid Hydroxylases Enzyme Family: Evolutionary Insights. In *eLS*; John Wiley & Sons, Ltd., 2014.

(2) Roberts, K. M.; Fitzpatrick, P. F. Mechanisms of tryptophan and tyrosine hydroxylase. *IUBMB Life* **2013**, *65*, 350−357.

(3) Willemsen, M. A.; Verbeek, M. M.; Kamsteeg, E. J.; de Rijk-van Andel, J. F.; Aeby, A.; Blau, N.; Burlina, A.; Donati, M. A.; Geurtz, B.; Grattan-Smith, P. J.; Haeussler, M.; Hoffmann, G. F.; Jung, H.; de Klerk, J. B.; van der Knaap, M. S.; Kok, F.; Leuzzi, V.; de Lonlay, P.; Megarbane, A.; Monaghan, H.; Renier, W. O.; Rondot, P.; Ryan, M. M.; Seeger, J.; Smeitink, J. A.; Steenbergen-Spanjers, G. C.; Wassmer, E.; Weschke, B.; Wijburg, F. A.; Wilcken, B.; Zafeiriou, D. I.; Wevers, R. A. Tyrosine hydroxylase deficiency: a treatable disorder of brain catecholamine biosynthesis. *Brain* **2010**, *133*, 1810−1822.

(4) Obeso, J. A.; Rodriguez-Oroz, M. C.; Goetz, C. G.; Marin, C.; Kordower, J. H.; Rodriguez, M.; Hirsch, E. C.; Farrer, M.; Schapira, A. H.; Halliday, G. Missing pieces in the Parkinson's disease puzzle. *Nat. Med.* **2010**, *16*, 653−661.

(5) Dunčko, R.; Kiss, A.; kultetyova, I. S.; Rusnak, M.; Jezova, D. Corticotropin-releasing hormone mRNA levels in response to chronic mild stress rise in male but not in female rats while tyrosine hydroxylase mRNA levels decrease in both sexes. *Psychoneuroendocrinology* **2001**, *21*, 77−89.

(6) Dahoun, T.; Trossbach, S. V.; Brandon, N. J.; Korth, C.; Howes, O. D. The impact of Disrupted-in-Schizophrenia 1 (DISC1) on the dopaminergic system: a systematic review. *Transl. Psychiatry* **2017**, *7*, No. e1015.

(7) Deuschl, G.; Schade-Brittinger, C.; Krack, P.; Volkmann, J.; Schäfer, H.; Bötzel, K.; Daniels, C.; Deutschländer, A.; Dillmann, U.; Eisner, W.; Gruber, D.; Hamel, W.; Herzog, J.; Hilker, R.; Klebe, S.; Kloß, M.; Koy, J.; Krause, M.; Kupsch, A.; Lorenz, D.; Lorenzl, S.; Mehdorn, H. M.; Moringlane, J. R.; Oertel, W.; Pinsker, M. O.; Reichmann, H.; Reuß, A.; Schneider, G.-H.; Schnitzler, A.; Steude, U.; Sturm, V.; Timmermann, L.; Tronnier, V.; Trottenberg, T.; Wojtecki, L.; Wolf, E.; Poewe, W.; Voges, J. A Randomized Trial of Deep-Brain Stimulation for Parkinson's Disease. *N. Engl. J. Med.* **2006**, *355*, 896−908.

(8) Tosi, G.; Duskey, J. T.; Kreuter, J. Nanoparticles as carriers for drug delivery of macromolecules across the blood-brain barrier. *Exp. Opin. Drug Delivery* **2019**, 1−10.

(9) Bezem, M. T.; Baumann, A.; Skjaerven, L.; Meyer, R.; Kursula, P.; Martinez, A.; Flydal, M. I. Stable preparations of tyrosine hydroxylase provide the solution structure of the full-length enzyme. *Sci. Rep.* **2016**, *6*, No. 30390.

(10) Baumann, A.; Jorge-Finnigan, A.; Jung-Kc, K.; Sauter, A.; Horvath, I.; Morozova-Roche, L. A.; Martinez, A. Tyrosine Hydroxylase Binding to Phospholipid Membranes Prompts Its Amyloid Aggregation and Compromises Bilayer Integrity. *Sci. Rep.* **2016**, *6*, No. 39488.

(11) Bezem, M. T.; Johannessen, F. G.; Jung-KC, K.; Gundersen, E. T.; Jorge-Finnigan, A.; Ying, M.; Betbeder, D.; Herfindal, L.; Martinez, A. Stabilization of Human Tyrosine Hydroxylase in Maltodextrin Nanoparticles for Delivery to Neuronal Cells and Tissue. *Bioconjugate Chem.* **2018**, *29*, 493−502.
(12) Jallouli, Y.; Paillard, A.; Chang, J.; Sevin, E.; Betbeder, D. Influence of surface charge and inner composition of porous nanoparticles to cross blood-brain barrier in vitro. *Int. J. Pharm.* **2007**, *344*, 103−109.
(13) Qin, Z.; Joo, J.; Gu, L.; Sailor, M. J. Size Control of Porous Silicon Nanoparticles by Electrochemical Perforation Etching. *Part. Part. Syst. Charact.* **2014**, *31*, 252−256.
(14) Canham, L. *Handbook Of Porous Silicon*; Springer, 2014.
(15) Jugdaohsingh, R.; Tucker, K. L.; Qiao, N.; Cupples, L. A.; Kiel, D. P.; Powell, J. J. Dietary silicon intake is positively associated with bone mineral density in men and premenopausal women of the Framingham Offspring cohort. *J. Bone Miner. Res.* **2004**, *19*, 297−307.
(16) Carlisle, E. M. Silicon: An Essential Element for the Chick. *Science* **1972**, *178*, 619−621.
(17) Henstock, J. R.; Canham, L. T.; Anderson, S. I. Silicon: the evolution of its use in biomaterials. *Acta Biomater.* **2015**, *11*, 17−26.
(18) Lin, V. S.-Y.; Motesharei, K.; Dancil, K.-P. S.; Sailor, M. J.; Ghadiri, M. R. A Porous Silicon-Based Optical Interferometric Biosensor. *Science* **1997**, *278*, 840−843.
(19) Orosco, M. M.; Pacholski, C.; Sailor, M. J. Real-time monitoring of enzyme activity in a mesoporous silicon double layer. *Nat. Nanotechnol.* **2009**, *4*, 255−258.
(20) Andrew, J. S.; Anglin, E. J.; Wu, E. C.; Chen, M. Y.; Cheng, L.; Freeman, W. R.; Sailor, M. J. Sustained Release of a Monoclonal Antibody from Electrochemically Prepared Mesoporous Silicon Oxide. *Adv. Funct. Mater.* **2010**, *20*, 4168−4174.
(21) Rosenberg, M.; Zilony, N.; Shefi, O.; Segal, E. Designing Porous Silicon Films as Carriers of Nerve Growth Factor. *J. Vis. Exp.* **2019**, *143*, No. e58982.
(22) Arshavsky-Graham, S.; Massad-Ivanir, N.; Paratore, F.; Scheper, T.; Bercovici, M.; Segal, E. On Chip Protein Pre-Concentration for Enhancing the Sensitivity of Porous Silicon Biosensors. *ACS Sens.* **2017**, *2*, 1767−1773.
(23) De Stefano, L.; Vitale, A.; Rea, I.; Staiano, M.; Rotiroti, L.; Labella, T.; Rendina, I.; Aurilia, V.; Rossi, M.; D'Auria, S. Enzymes and proteins from extremophiles as hyperstable probes in nanotechnology: the use of D-trehalose/D-maltose-binding protein from the hyperthermophilic archaeon Thermococcus litoralis for sugars monitoring. *Extremophiles* **2008**, *12*, 69−73.
(24) Wu, C.-C.; Hu, Y.; Miller, M.; Aroian, R. V.; Sailor, M. J. Protection and Delivery of Anthelmintic Protein Cry5B to Nematodes Using Mesoporous Silicon Particles. *ACS Nano* **2015**, *9*, 6158−6167.
(25) Wang, J.; Kumeria, T.; Bezem, M. T.; Wang, J.; Sailor, M. J. Self-Reporting Photoluminescent Porous Silicon Microparticles for Drug Delivery. *ACS Appl. Mater. Interfaces* **2018**, *10*, 3200−3209.
(26) Sahare, P.; Ayala, M.; Vazquez-Duhalt, R.; Pal, U.; Loni, A.; Canham, L. T.; Osorio, I.; Agarwal, V. Enhancement of Peroxidase Stability Against Oxidative Self-Inactivation by Co-immobilization with a Redox-Active Protein in Mesoporous Silicon and Silica Microparticles. *Nanoscale Res. Lett.* **2016**, *11*, 417.
(27) Park, J. H.; Gu, L.; von Maltzahn, G.; Ruoslahti, E.; Bhatia, S. N.; Sailor, M. J. Biodegradable luminescent porous silicon nanoparticles for in vivo applications. *Nat. Mater.* **2009**, *8*, 331−336.
(28) Kang, J.; Joo, J.; Kwon, E. J.; Skalak, M.; Hussain, S.; She, Z. G.; Ruoslahti, E.; Bhatia, S. N.; Sailor, M. J. Self-Sealing Porous Silicon-Calcium Silicate Core-Shell Nanoparticles for Targeted siRNA Delivery to the Injured Brain. *Adv. Mater.* **2016**, *28*, 7962−7969.
(29) Kim, D.; Zuidema, J. M.; Kang, J.; Pan, Y.; Wu, L.; Warther, D.; Arkles, B.; Sailor, M. J. Facile Surface Modification of Hydroxylated Silicon Nanostructures Using Heterocyclic Silanes. *J. Am. Chem. Soc.* **2016**, *138*, 15106−15109.
(30) Zuidema, J. M.; Kumeria, T.; Kim, D.; Kang, J.; Wang, J.; Hollett, G.; Zhang, X.; Roberts, D. S.; Chan, N.; Dowling, C.; Blanco-Suarez, E.; Allen, N. J.; Tuszynski, M. H.; Sailor, M. J. Oriented Nanofibrous Polymer Scaffolds Containing Protein-Loaded Porous Silicon Generated by Spray Nebulization. *Adv. Mater.* **2018**, *30*, No. e1706785.
(31) Gu, L.; Ruff, L. E.; Qin, Z.; Corr, M.; Hedrick, S. M.; Sailor, M. J. Multivalent porous silicon nanoparticles enhance the immune activation potency of agonistic CD40 antibody. *Adv Mater.* **2012**, *24*, 3981−3987.
(32) Goodwill, K. E.; Sabatier, C.; Stevens, R. C. Crystal Structure of Tyrosine Hydroxylase with Bound Cofactor Analogue and Iron at 2.3 Å Resolution: Self-Hydroxylation of Phe300 and the Pterin-Binding Site. *Biochemistry* **1998**, *37*, No. 13437.
(33) Zhang, S.; Huang, T.; Ilangovan, U.; Hinck, A. P.; Fitzpatrick, P. F. The Solution Structure of the Regulatory Domain of Tyrosine Hydroxylase. *J. Mol. Biol.* **2014**, *426*, 1483−1497.
(34) Døskeland, A. P.; Flatmark, T. Ubiquitination of soluble and membrane-bound tyrosine hydroxylase and degradation of the soluble form. *Eur. J. Biochem.* **2002**, *269*, 1561−1569.
(35) Chen, M. Y.; Sailor, M. J. Charge-gated transport of proteins in nanostructured optical films of mesoporous silica. *Anal. Chem.* **2011**, *83*, 7186−7193.
(36) Thórólfsson, M.; Døskeland, A. P.; Muga, A.; Martinez, A. The binding of tyrosine hydroxylase to negatively charged lipid bilayers involves the N-terminal region of the enzyme. *FEBS Lett.* **2002**, *519*, 221−226.
(37) Halskau, Ø.; Ying, M.; Baumann, A.; Kleppe, R.; Rodriguez-Larrea, D.; Almås, B.; Haavik, J.; Martinez, A. Three-way Interaction between 14-3-3 Proteins, the N-terminal Region of Tyrosine Hydroxylase, and Negatively Charged Membranes. *J. Biol. Chem.* **2009**, *284*, 32758−32769.
(38) Skjevik, A. A.; Mileni, M.; Baumann, A.; Halskau, O.; Teigen, K.; Stevens, R. C.; Martinez, A. The N-terminal sequence of tyrosine hydroxylase is a conformationally versatile motif that binds 14-3-3 proteins and membranes. *J. Mol. Biol.* **2014**, *426*, 150−168.
(39) Dolinsky, T. J.; Nielsen, J. E.; McCammon, J. A.; Baker, N. A. PDB2PQR: an automated pipeline for the setup of Poisson-Boltzmann electrostatics calculations. *Nucleic Acids Res* **2004**, *32*, W665−W667.
(40) Baker, N. A.; Sept, D.; Joseph, S.; Holst, M. J.; McCammon, J. A. Electrostatics of nanosystems: Application to microtubules and the ribosome. *Proc. Natl. Acad. Sci. U.S.A.* **2001**, *98*, 10037−10041.
(41) APBS. poissonboltzmann.org. http://apbs.poissonboltzmann.org/pdb2pqr (14 May, 2020).
(42) Anderson, S. H. C.; Elliott, H.; Wallis, D. J.; Canham, L. T.; Powell, J. J. Dissolution of different forms of partially porous silicon wafers under simulated physiological conditions. *Phys. Status Solidi A* **2003**, *197*, 331−335.
(43) Haavik, J.; Le Bourdelles, B.; Martinez, A.; Flatmark, T.; Mallet, J. Recombinant human tyrosine hydroxylase isozymes-Reconstitution with iron and inhibitory effect of other metal ions. *Eur. J. Biochem.* **1991**, *199*, 371−378.
(44) Nasrin, S.; Ichinose, H.; Hidaka, H.; Nagatsu, T. Recombinant Human Tyrosine Hydroxylase Types 1-4 Show Regulatory Kinetic Properties for the Natural (6R)-Tetrahydrobiopterin Cofactor. *J. Biochem.* **1994**, *116*, 393−398.
(45) Aliyan, A.; Cook, N. P.; Marti, A. A. Interrogating Amyloid Aggregates using Fluorescent Probes. *Chem. Rev.* **2019**, *119*, 11819−11856.
(46) Azakami, H.; Mukai, A.; Kato, A. Role of Amyloid Type Cross â-Structure in the Formation of Soluble Aggregate and Gel in Heat-Induced Ovalbumin. *J. Agric. Food Chem.* **2005**, *53*, 1254−1257.
(47) Linse, S.; Cabaleiro-Lago, C.; Xue, W.-F.; Lynch, I.; Lindman, S.; Thulin, E.; Radford, S. E.; Dawson, K. A. Nucleation of protein fibrillation by nanoparticles. *Proc. Natl. Acad. Sci. U.S.A.* **2007**, *104*, 8691−8696.
(48) Chayen, N. E.; Saridakis, E.; El-Bahar, R.; Nemirovsky, Y. Porous silicon: an effective nucleation-inducing material for protein crystallization. *J. Mol. Biol.* **2001**, *312*, 591−595.
(49) Görg, A.; Obermaier, C.; Boguth, G.; Harder, A.; Scheibe, B.; Wildgruber, R.; Weiss, W. The current state of two-dimensional

electrophoresis with immobilized gradients. *Electrophoresis* **2000**, *21*, 1037−1053.
(50) Cha, T.; Guo, A.; Zhu, X. Y. Enzymatic activity on a chip: the critical role of protein orientation. *Proteomics* **2005**, *5*, 416−419.
(51) Liu, F.; Wang, L.; Wang, H.; Yuan, L.; Li, J.; Brash, J. L.; Chen, H. Modulating the activity of protein conjugated to gold nanoparticles by site-directed orientation and surface density of bound protein. *ACS Appl. Mater. Interfaces* **2015**, *7*, 3717−3724.
(52) Kappock, T. J.; Caradonna, J. P. Pterin-Dependent Amino Acid Hydroxylases. *Chem. Rev.* **1996**, *96*, 2659−2756.
(53) Thny, B.; Calvo, A. C.; Scherer, T.; Svebak, R. M.; Haavik, J.; Blau, N.; Martinez, A. Tetrahydrobiopterin shows chaperone activity for tyrosine hydroxylase. *J. Neurochem.* **2008**, *106*, 672−681.
(54) Sadidi, M.; Geddes, T. J.; Kuhn, D. M. S-thiolation of tyrosine hydroxylase by reactive nitrogen species in the presence of cysteine or glutathione. *Antioxid. Redox Signaling* **2005**, *7*, 863−869.
(55) Di Giovanni, G.; Pessia, M.; Di Maio, R. Redox sensitivity of tyrosine hydroxylase activity and expression in dopaminergic dysfunction. *CNS Neurol. Disord.: Drug Targets* **2012**, *11*, 419−429.
(56) Hole, M.; Underhaug, J.; Diez, H.; Ying, M.; Røhr, Å. K.; Jorge-Finnigan, A.; Fernàndez-Castillo, N.; García-Cazorla, A.; Andersson, K. K.; Teigen, K.; Martinez, A. Discovery of compounds that protect tyrosine hydroxylase activity through different mechanisms. *Biochim. Biophys. Acta, Proteins Proteomics* **2015**, *1854*, 1078−1089.
(57) Parks, G. A. The Isoelectric Points of Solid Oxides, Solid Hydroxides, and Aqueous Hydroxo Complex Systems. *Chem. Rev.* **1965**, *65*, 177−198.
(58) Lang, E. J.; Cross, P. J.; Mittelstadt, G.; Jameson, G. B.; Parker, E. J. Allosteric ACTion: the varied ACT domains regulating enzymes of amino-acid metabolism. *Curr. Opin. Struct. Biol.* **2014**, *29*, 102−111.
(59) Meissner, J.; Wu, Y.; Jestin, J.; Shelton, W. A.; Findenegg, G. H.; Bharti, B. pH-Induced reorientation of cytochrome c on silica nanoparticles. *Soft Matter* **2019**, *15*, 350−354.
(60) Yu, G.; Zhou, J. Understanding the curvature effect of silica nanoparticles on lysozyme adsorption orientation and conformation: a mesoscopic coarse-grained simulation study. *Phys. Chem. Chem. Phys.* **2016**, *18*, 23500−23507.
(61) Hung, A.; Mwenifumbo, S.; Mager, M.; Kuna, J. J.; Stellacci, F.; Yarovsky, I.; Stevens, M. M. Ordering surfaces on the nanoscale: implications for protein adsorption. *J. Am. Chem. Soc.* **2011**, *133*, 1438−1450.
(62) Peng, C.; Liu, J.; Zhao, D.; Zhou, J. Adsorption of hydrophobin on different self-assembled monolayers: the role of the hydrophobic dipole and the electric dipole. *Langmuir* **2014**, *30*, 11401−11411.
(63) Zheng, H.; Yang, S. J.; Zheng, Y. C.; Cui, Y.; Zhang, Z.; Zhong, J. Y.; Zhou, J. Electrostatic Effect of Functional Surfaces on the Activity of Adsorbed Enzymes: Simulations and Experiments. *ACS Appl. Mater. Interfaces* **2020**, *12*, 35676−35687.
(64) Quan, X.; Liu, J.; Zhou, J. Multiscale modeling and simulations of protein adsorption: progresses and perspectives. *Curr. Opin. Colloid Interface Sci.* **2019**, *41*, 74−85.
(65) Martin, L. J.; Akhavan, B.; Bilek, M. M. M. Electric fields control the orientation of peptides irreversibly immobilized on radical-functionalized surfaces. *Nat. Commun.* **2018**, *9*, No. 357.
(66) Ries, M. Enzyme replacement therapy and beyond-in memoriam Roscoe O. Brady, M.D. (1923-2016). *J. Inherited Metab. Dis.* **2017**, *40*, 343−356.
(67) Suh, K. Y.; Yang, J. M.; Khademhosseini, A.; Berry, D.; Tran, T. N.; Park, H.; Langer, R. Characterization of chemisorbed hyaluronic acid directly immobilized on solid substrates. *J. Biomed. Mater. Res., Part B* **2005**, *72*, 292−298.
(68) Hou, S.; Xu, Q.; Tian, W.; Cui, F.; Cai, Q.; Ma, J.; Lee, I. S. The repair of brain lesion by implantation of hyaluronic acid hydrogels modified with laminin. *J. Neurosci. Methods* **2005**, *148*, 60−70.
(69) Bjugstad, K. B.; Redmond, D. E.; Lampe, K. J.; Kern, D. S.; Sladek, J. R., Jr.; Mahoney, M. J. Biocompatibility of PEG-Based Hydrogels in Primate Brain. *Cell Transplant.* **2008**, *17*, 409−415.
(70) Basso, J.; Miranda, A.; Nunes, S.; Cova, T.; Sousa, J.; Vitorino, C.; Pais, A. Hydrogel-Based Drug Delivery Nanosystems for the Treatment of Brain Tumors. *Gels* **2018**, *4*, No. 62.
(71) Giordano, C.; Albani, D.; Gloria, A.; Tunesi, M.; Batelli, S.; Russo, T.; Forloni, G.; Ambrosio, L.; Cigada, A. Multidisciplinary Perspectives for Alzheimer's and Parkinson's Diseases: Hydrogels for Protein Delivery and Cell-Based Drug Delivery as Therapeutic Strategies. *Int. J. Artif. Organs* **2009**, *32*, 836−850.
(72) Li, J.; Darabi, M.; Gu, J.; Shi, J.; Xue, J.; Huang, L.; Liu, Y.; Zhang, L.; Liu, N.; Zhong, W.; Zhang, L.; Xing, M.; Zhang, L. A drug delivery hydrogel system based on activin B for Parkinson's disease. *Biomaterials* **2016**, *102*, 72−86.

https://dx.doi.org/10.1021/acs.molpharmaceut.0c00960
Mol. Pharmaceutics 2021, 18, 976−985

Graphic design: Communication Division, UiB / Print: Skipnes Kommunikasjon AS

uib.no

ISBN: 9788230857779 (print)
9788230854167 (PDF)